Recent advances in radio channel characterization:

Some contributions from the NoE NEWCOM

Xuefeng Yin[1] Troels Pedersen[1] Bernard H. Fleury[1,2]

[1]Department of Electronic Systems, Aalborg University, Denmark
[2]Forschungszentrum Telekommunikation Wien (ftw.), Vienna, Austria

{xuefeng,troels,fleury}@es.aau.dk

The 4th COST 289 Workshop, April 11-12, 2007, Gothenburg, Sweden

Contents

Short Presentation of NEWCOM Dept2 Radio Channel Modelling for Next Generation Communication Systems

Contents

- Partners involved in Dept2
- Workpackages
- Operation of Dept2 in Conducting Integrated Research
- Outcome and Benefits
- Conclusions

Partners Involved in Dept2

- (BE) Universté Catholique de Louvain
- (DE) Technical University of Ilmenau
- (DK) Aalborg University
- (FI) Elektrobit
- (FI) University of Oulu
- (UK) University of Bristol
- (UK) University of Edinburg
- (UK) University of York
- (FR) Eurecom
- (FR) Thales Communications
- (SE) Lund University
- (SE) Royal Institute of Technology
- (FR) Centre National de la Recherche Scientifique
- (GR) National and Kapodistrian University of Athens
- (AU) Forschungszentrum Telekommunilation Wien, ftw.
- (AU) Vienna University of Technology
- (IT) Consorzio Nationale Interuniversitario per le Telecommunicazioni
- (PT) Technical University of Lisboa
- (SP) Universitad Politécnica de Valencia
- (TR) Bilkent University

Workpackages

- WP2.1: Channel Modelling
- WP2.2: Channel Simulation
- WP2.3: Channel Sounding

Operation of Dept2 in Conducting Integrated Research

Dept2 is operated like a decentralized, self-organizing, ad-hoc network:

- Nodes, i.e. partners, cluster into "integrated activity" groups.
- Initiatives are left to the nodes.
- Dynamic, time-varying clustering (integrated activities) driven by emerging critical open issues in research.

Outcome and Benefits

- New long-lasting integrated activities have been established.
- Exchanges of tools, data, methods, and software packages have enabled new research initiatives to be launched at partner institutions.
- Dissemination of competence and expertise within the NoE.
- Significantly increased research mobility.
- Significant amount of scientific publications:
  $\sim$40 publications per year
  $\sim$83% joint papers, $\sim$17% NEWCOM inspired papers
  $\sim$20% journal papers, $\sim$80% conference papers

Some Further Conclusions

- Dept2, like the other departments and projects in NEWCOM, is operated in a COST-like manner.
- The add-on compared to COST actions is that more financing means are available in NoEs to implement networking and integration.
  - A high degree of integration has been achieved in Dept2.
- The negative side is the heavy reporting load requested by the EC compared to the actually modest financing of NoEs.
  - NoEs only finance networking and integration, not research.
- Effective networking and integration in a NoE require specific skills from the "partner nodes". Acquiring these skills has proven to be not self-evident.
  - Dept2 has strongly beneficiated from the cooperation spirit developed in the past COST 273, COST 231, ...

Parametric Characterization and Estimation of Dispersion of Individual Path Components

Contents

Contents

Multipath Propagation

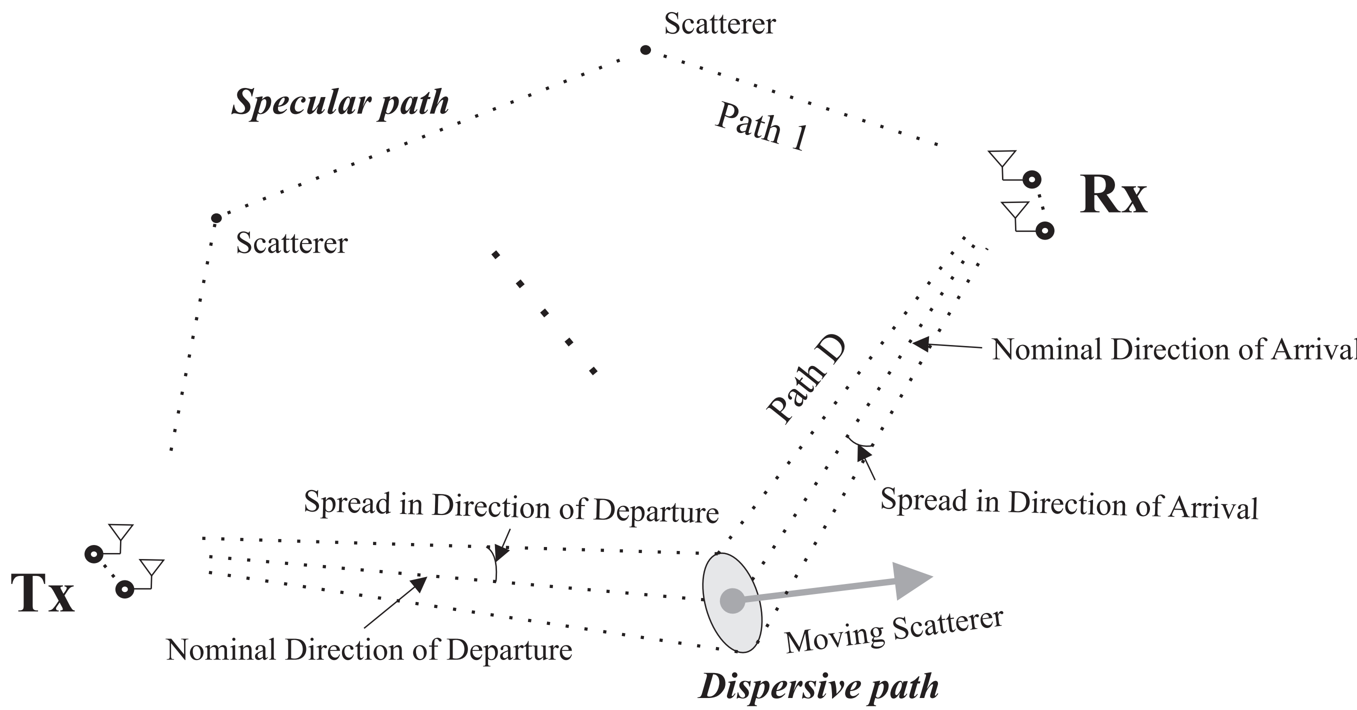

- Dispersion dimensions: delay, direction of departure, direction of arrival, Doppler frequency and polarization.
- Path component: the contribution of a wave propagating along a propagation path in the response of the channel.
- Parameters of a path component: center of gravity and spread in each dispersion dimension and dependencies across the dispersion dimensions.

Radio Channel Estimation Based on a Specular Path Model

View from Receiver

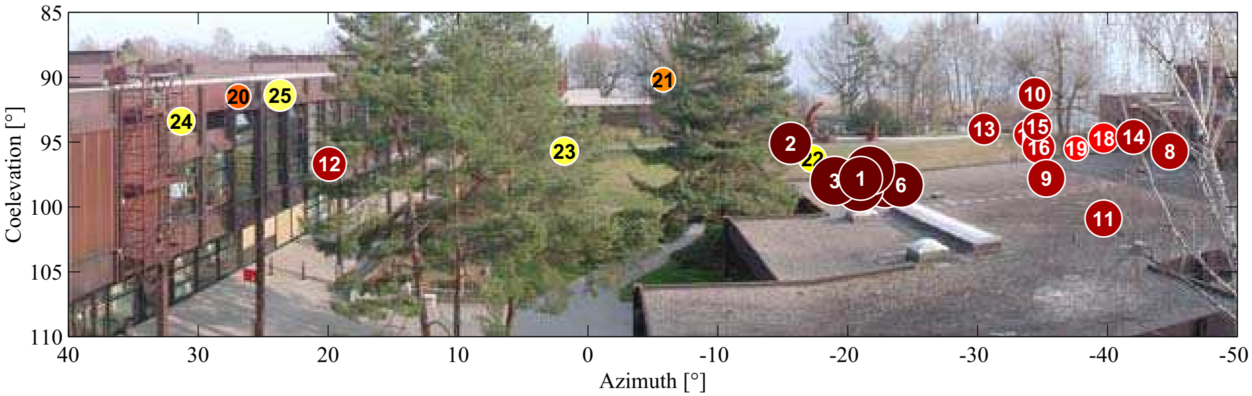

View from Transmitter

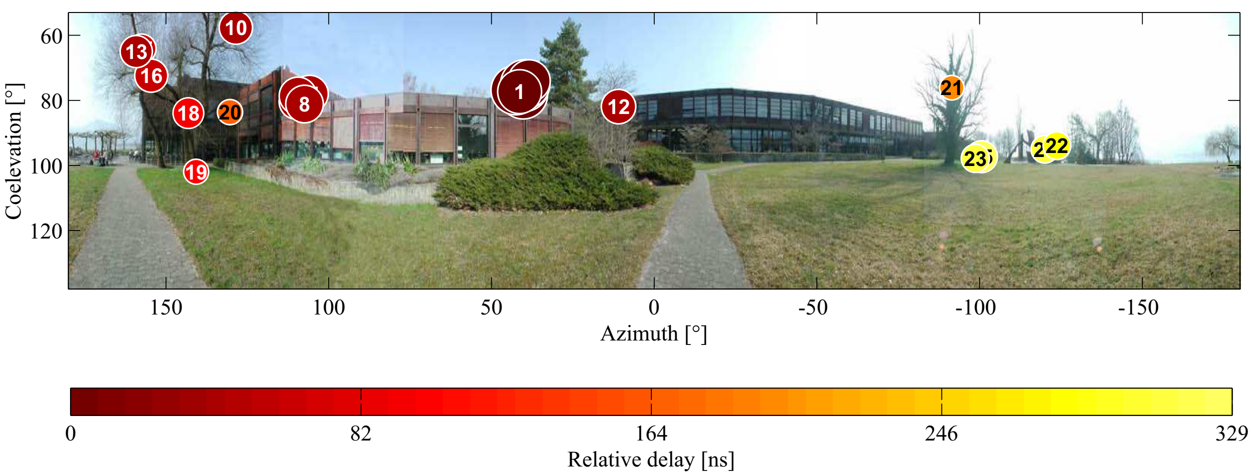

Reconstructed Paths

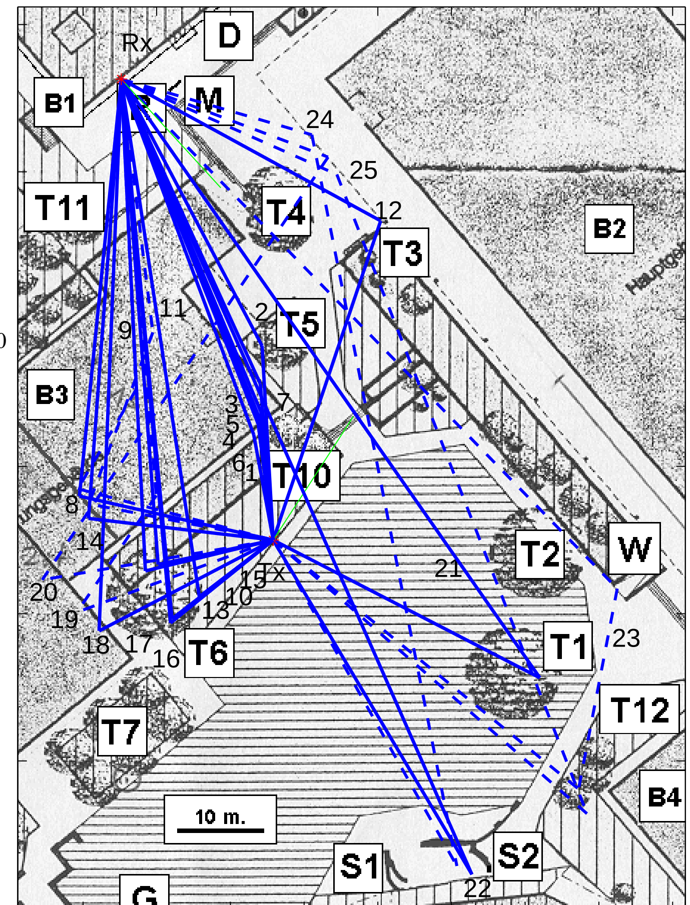

Dispersion of Individual Path Components

Bartlett spectra with respect to azimuth of departure (AoD) and azimuth of arrival (AoA) computed at a specific delay from measurement data

- 5.25 GHz carrier frequency and 200 MHz bandwidth
- The Rx and Tx are equipped with similar 9-element circular arrays.

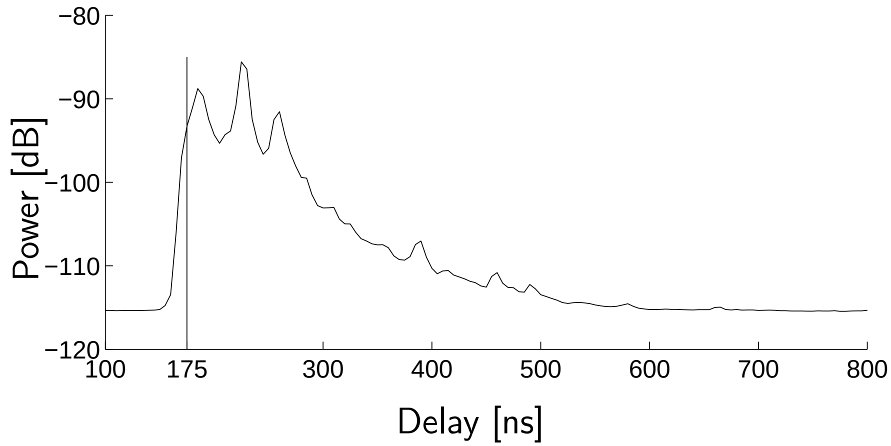

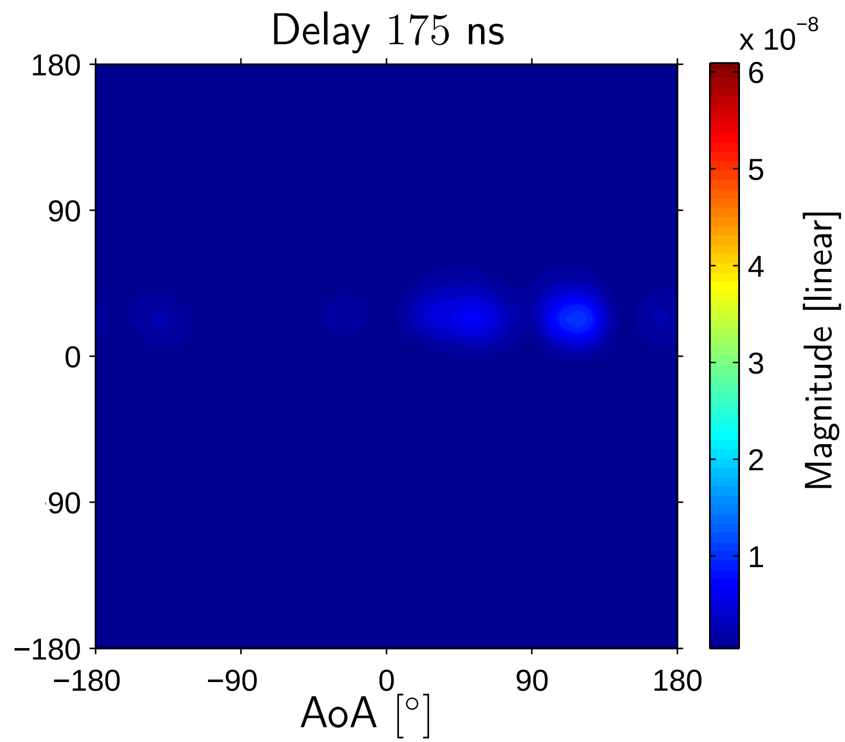

Dispersion of Individual Path Components

Bartlett spectra with respect to azimuth of departure (AoD) and azimuth of arrival (AoA) computed at a specific delay from measurement data

- 5.25 GHz carrier frequency and 200 MHz bandwidth
- The Rx and Tx are equipped with similar 9-element circular arrays.

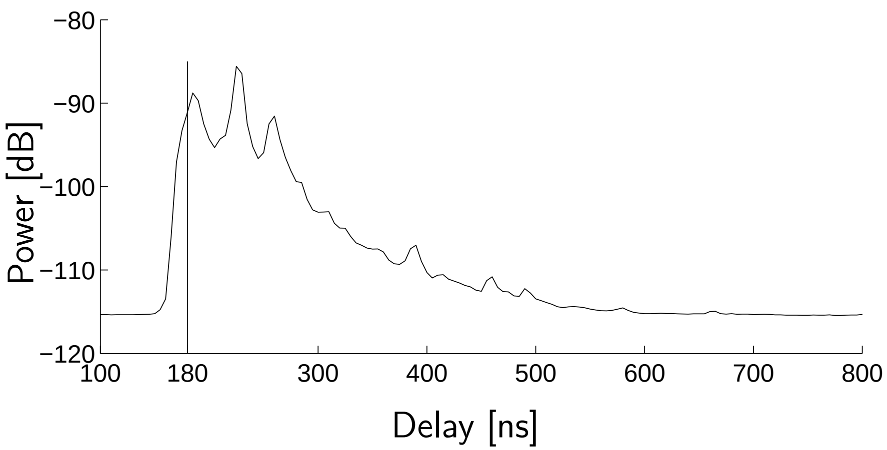

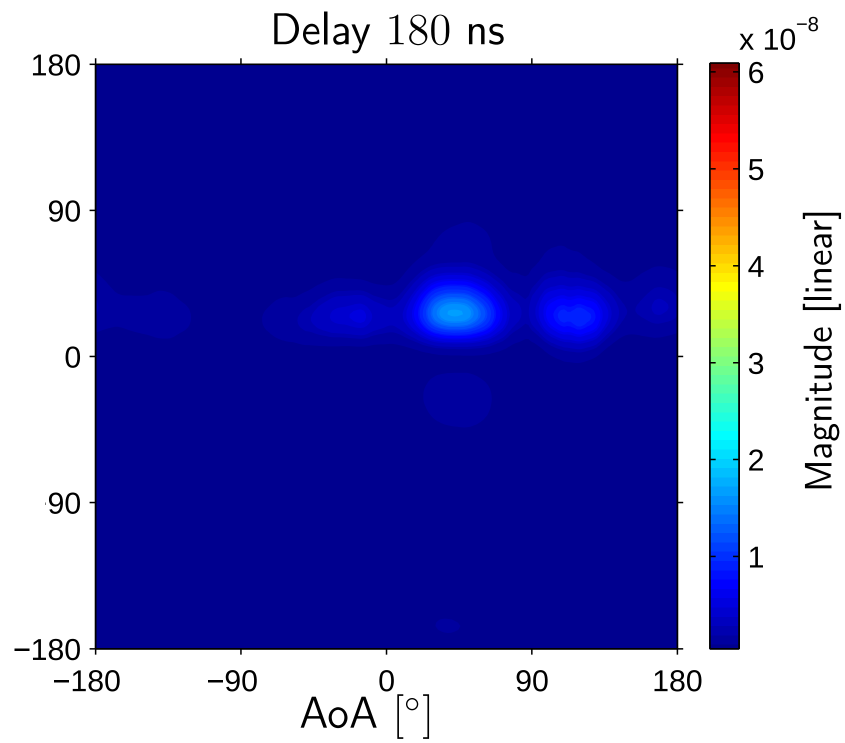

Dispersion of Individual Path Components

Bartlett spectra with respect to azimuth of departure (AoD) and azimuth of arrival (AoA) computed at a specific delay from measurement data

- 5.25 GHz carrier frequency and 200 MHz bandwidth
- The Rx and Tx are equipped with similar 9-element circular arrays.

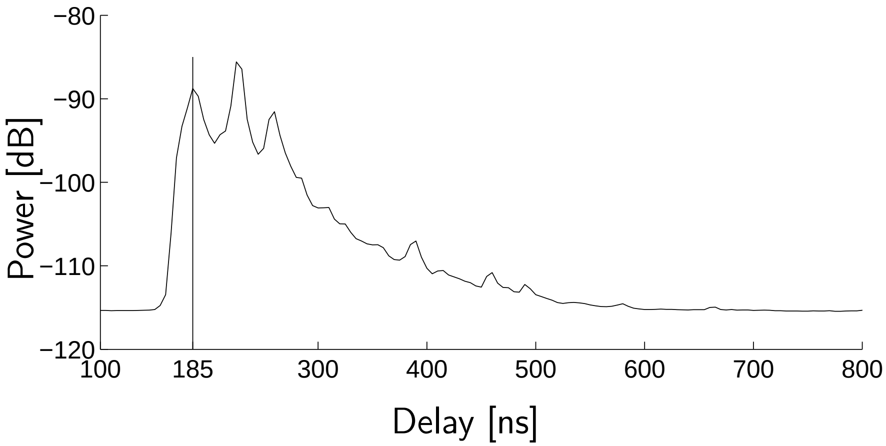

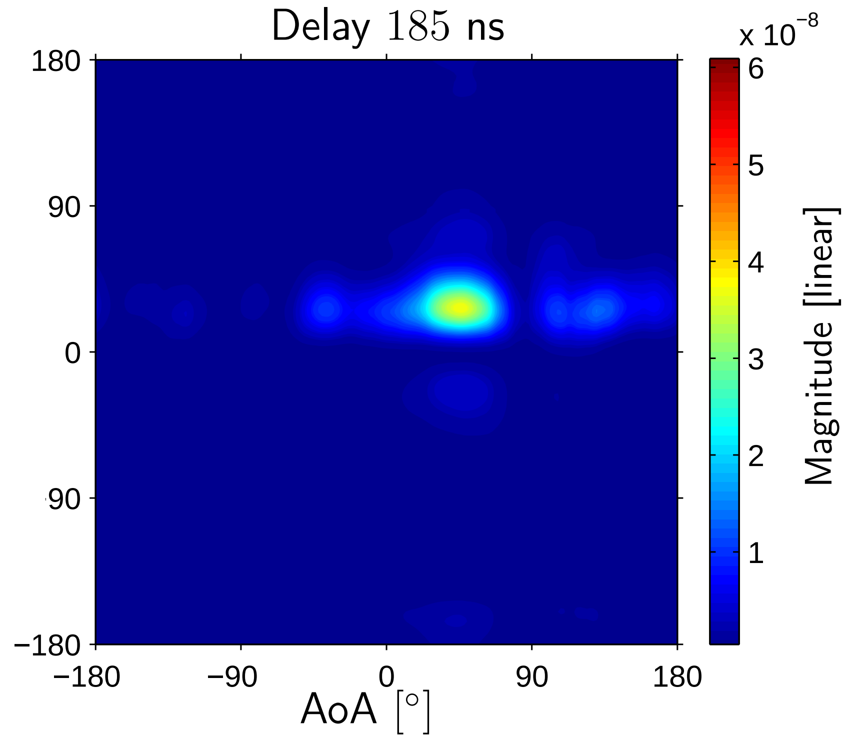

Dispersion of Individual Path Components

Bartlett spectra with respect to azimuth of departure (AoD) and azimuth of arrival (AoA) computed at a specific delay from measurement data

- 5.25 GHz carrier frequency and 200 MHz bandwidth
- The Rx and Tx are equipped with similar 9-element circular arrays.

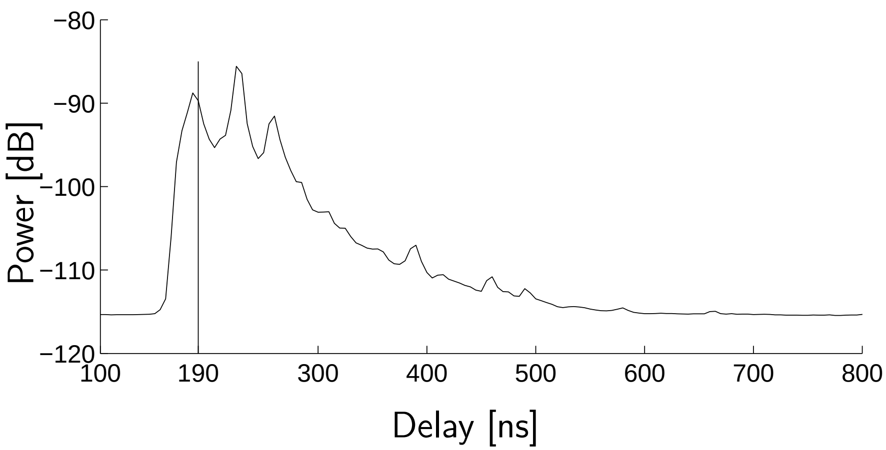

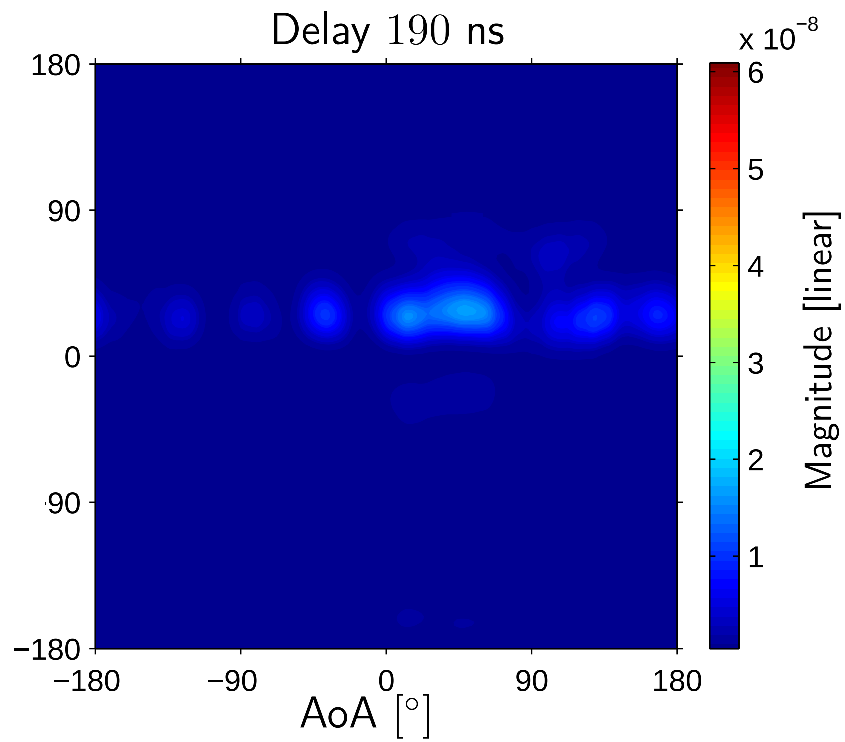

Dispersion of Individual Path Components

Bartlett spectra with respect to azimuth of departure (AoD) and azimuth of arrival (AoA) computed at a specific delay from measurement data

- 5.25 GHz carrier frequency and 200 MHz bandwidth
- The Rx and Tx are equipped with similar 9-element circular arrays.

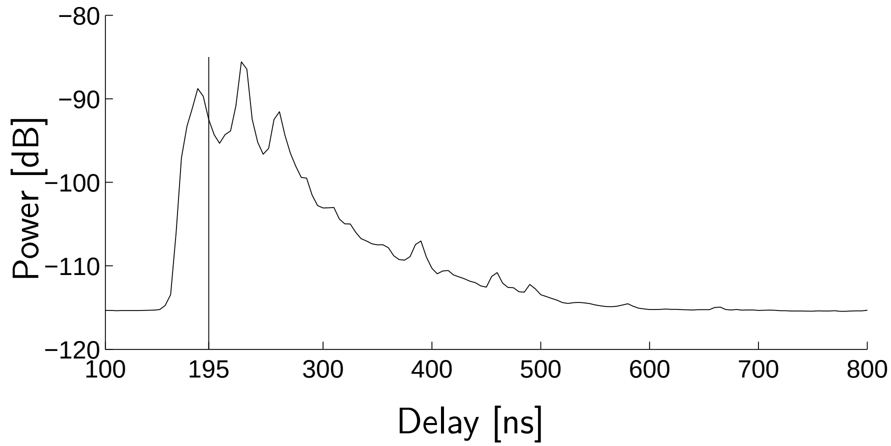

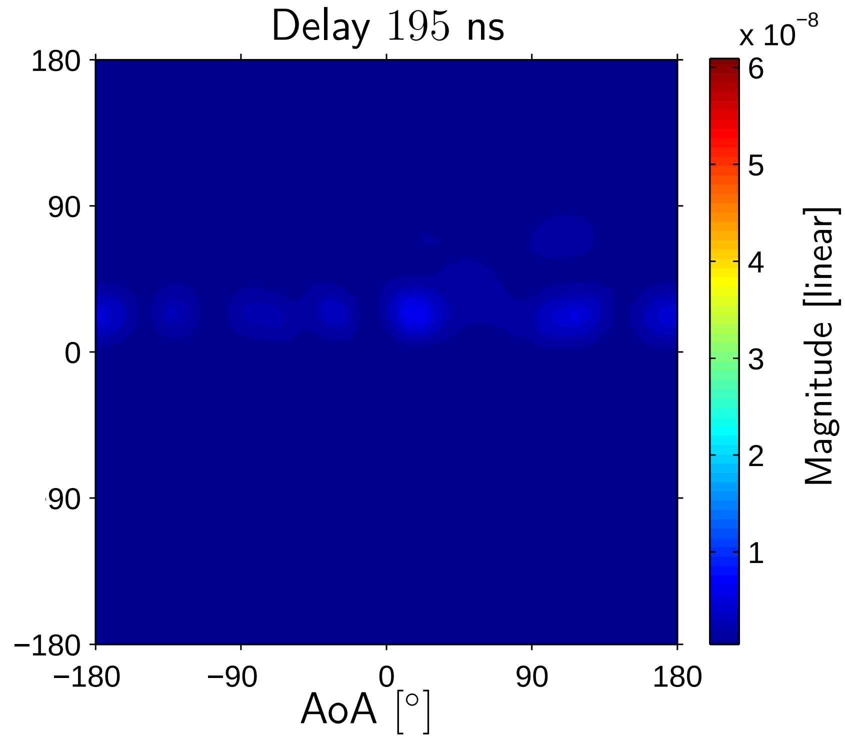

Dispersion of Individual Path Components

Bartlett spectra with respect to azimuth of departure (AoD) and azimuth of arrival (AoA) computed at a specific delay from measurement data

- 5.25 GHz carrier frequency and 200 MHz bandwidth
- The Rx and Tx are equipped with similar 9-element circular arrays.

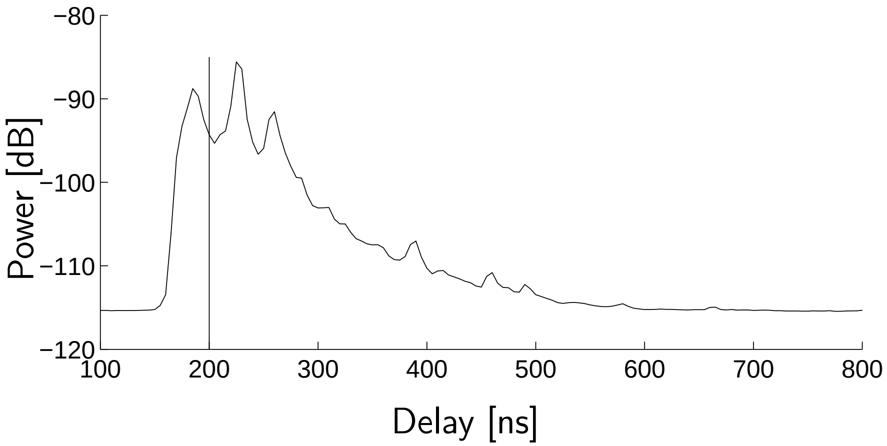

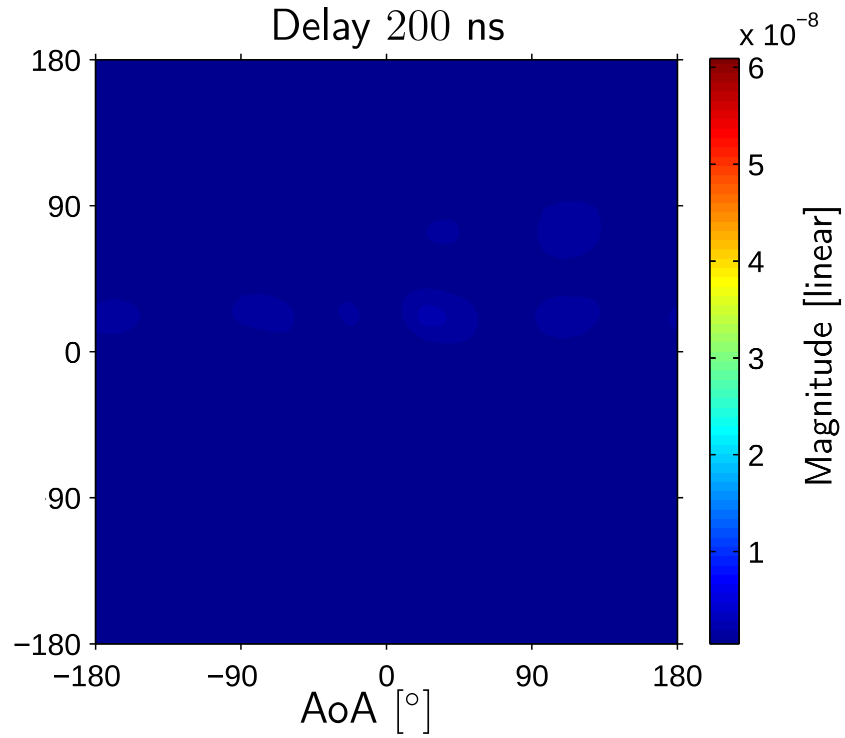

Dispersion of Individual Path Components

Bartlett spectra with respect to azimuth of departure (AoD) and azimuth of arrival (AoA) computed at a specific delay from measurement data

- 5.25 GHz carrier frequency and 200 MHz bandwidth
- The Rx and Tx are equipped with similar 9-element circular arrays.

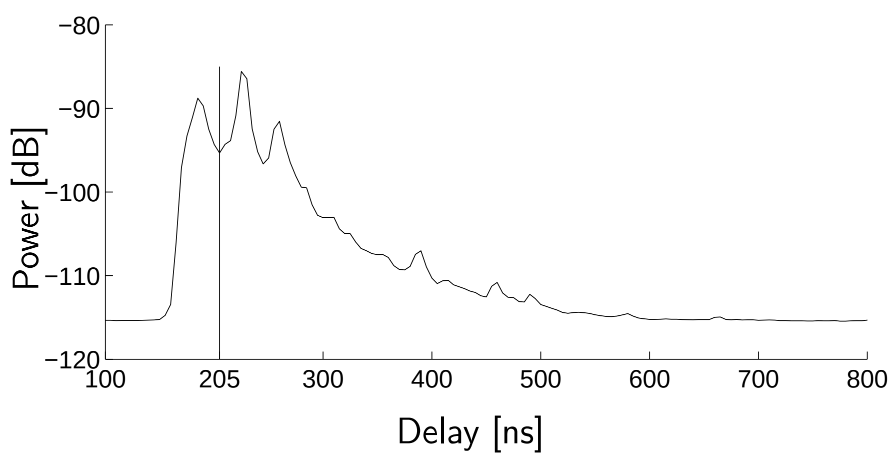

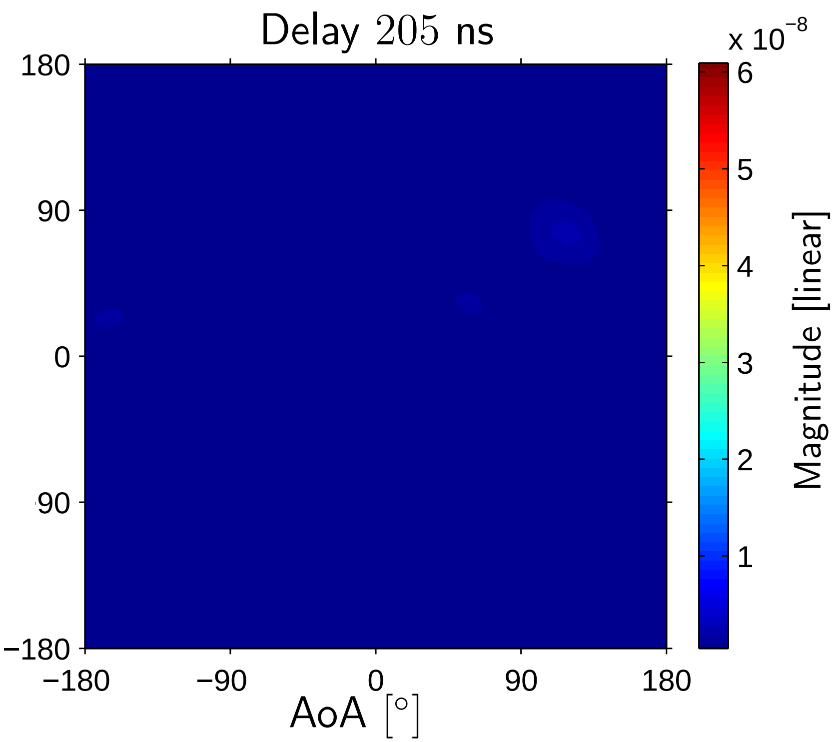

Dispersion of Individual Path Components

Bartlett spectra with respect to azimuth of departure (AoD) and azimuth of arrival (AoA) computed at a specific delay from measurement data

- 5.25 GHz carrier frequency and 200 MHz bandwidth
- The Rx and Tx are equipped with similar 9-element circular arrays.

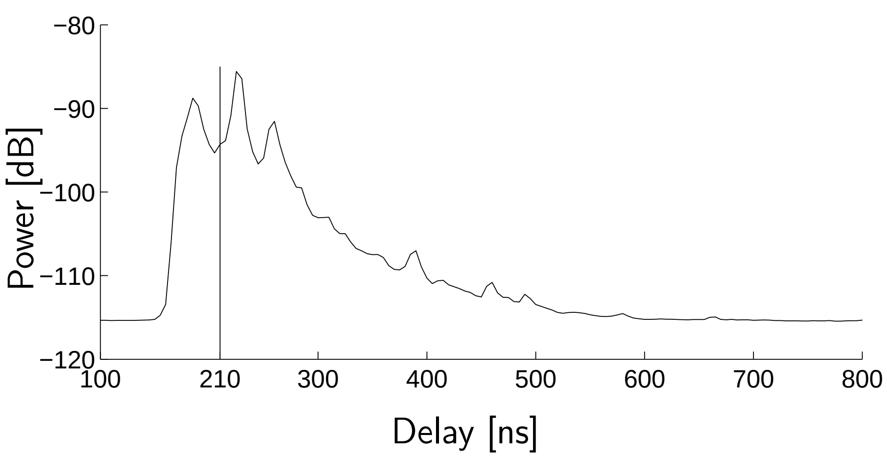

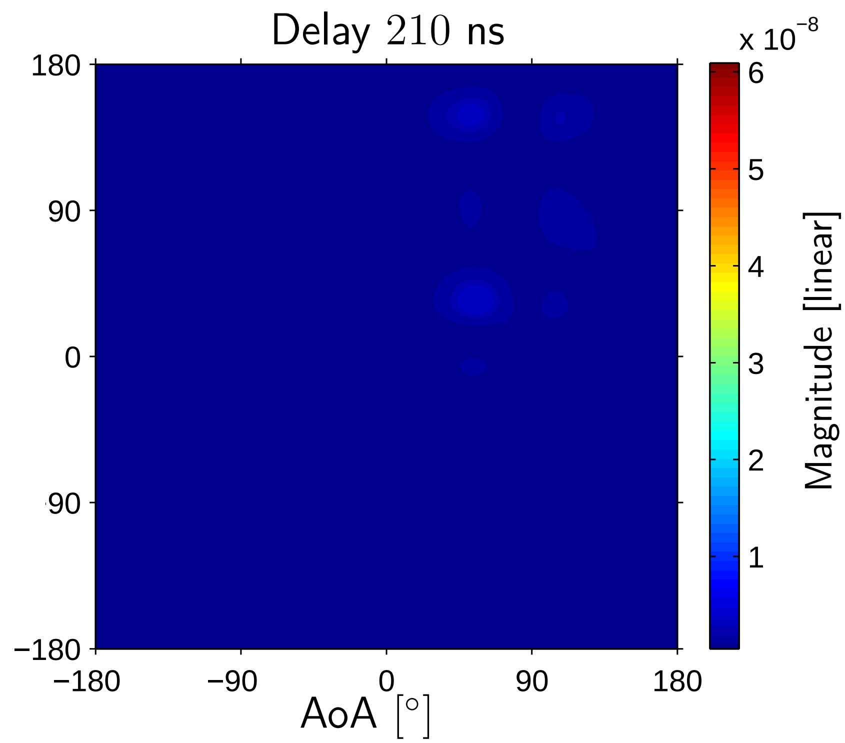

Dispersion of Individual Path Components

Bartlett spectra with respect to azimuth of departure (AoD) and azimuth of arrival (AoA) computed at a specific delay from measurement data

- 5.25 GHz carrier frequency and 200 MHz bandwidth
- The Rx and Tx are equipped with similar 9-element circular arrays.

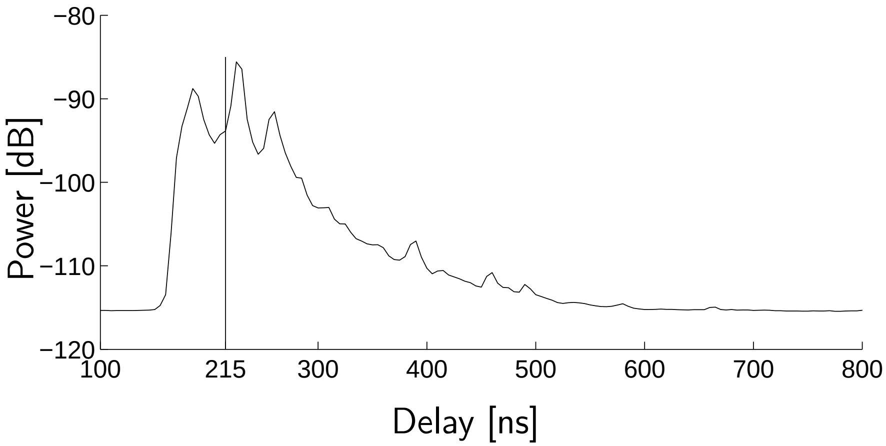

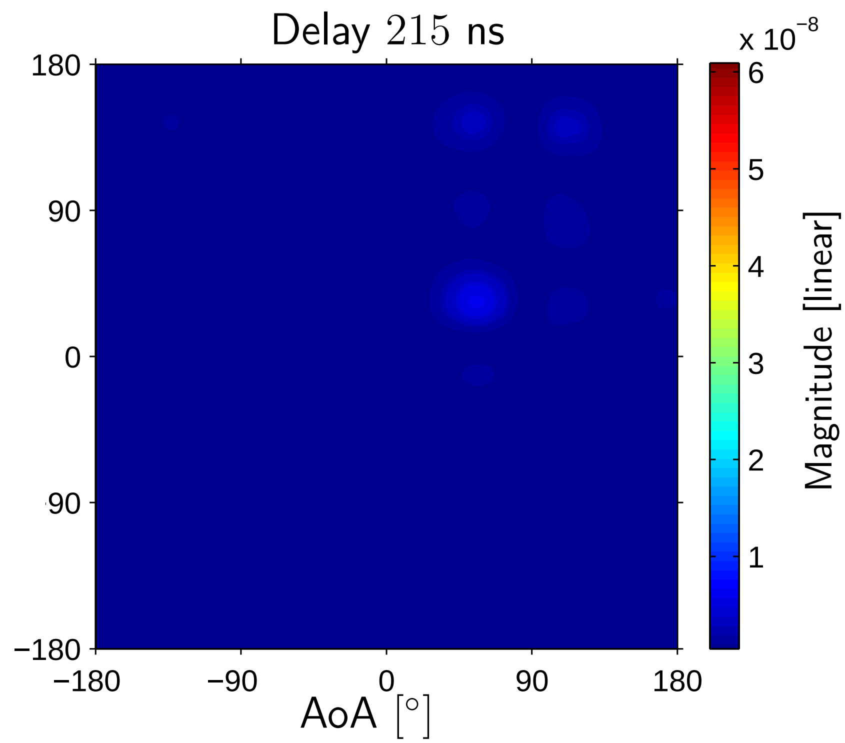

Dispersion of Individual Path Components

Bartlett spectra with respect to azimuth of departure (AoD) and azimuth of arrival (AoA) computed at a specific delay from measurement data

- 5.25 GHz carrier frequency and 200 MHz bandwidth
- The Rx and Tx are equipped with similar 9-element circular arrays.

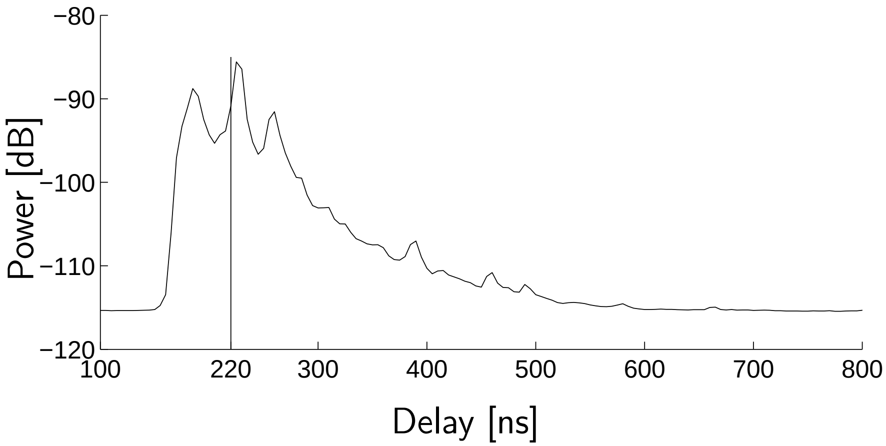

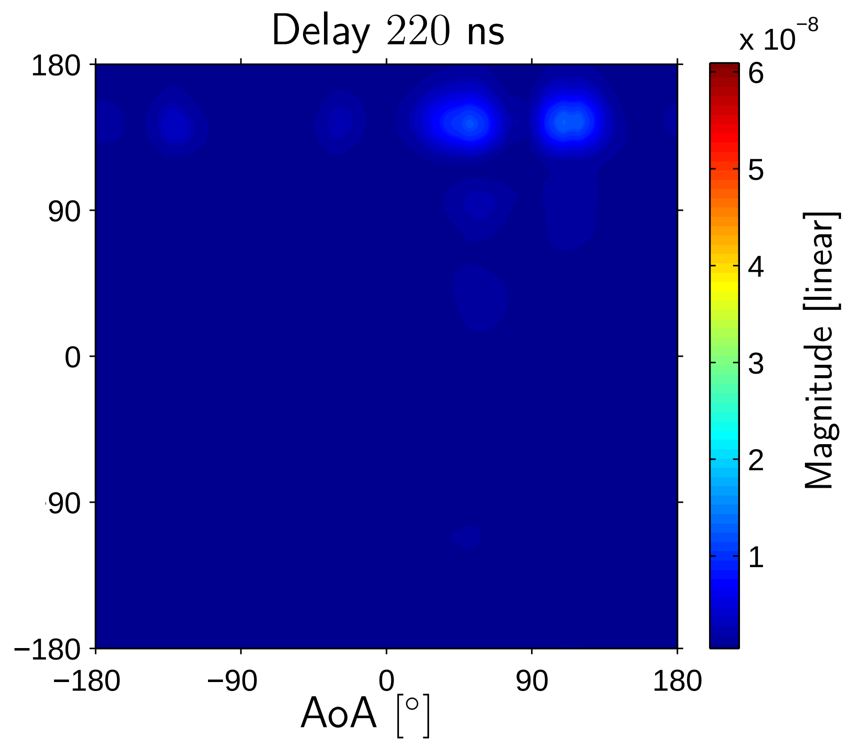

Dispersion of Individual Path Components

Bartlett spectra with respect to azimuth of departure (AoD) and azimuth of arrival (AoA) computed at a specific delay from measurement data

- 5.25 GHz carrier frequency and 200 MHz bandwidth
- The Rx and Tx are equipped with similar 9-element circular arrays.

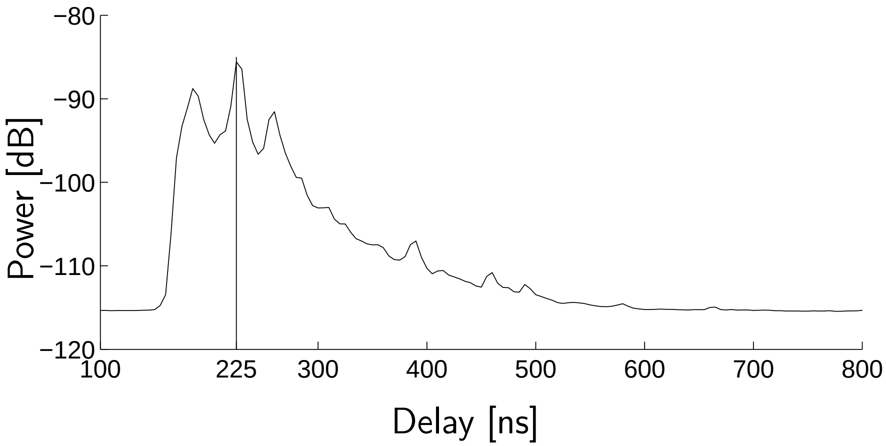

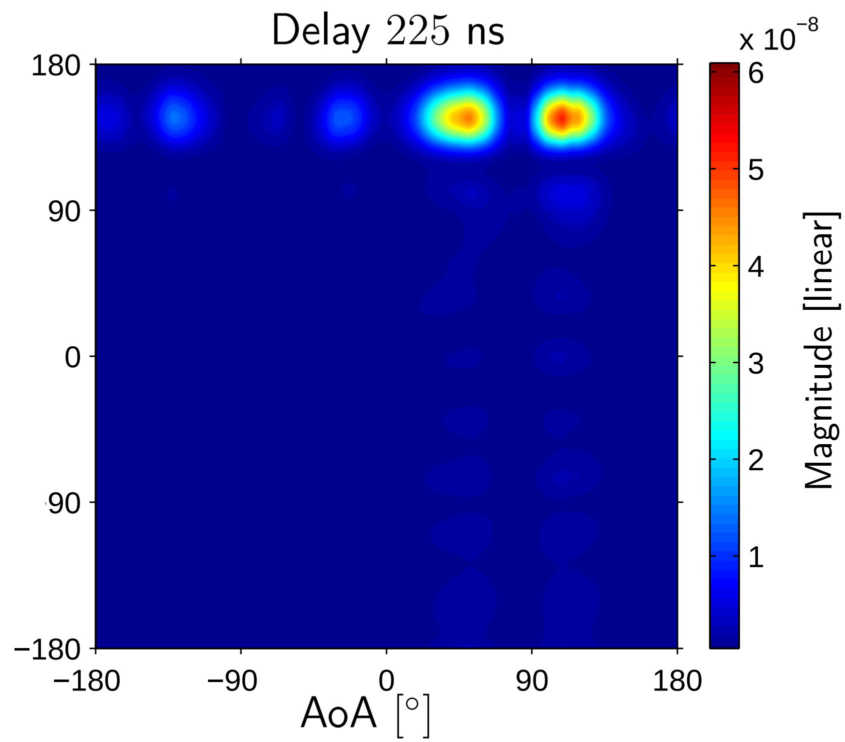

Dispersion of Individual Path Components

Bartlett spectra with respect to azimuth of departure (AoD) and azimuth of arrival (AoA) computed at a specific delay from measurement data

- 5.25 GHz carrier frequency and 200 MHz bandwidth
- The Rx and Tx are equipped with similar 9-element circular arrays.

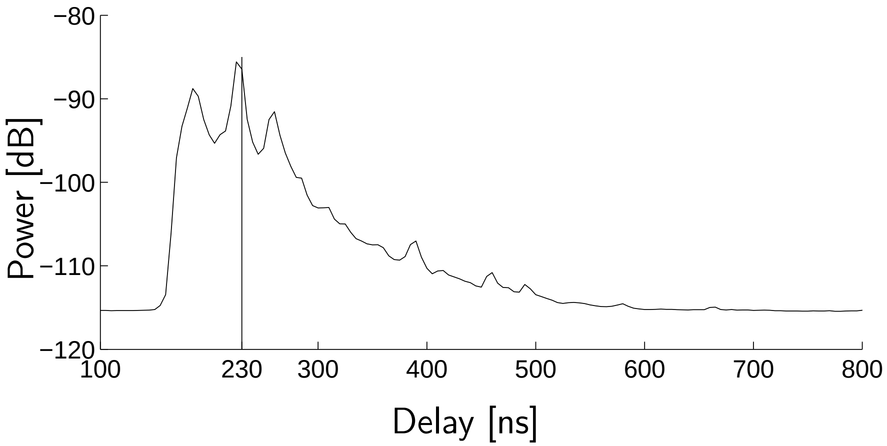

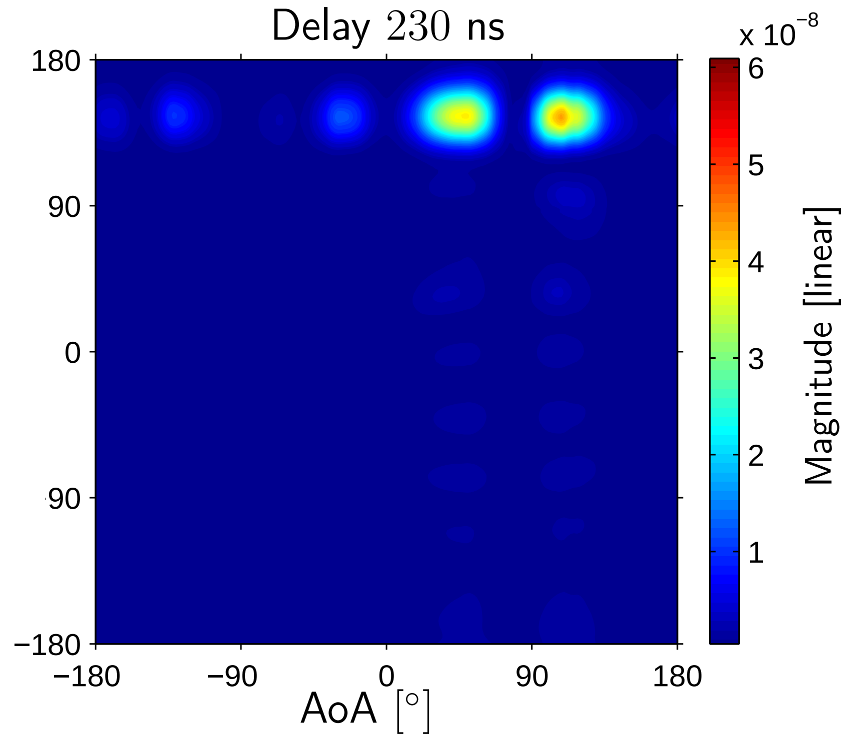

Dispersion of Individual Path Components

Bartlett spectra with respect to azimuth of departure (AoD) and azimuth of arrival (AoA) computed at a specific delay from measurement data

- 5.25 GHz carrier frequency and 200 MHz bandwidth
- The Rx and Tx are equipped with similar 9-element circular arrays.

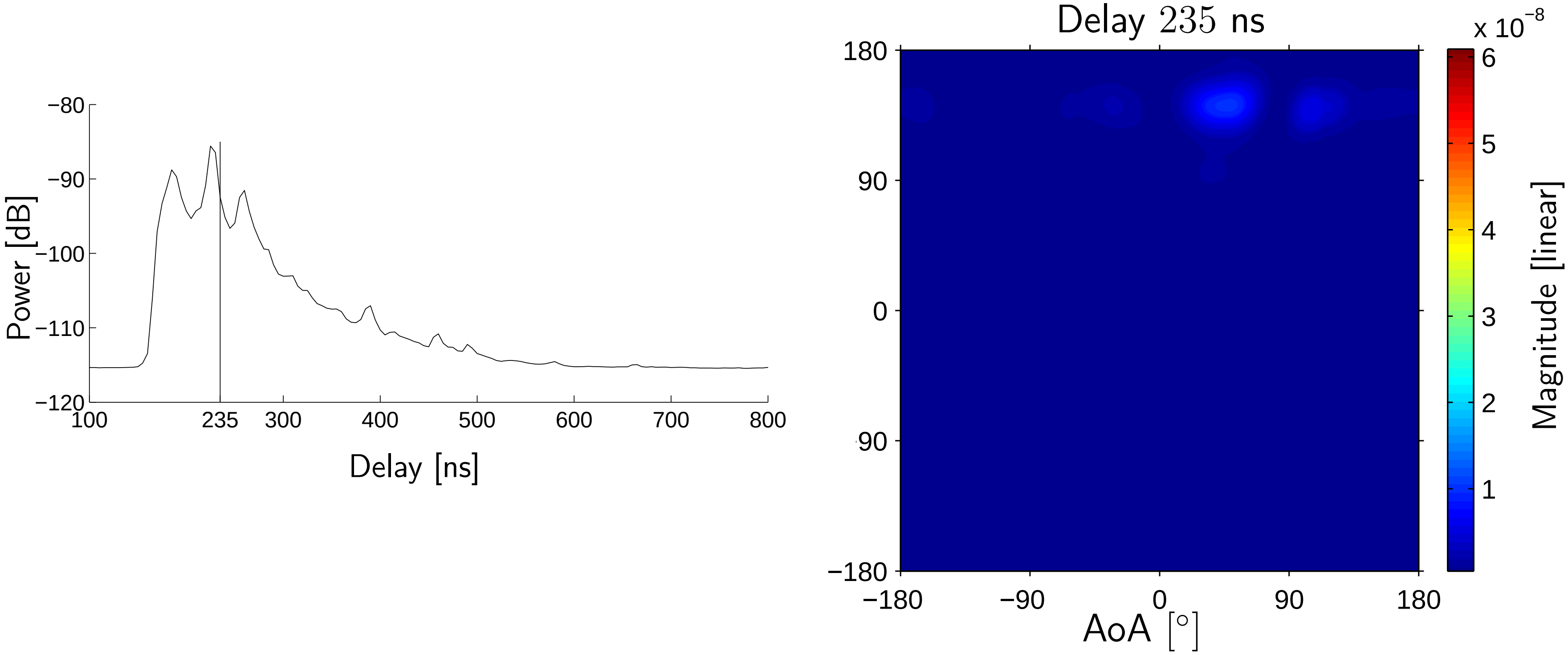

Dispersion of Individual Path Components

Bartlett spectra with respect to azimuth of departure (AoD) and azimuth of arrival (AoA) computed at a specific delay from measurement data

- 5.25 GHz carrier frequency and 200 MHz bandwidth
- The Rx and Tx are equipped with similar 9-element circular arrays.

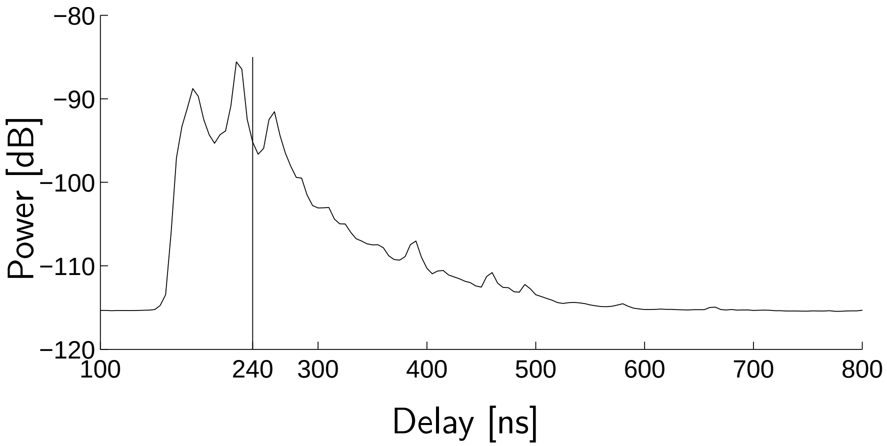

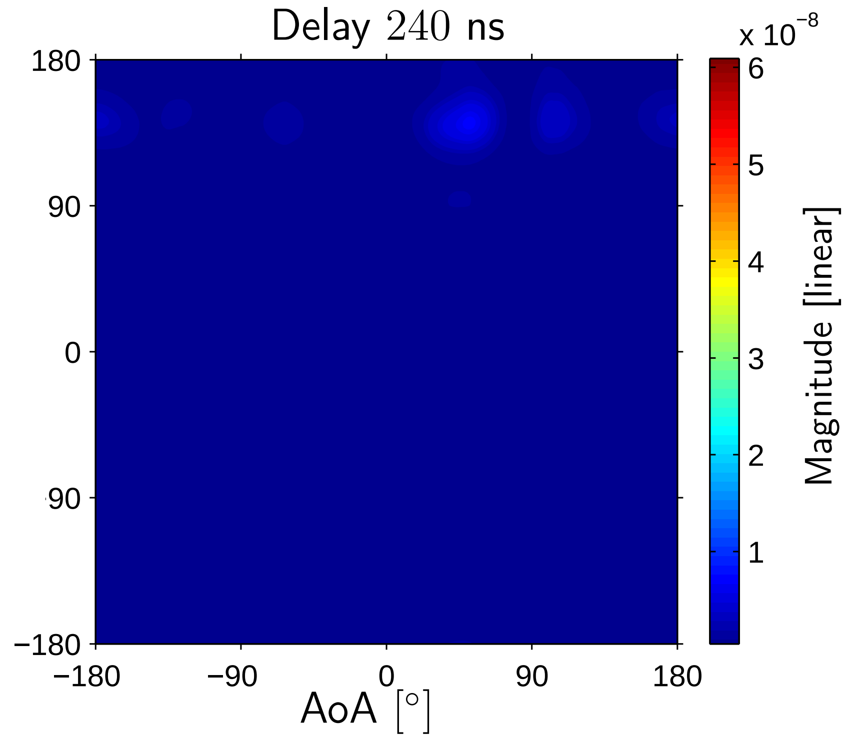

Dispersion of Individual Path Components

Bartlett spectra with respect to azimuth of departure (AoD) and azimuth of arrival (AoA) computed at a specific delay from measurement data

- 5.25 GHz carrier frequency and 200 MHz bandwidth
- The Rx and Tx are equipped with similar 9-element circular arrays.

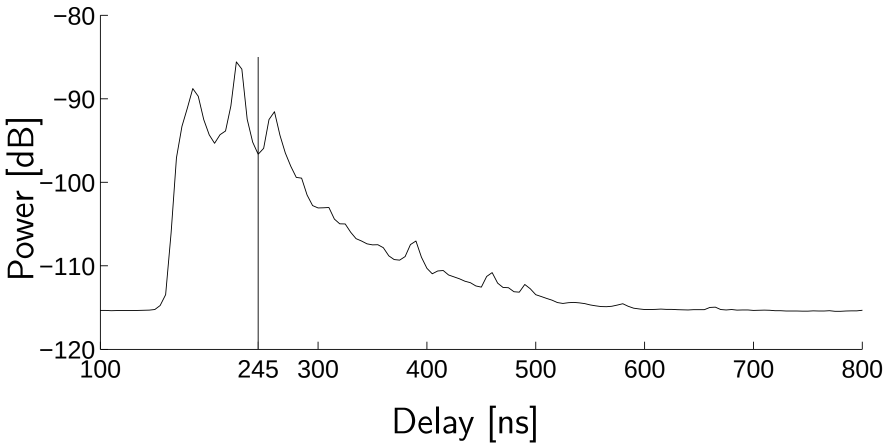

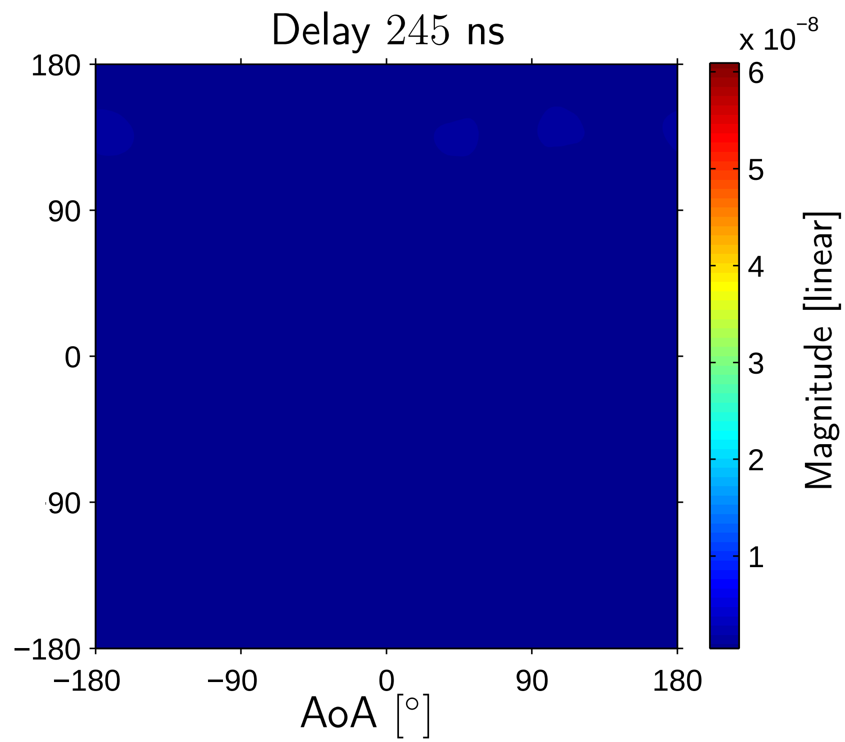

Dispersion of Individual Path Components

Bartlett spectra with respect to azimuth of departure (AoD) and azimuth of arrival (AoA) computed at a specific delay from measurement data

- 5.25 GHz carrier frequency and 200 MHz bandwidth
- The Rx and Tx are equipped with similar 9-element circular arrays.

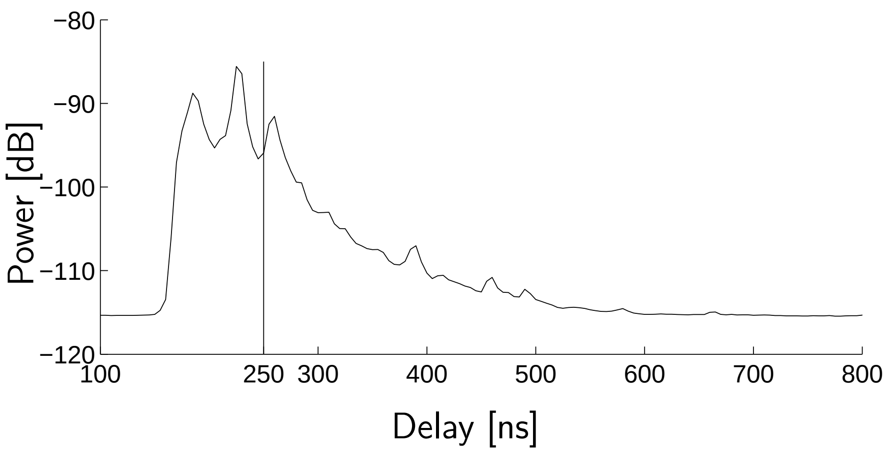

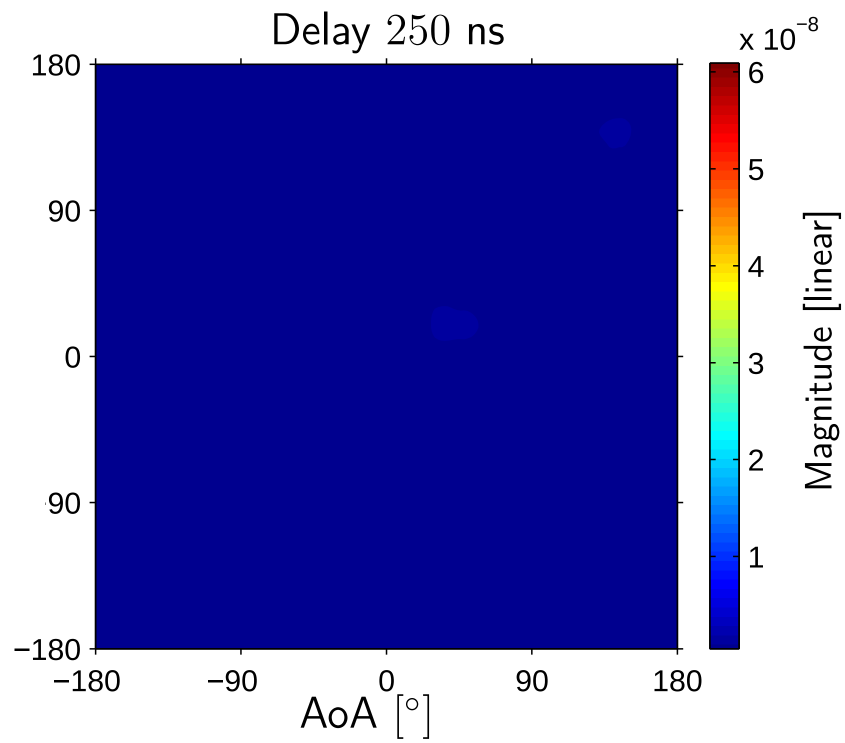

Dispersion of Individual Path Components

Bartlett spectra with respect to azimuth of departure (AoD) and azimuth of arrival (AoA) computed at a specific delay from measurement data

- 5.25 GHz carrier frequency and 200 MHz bandwidth
- The Rx and Tx are equipped with similar 9-element circular arrays.

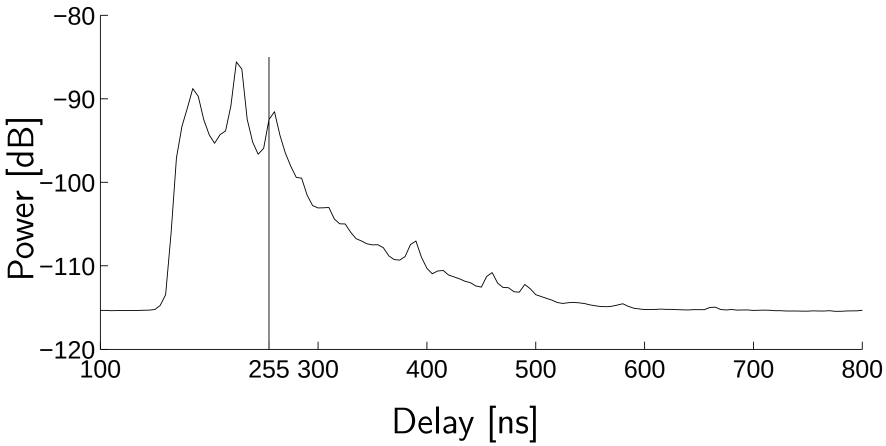

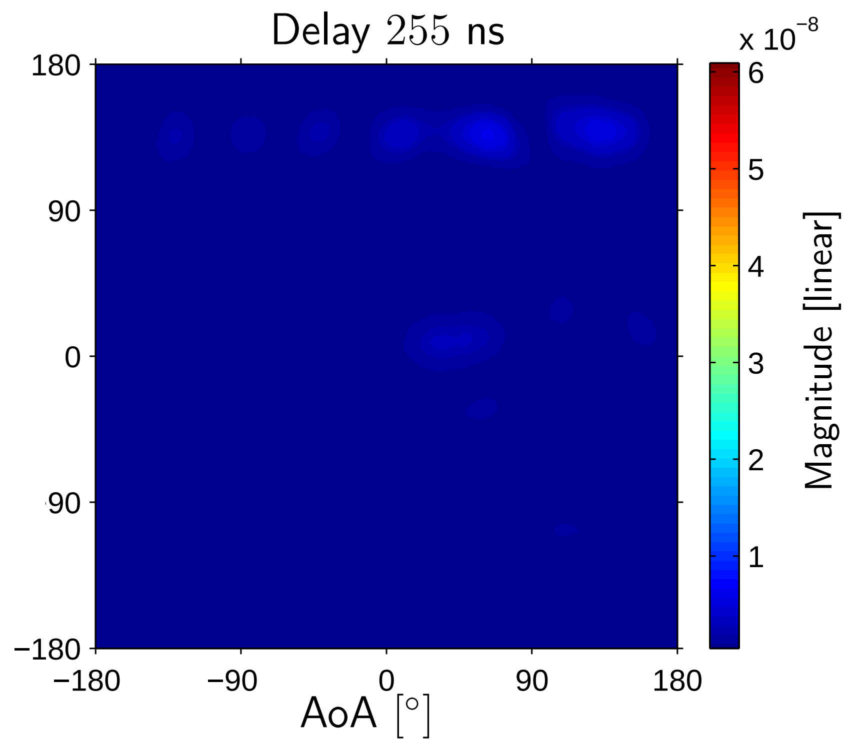

Dispersion of Individual Path Components

Bartlett spectra with respect to azimuth of departure (AoD) and azimuth of arrival (AoA) computed at a specific delay from measurement data

- 5.25 GHz carrier frequency and 200 MHz bandwidth
- The Rx and Tx are equipped with similar 9-element circular arrays.

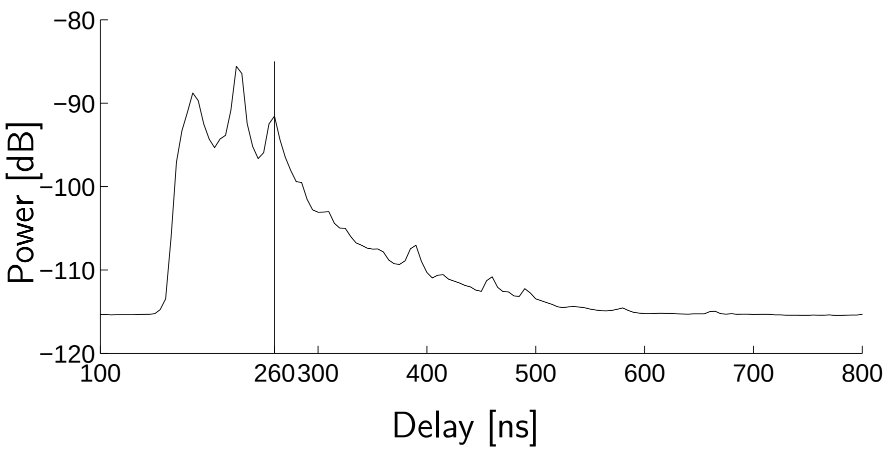

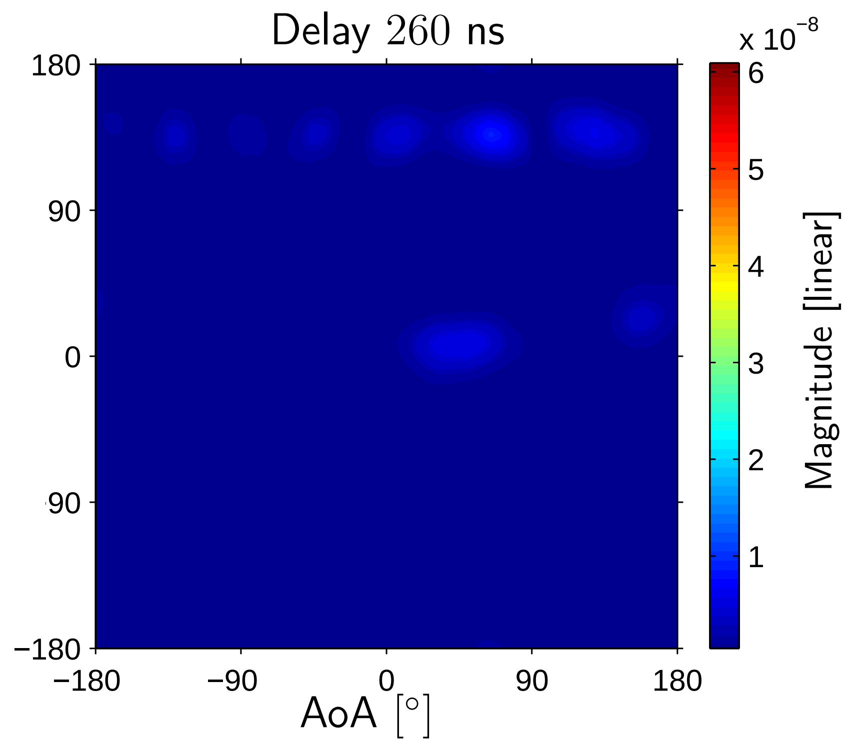

Dispersion of Individual Path Components

Bartlett spectra with respect to azimuth of departure (AoD) and azimuth of arrival (AoA) computed at a specific delay from measurement data

- 5.25 GHz carrier frequency and 200 MHz bandwidth
- The Rx and Tx are equipped with similar 9-element circular arrays.

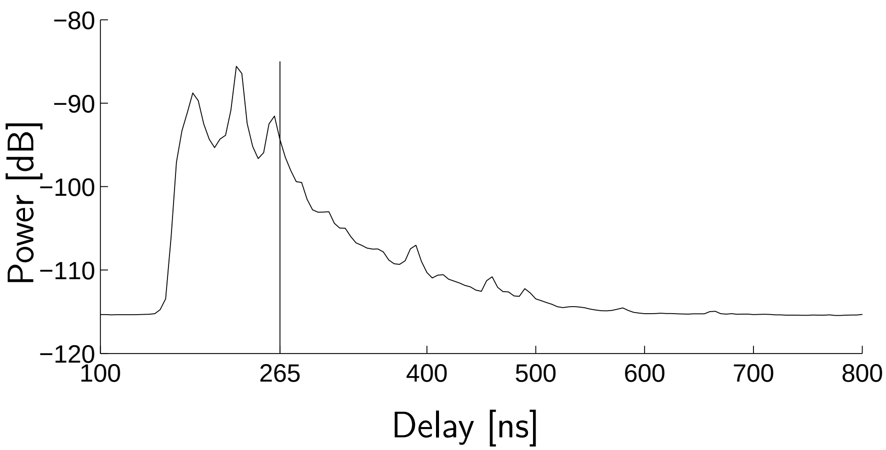

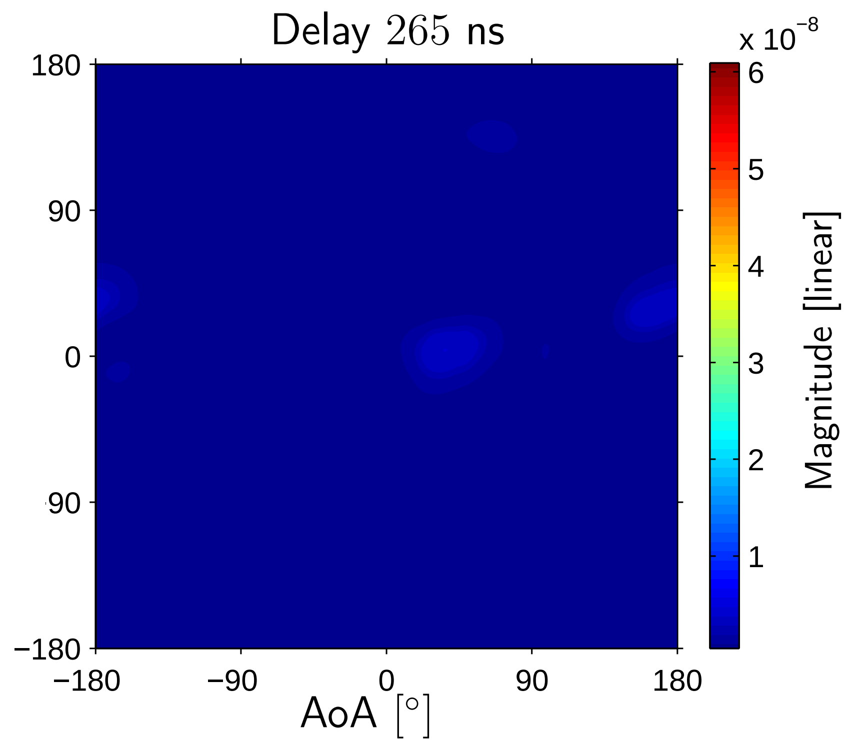

Dispersion of Individual Path Components

Bartlett spectra with respect to azimuth of departure (AoD) and azimuth of arrival (AoA) computed at a specific delay from measurement data

- 5.25 GHz carrier frequency and 200 MHz bandwidth
- The Rx and Tx are equipped with similar 9-element circular arrays.

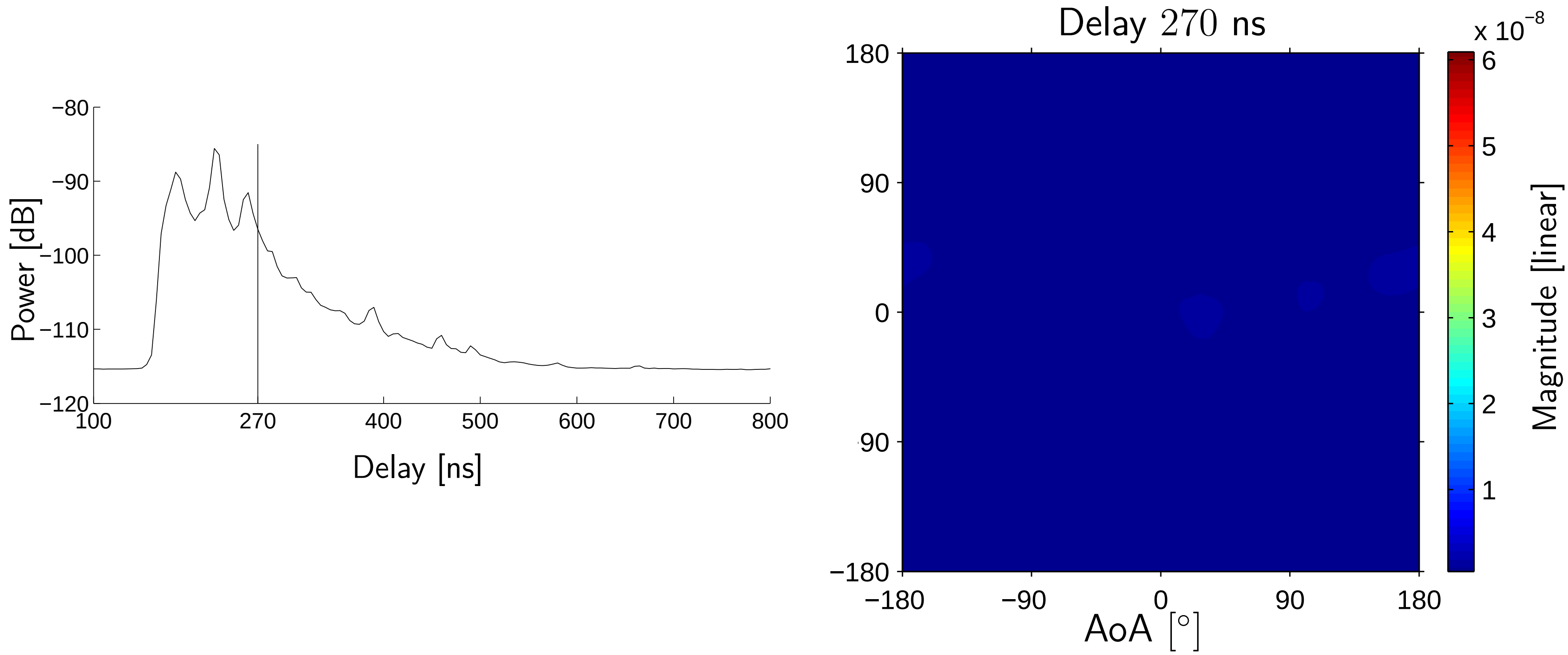

Conventional Methods for Estimation of Dispersion of Individual Path Components

- Beamformers, such as Bartlett and Capon beamformers.
- Dispersion estimates computed from "clustering" specular path estimates.

Numerical example: Pdf of the maximum-likelihood estimate of the azimuth of arrival of a specular path:

Simulation setting:

- A single dispersed path component scenario
- Azimuth power spectrum: uniform within $[-3^\circ, +3^\circ]$
- SNR$=40$ dB

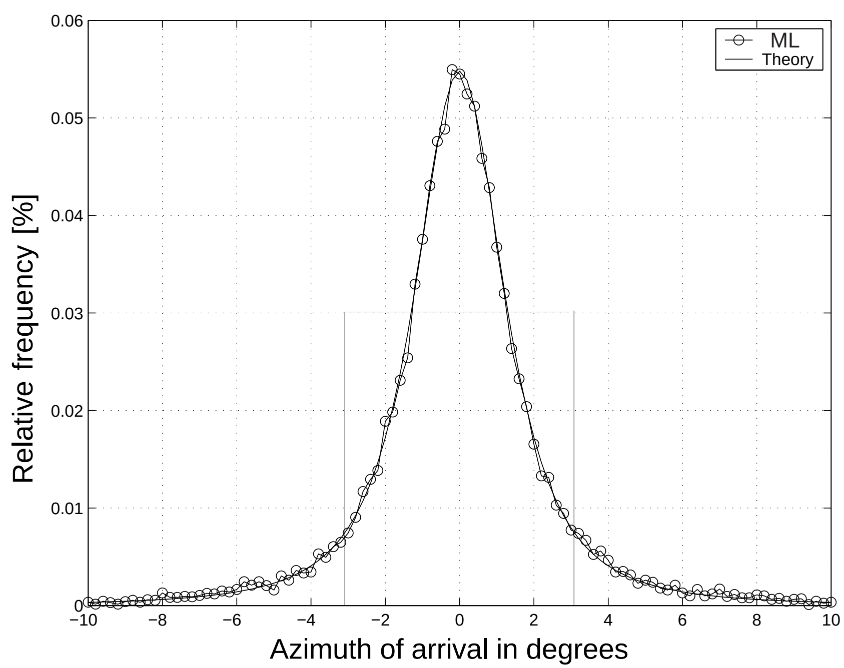

Contents

Dispersion Characterization

Distribution models are applied to characterize dispersion of individual path components in

- AoA only
  - Uniform distribution in a confined range [Besson & Stoica, 1999]
  - Truncated Gaussian distribution [Trump & Ottersten, 1996]
  - Von-Mises distribution [Riberio, *et al.* 2005a]
- Multiple dispersion dimensions
  - Von-Mises and Exp. distribution (azimuth-delay) [Ribeiro, *et al.* 2005b]
  - Von-Mises-Fisher distribution (biazimuth) [Yin, Fleury & Pedersen, *et al.* 2006a]
  - Extended von-Mises-Fisher distribution (biazimuth-delay) [—, 2006b]
  - Fisher-Bingham-5 distribution (elevation-azimuth) [—, 2007a] [—, 2007b]

Dispersion in Direction (Azimuth-Elevation)

A direction is defined by a unit vector $\boldsymbol{\Omega}$ with end point on a sphere $\mathbb{S}_2$

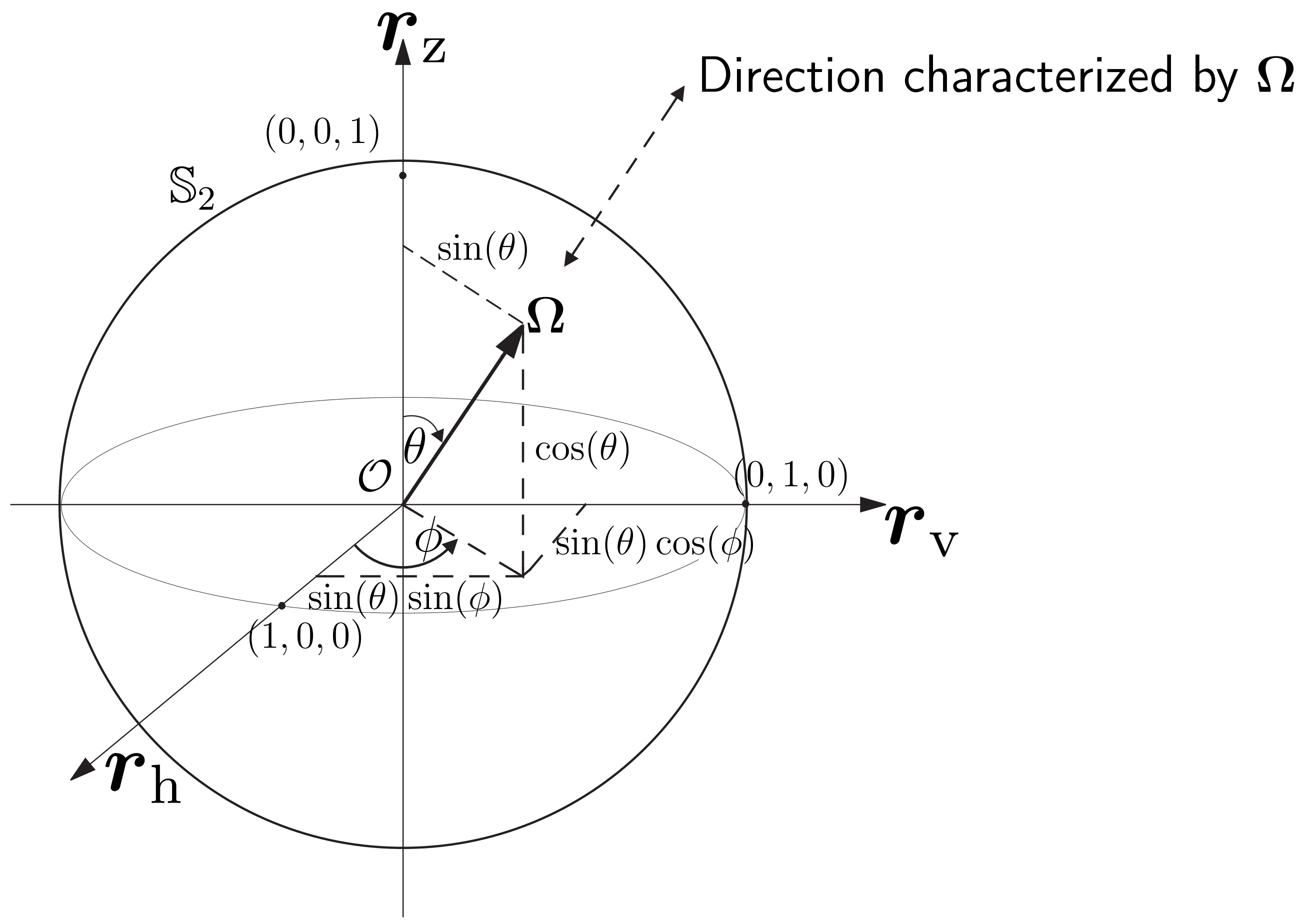

$$\boldsymbol{\Omega} = [\sin(\theta)\cos(\phi),\ \ \sin(\theta)\sin(\phi),\ \ \cos(\theta)]^{\mathrm{T}}$$

with ϕ and θ representing the azimuth and elevation of $\boldsymbol{\Omega}$ respectively.

Dispersion in Direction (Azimuth-Elevation)

The entropy-maximizing density function with specified

- first moment $\mu_{\mathbf{\Omega}} = \int \mathbf{\Omega} f(\mathbf{\Omega})\mathrm{d}\mathbf{\Omega}$
- second moment matrix $\int \mathbf{\Omega}\mathbf{\Omega}^{\mathrm{T}} f(\mathbf{\Omega})\mathrm{d}\mathbf{\Omega}$

is the Fisher-Bingham 5 density function [Kent 1982]:

$$f(\mathbf{\Omega}) = c(\kappa, \beta) \cdot \exp\left\{\kappa \boldsymbol{\gamma}_1^{\mathrm{T}} \mathbf{\Omega} + \beta[(\boldsymbol{\gamma}_2^{\mathrm{T}} \mathbf{\Omega})^2 - (\boldsymbol{\gamma}_3^{\mathrm{T}} \mathbf{\Omega})^2]\right\},$$

where

- κ: concentration parameter
- β: ovalness parameter
- $\boldsymbol{\gamma}_1, \boldsymbol{\gamma}_2, \boldsymbol{\gamma}_3$: orthonormal vectors determined by angles $\bar{\phi}, \bar{\theta}, \alpha$.

Dispersion in Direction (Azimuth-Elevation)

Plots of $f(\mathbf{\Omega})$:

$$(\bar{\phi}, \bar{\theta}, \alpha, \kappa, \beta) = (0°, 45°, 160°, 5, 1.5)$$

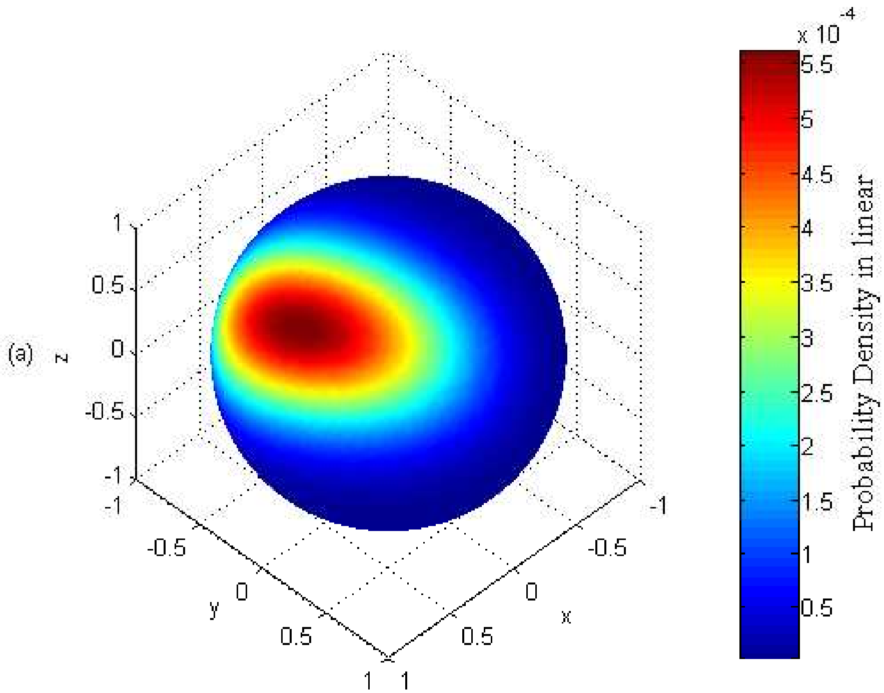

$$(\bar{\phi}, \bar{\theta}, \alpha, \kappa, \beta) = (45°, 70°, 35°, 200, 100)$$

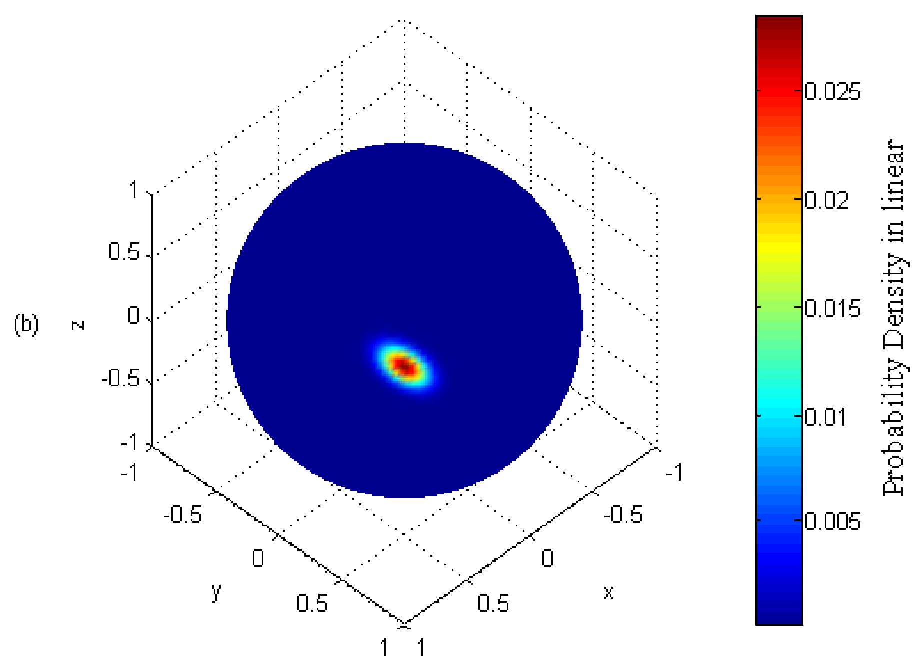

Dispersion in Biazimuth (AoA-AoD)

For horizontal-only propagation with azimuth of departure (AoD) ϕ_1 and azimuth of arrival (AoA) ϕ_2 we define

$$\boldsymbol{\Omega}_1 = [\cos(\phi_1) \quad \sin(\phi_1)]^{\mathrm{T}}, \quad \text{and} \quad \boldsymbol{\Omega}_2 = [\cos(\phi_2) \quad \sin(\phi_2)]^{\mathrm{T}}.$$

The entropy-maximizing density function $f(\boldsymbol{\Omega}_1, \boldsymbol{\Omega}_2)$ with specified

- first moments $\boldsymbol{\mu}_{\boldsymbol{\Omega}_1}$, $\boldsymbol{\mu}_{\boldsymbol{\Omega}_2}$
- second moment matrix $\iint \boldsymbol{\Omega}_1 \boldsymbol{\Omega}_2^{\mathrm{T}} f(\boldsymbol{\Omega}_1, \boldsymbol{\Omega}_2) \mathrm{d}\boldsymbol{\Omega}_1 \mathrm{d}\boldsymbol{\Omega}_2$

is the density function of the von-Mises-Fisher distribution [Mardia, 1975]

$$f(\boldsymbol{\Omega}_1, \boldsymbol{\Omega}_2) = C \cdot \exp\{\boldsymbol{a}_1^{\mathrm{T}} \boldsymbol{\Omega}_1 + \boldsymbol{a}_2^{\mathrm{T}} \boldsymbol{\Omega}_2 + \boldsymbol{\Omega}_1^{\mathrm{T}} \boldsymbol{A} \boldsymbol{\Omega}_2\},$$

where

- C : normalization constant
- $\boldsymbol{a}_1$, $\boldsymbol{a}_2$ and $\boldsymbol{A}$: free parameters.

Dispersion in Biazimuth (AoA-AoD)

The biazimuth density function $f(\phi_1, \phi_2)$ induced by $f(\mathbf{\Omega}_1, \mathbf{\Omega}_2)$ via the mapping $(\phi_1, \phi_2) \mapsto (\mathbf{\Omega}_1, \mathbf{\Omega}_2)$ reads

$$\begin{aligned} f(\phi_1, \phi_2) &= c(\kappa_1, \kappa_2, \rho) \cdot \exp\Big\{ \Big(\frac{\kappa_1 - \rho\sqrt{\kappa_1 \kappa_2}}{1-\rho^2} \Big) \cos(\phi_1 - \bar{\phi}_1) \\ &\quad + \Big(\frac{\kappa_2 - \rho\sqrt{\kappa_1 \kappa_2}}{1-\rho^2} \Big) \cos(\phi_2 - \bar{\phi}_2) + \frac{\rho\sqrt{\kappa_1 \kappa_2}}{1-\rho^2} \cos[(\phi_1 - \bar{\phi}_1) - (\phi_2 - \bar{\phi}_2)] \Big\}. \end{aligned}$$

Contour plots of $f(\phi_1, \phi_2)$:

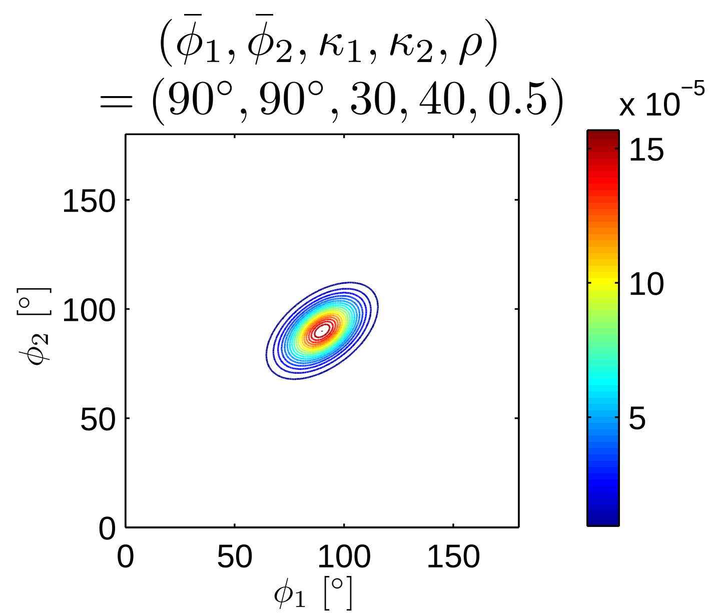

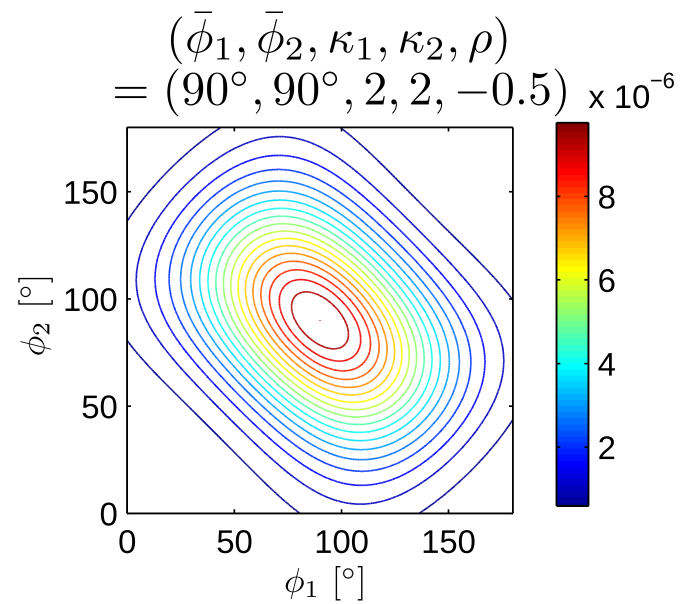

Dispersion in Biazimuth and Delay

Let τ be the delay variable and define

$$\boldsymbol{\psi} = [\boldsymbol{\Omega}_1^{\mathrm{T}}, \boldsymbol{\Omega}_2^{\mathrm{T}}, \tau]^{\mathrm{T}}$$

The entropy-maximizing density function $f(\boldsymbol{\psi})$ with specified

- first moment vector $\boldsymbol{\mu}_{\boldsymbol{\psi}}$
- second moment matrix $\int \boldsymbol{\psi}\boldsymbol{\psi}^{\mathrm{T}} f(\boldsymbol{\psi})\mathrm{d}\boldsymbol{\psi}$

reads [Mardia, 1975]

$$f(\boldsymbol{\psi}) = C \cdot \exp\{\boldsymbol{b}^{\mathrm{T}}\boldsymbol{\psi} + \boldsymbol{\psi}^{\mathrm{T}}\boldsymbol{B}\boldsymbol{\psi}\},$$

where

- C : normalization constant
- $\boldsymbol{b} \in \mathbb{R}^{5\times 1}$ and $\boldsymbol{B} \in \mathbb{R}^{5\times 5}$: free parameters.

Dispersion in Biazimuth and Delay

The biazimuth-delay density function $f(\phi_1, \phi_2, \tau)$ induced by $f(\boldsymbol{\psi})$ via the mapping $(\phi_1, \phi_2, \tau) \mapsto (\boldsymbol{\Omega}_1, \boldsymbol{\Omega}_2, \tau)$ reads

$$\begin{aligned} f(\phi_1, \phi_2, \tau; \boldsymbol{\theta}) = C' \cdot \exp\Big\{ & c_1 \cos(\phi_1 - \bar{\phi}_1) + c_2 \cos(\phi_2 - \bar{\phi}_2) \\ & + (\tau - \bar{\tau})[c_3 \sin(\phi_1 - \bar{\phi}_1) + c_4 \sin(\phi_2 - \bar{\phi}_2)] \\ & + c_5 (\tau - \bar{\tau})^2 + c_6 \cos[(\phi_1 - \bar{\phi}_1) - (\phi_2 - \bar{\phi}_2)] \Big\} \end{aligned}$$

with

- $\boldsymbol{\theta}$: parameter vector $\boldsymbol{\theta} = [\underbrace{\bar{\phi}_1, \bar{\phi}_2, \bar{\tau}}_{\text{center of gravity}}, \underbrace{\kappa_1, \kappa_2, \sigma_\tau}_{\text{spreads}}, \underbrace{\rho_{12}, \rho_1, \rho_2}_{\text{dependencies}}]$
- C' : normalization constant
- $c_1, \ldots, c_6$: functions of $\kappa_1, \kappa_2, \sigma_\tau, \rho_{12}, \rho_1, \rho_2$.

Dispersion in Biazimuth and Delay

3 dB-spread surface $\left\{(\phi_1, \phi_2, \tau) : f(\phi_1, \phi_2, \tau) = \frac{1}{2} f(\bar{\phi}_1, \bar{\phi}_2, \bar{\tau})\right\}$:

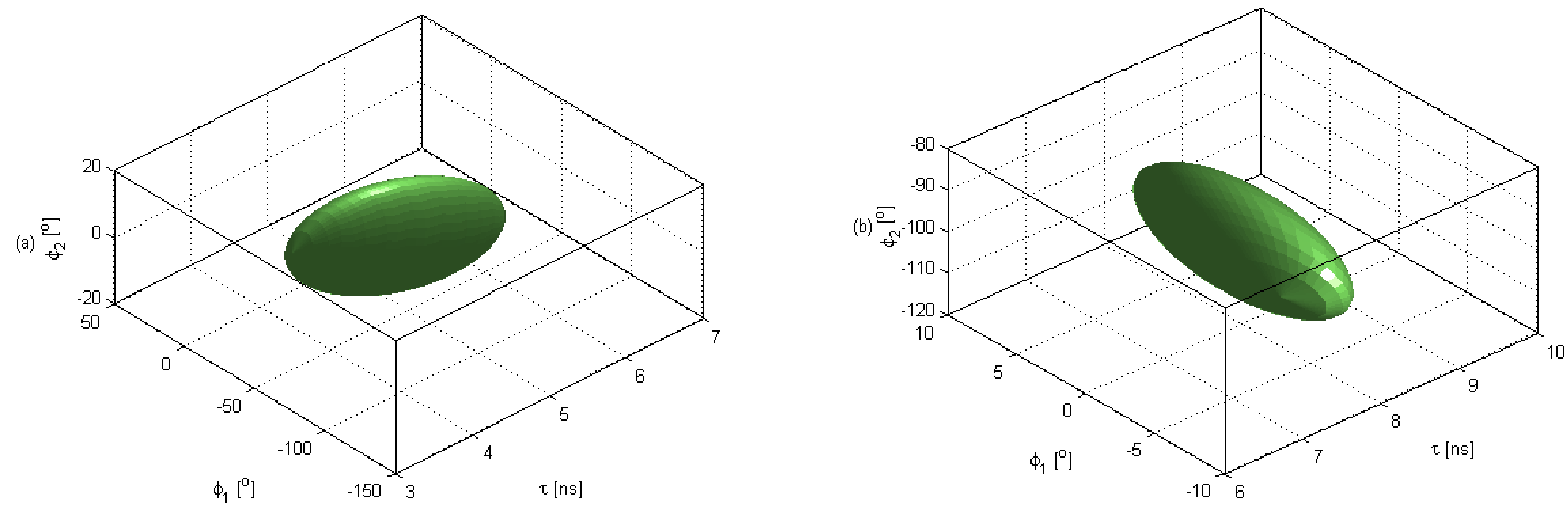

	$\bar{\tau}$ [ns]	$\bar{\phi}_1$ [°]	$\bar{\phi}_2$ [°]	σ_τ [ns]	κ_1	σ_{ϕ_1} [°]	κ_2	σ_{ϕ_2} [°]	ρ_{12}	ρ_1	ρ_2
(a)	5	-40	0	1	5	25.6	10	18.1	-0.4	-0.3	-0.3
(b)	8	0	-100	0.5	50	8.1	30	10.5	-0.5	0.6	-0.2

Contents

Signal Model for MIMO Channel Sounding

In the scenario where dispersion of the propagation channel in AoA, AoD and Delay is considered,

$$\boldsymbol{Y}(t) = \int_{-\pi}^{+\pi}\int_{-\pi}^{+\pi}\int_{-\infty}^{+\infty} \boldsymbol{c}_2(\phi_2)\boldsymbol{c}_1(\phi_1)^{\mathrm{T}}\boldsymbol{s}(t-\tau)h(t;\phi_1,\phi_2,\tau)\mathrm{d}\phi_1\mathrm{d}\phi_2\mathrm{d}\tau + \boldsymbol{W}(t),$$

where

- $\boldsymbol{Y}(t) \in \mathbb{C}^{M_2}$: output signals of the Rx array
- $\boldsymbol{c}_i(\phi) \in \mathbb{C}^{M_i}$, $i = 1, 2$: antenna array responses
- $\boldsymbol{s}(t) \in \mathbb{C}^{M_1}$: complex envelope of the transmitted signal
- $h(t;\phi_1,\phi_2,\tau) \in \mathbb{C}$: (time-variant) biazimuth-delay spread function of the propagation channel
- $\boldsymbol{W}(t) \in \mathbb{C}^{M_2}$: complex temporally and spatially white Gaussian noise.

Signal Model for MIMO Channel Sounding

Scenario with D path components:

$$h(t;\phi_1,\phi_2,\tau)=\sum_{d=1}^{D}h_d(t;\phi_1,\phi_2,\tau).$$

Under the uncorrelated scattering assumption, the biazimuth-delay power spectrum is of the form

$$\begin{aligned}P(\phi_1,\phi_2,\tau)&=\mathrm{E}\left[|h(t;\phi_1,\phi_2,\tau)|^2\right]\\&=\sum_{d=1}^{D}P_d(\phi_1,\phi_2,\tau).\end{aligned}$$

Signal Model for MIMO Channel Sounding

Power spectrum $P_d(\phi_1, \phi_2, \tau)$ of the dth path component:

$$\begin{aligned} P_d(\phi_1, \phi_2, \tau) &= \mathrm{E}\left[|h_d(t; \phi_1, \phi_2, \tau)|^2 \right] \\ &= P_d \cdot f_d(\phi_1, \phi_2, \tau), \end{aligned}$$

with average power

$$P_d = \int_{-\pi}^{+\pi} \int_{-\pi}^{+\pi} \int_{-\infty}^{+\infty} P_d(\phi_1, \phi_2, \tau) \mathrm{d}\phi_1 \mathrm{d}\phi_2 \mathrm{d}\tau$$

and

$$f_d(\phi_1, \phi_2, \tau) = \frac{1}{P_d} \cdot P_d(\phi_1, \phi_2, \tau).$$

Signal Model for MIMO Channel Sounding

We assume that

$$f_d(\phi_1, \phi_2, \tau) = f(\phi_1, \phi_2, \tau; \boldsymbol{\theta}_d),$$

where $f(\phi_1, \phi_2, \tau; \boldsymbol{\theta}_d)$ is the derived biazimuth-delay density function with the parameter vector

$$\boldsymbol{\theta}_d = [\bar{\phi}_{1,d}, \bar{\phi}_{2,d}, \bar{\tau}_d, \kappa_{1,d}, \kappa_{2,d}, \sigma_{\tau_d}, \rho_{1,d}, \rho_{2,d}, \rho_{12,d}].$$

Parameter vector for the D-path-component scenario:

$$\boldsymbol{\Theta} = [P_d, \boldsymbol{\theta}_d; d = 1, \ldots, D].$$

The SAGE algorithm can be applied to obtain an approximation of the maximum likelihood estimate $(\hat{\boldsymbol{\Theta}})_{\mathrm{ML}}$.

Contents

Direction-of-Departure Power Spectra

Measurement set-up:

- Channel sounder: Elektrobit channel sounder – Propsound
- Carrier frequency: 5.2 GHz
- Bandwidth: 200 MHz
- 50 measurement cycles (about 4 seconds)
- Tx array height: 1.53 m; Rx array height: 0.82 m
- Office environment

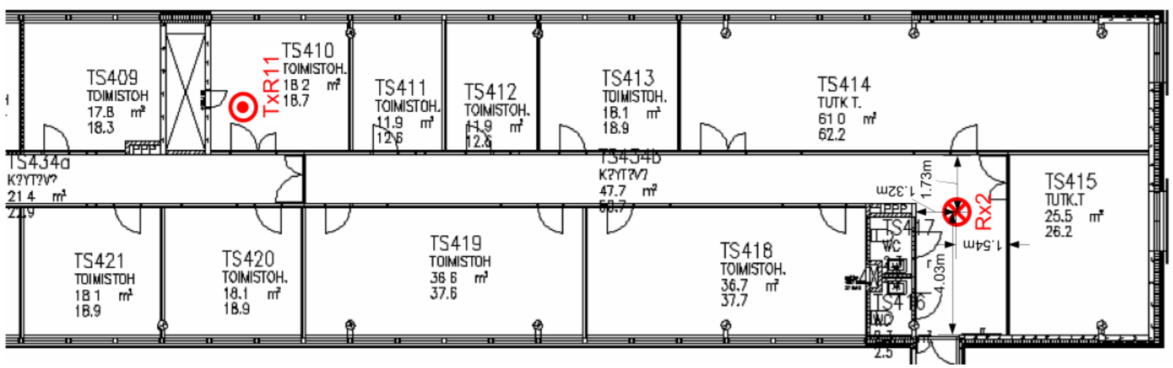

- People walking (time-variant scenario)

Direction-of-Departure Power Spectra

Measurement set-up:

- A single Rx antenna, 50-element Tx array:

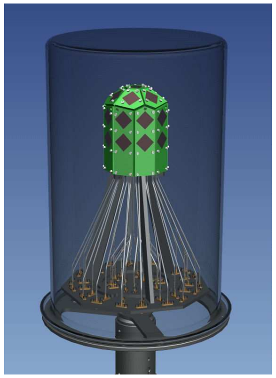

- Surroundings of the Tx (Left) and the Rx (Right)

Estimated Direction-of-Departure Power Spectra

Delay 115 ns

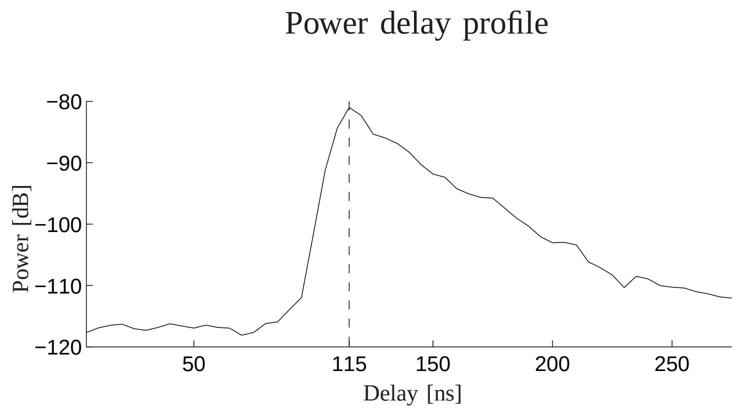

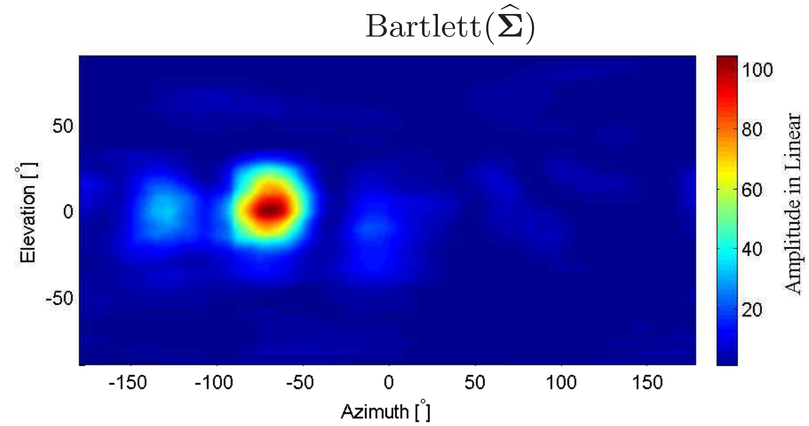

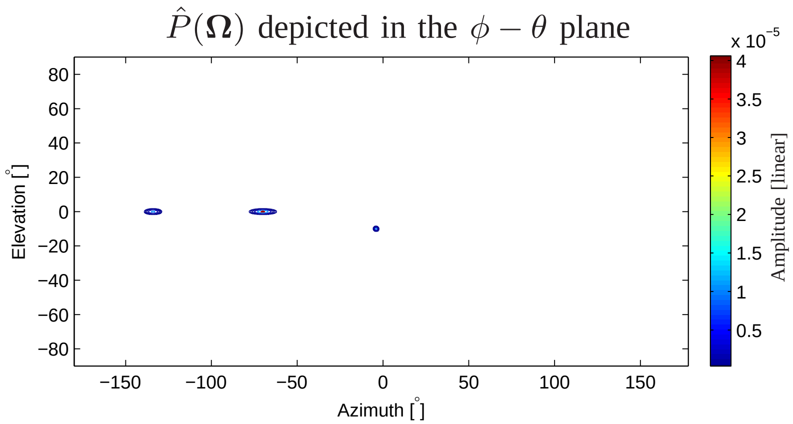

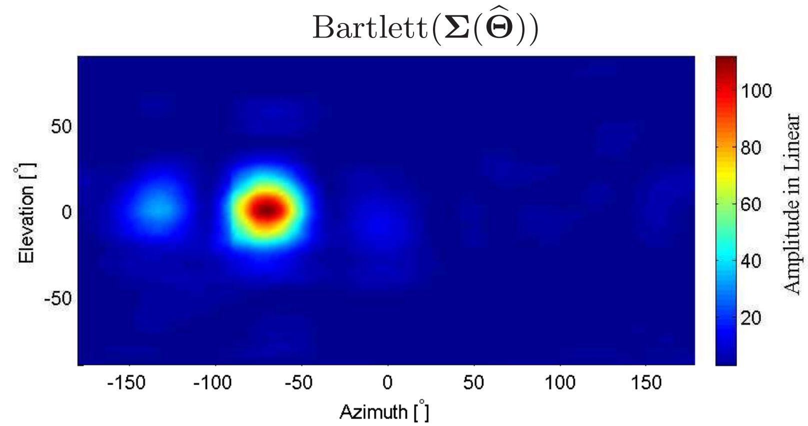

$\mathrm{Bartlett}(\cdot)$: Bartlett spectrum of the matrix given as an argument.
$\hat{P}(\cdot)$: Estimated power spectrum.

Estimated Direction-of-Departure Power Spectra

Delay 160 ns

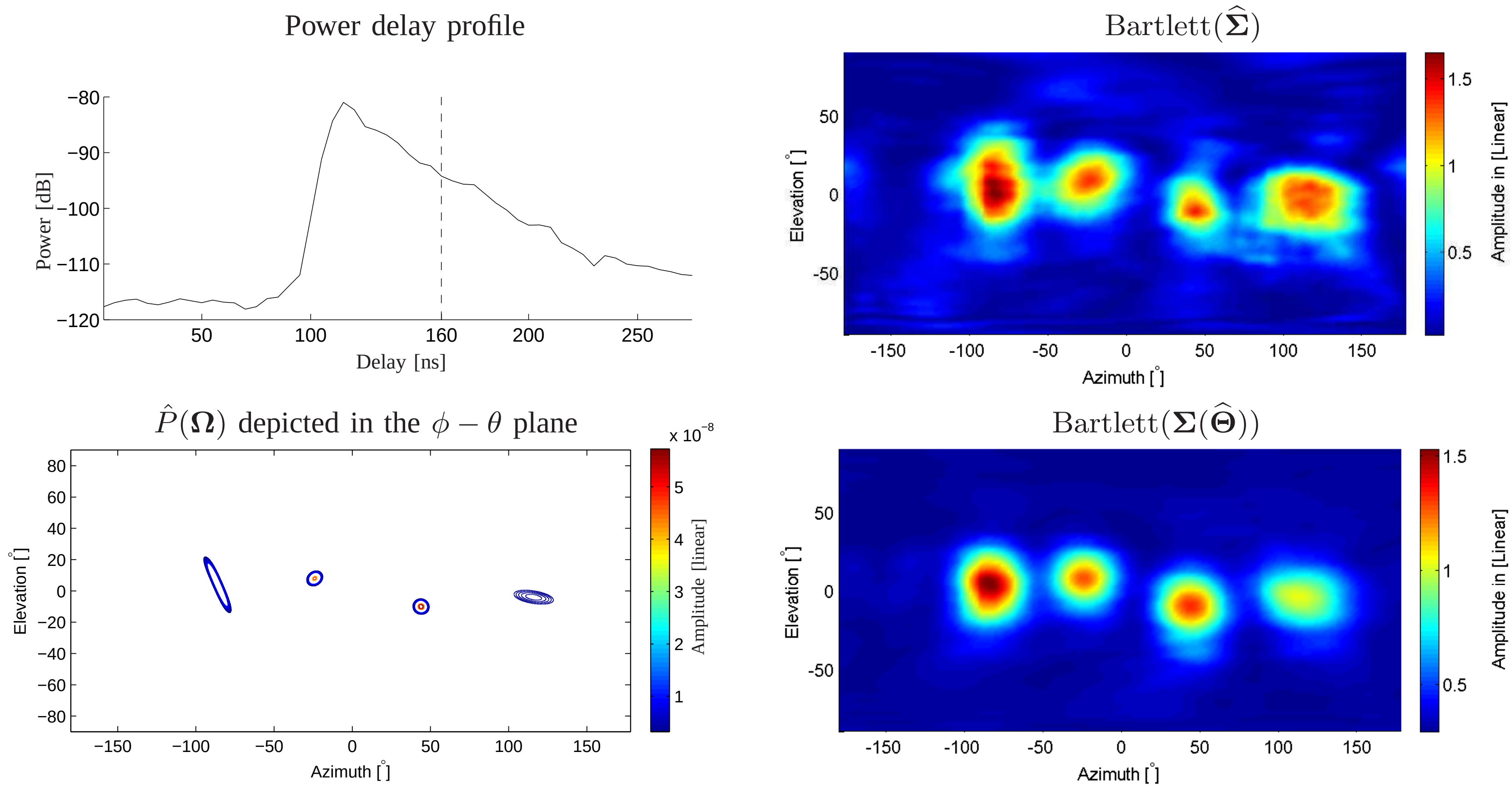

Bartlett$(\cdot)$: Bartlett spectrum of the matrix given as an argument.
$\hat{P}(\cdot)$: Estimated power spectrum.

Biazimuth Power Spectrum Estimation

Measurement set-up:

- Channel sounder: Elektrobit channel sounder – Propsound
- Carrier frequency: 5.2 GHz
- Bandwidth: 200 MHz
- 900 measurement cycles (60 s)
- Big hall and time-variant scenario

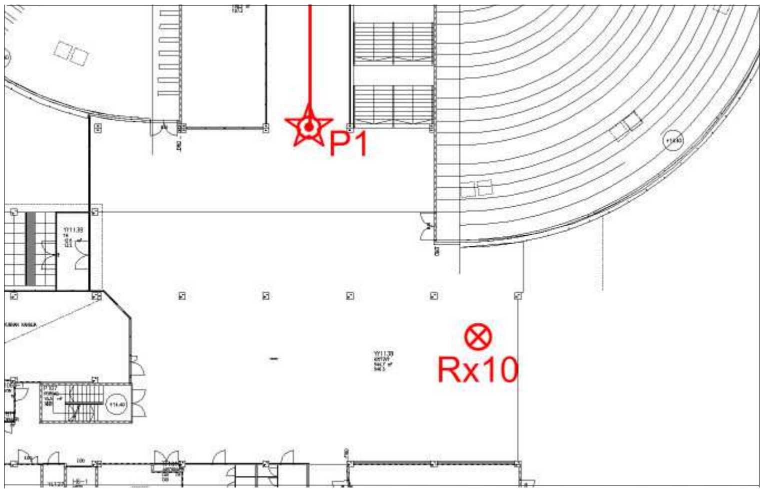

- Tx array height: 1.53 m; Rx array height: 0.82 m

Biazimuth Power Spectrum Estimation

Measurement set-up:

- 9-element circular Tx and Rx arrays:

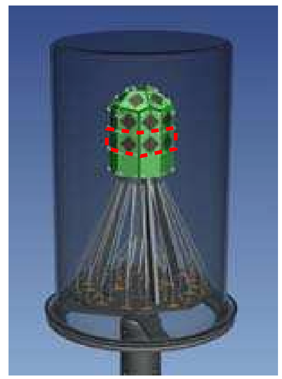

- Surroundings of the Tx (Left) and the Rx (Right)

Estimated Biazimuth Power Spectra

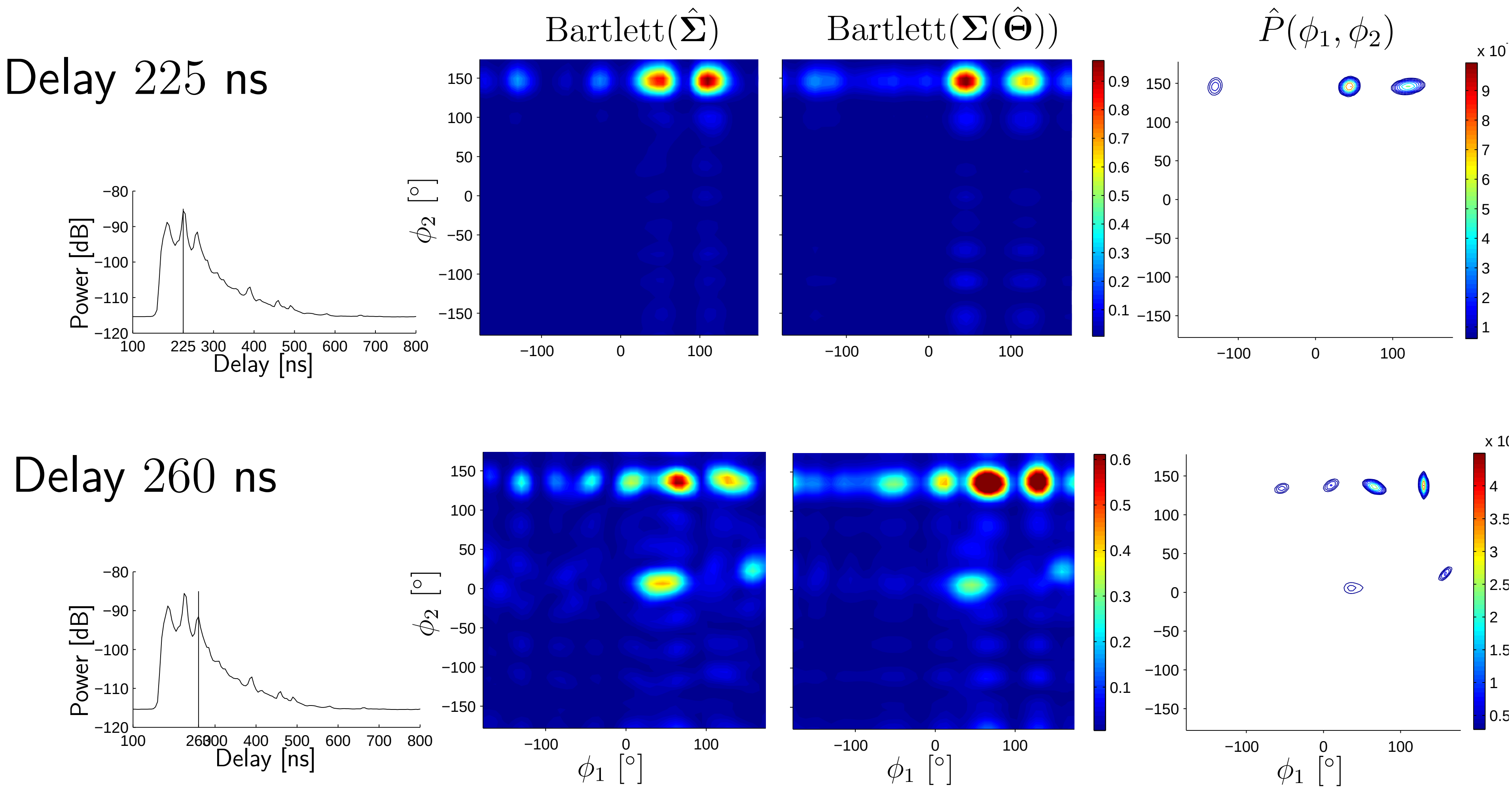

Estimated Biazimuth-Delay Power Spectrum

Estimated 3 dB-spread surfaces of individual path components:

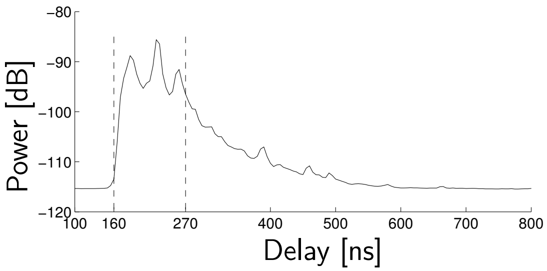

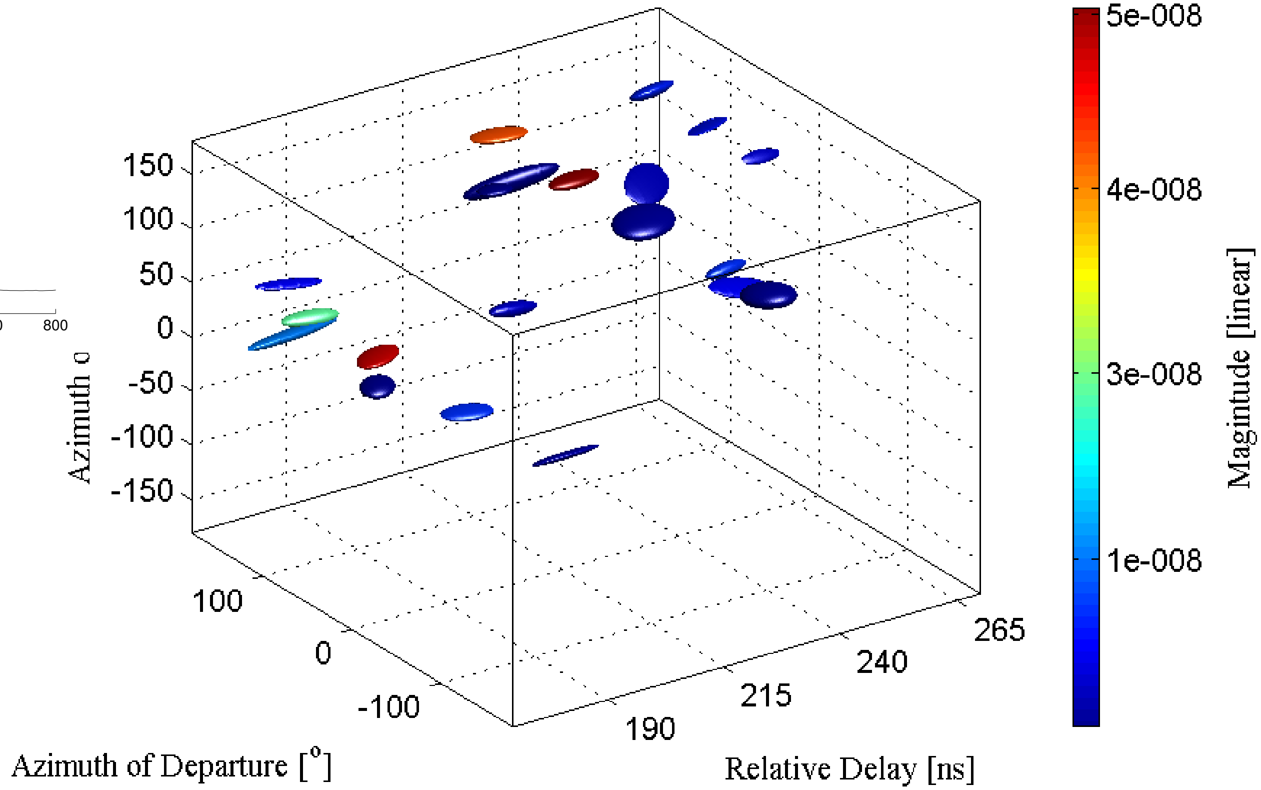

The power estimates $\hat{P}_d$ are coded using the color bar.

Estimated Biazimuth-Delay Power Spectrum

Dispersion dependence of individual path components across multiple dimensions:

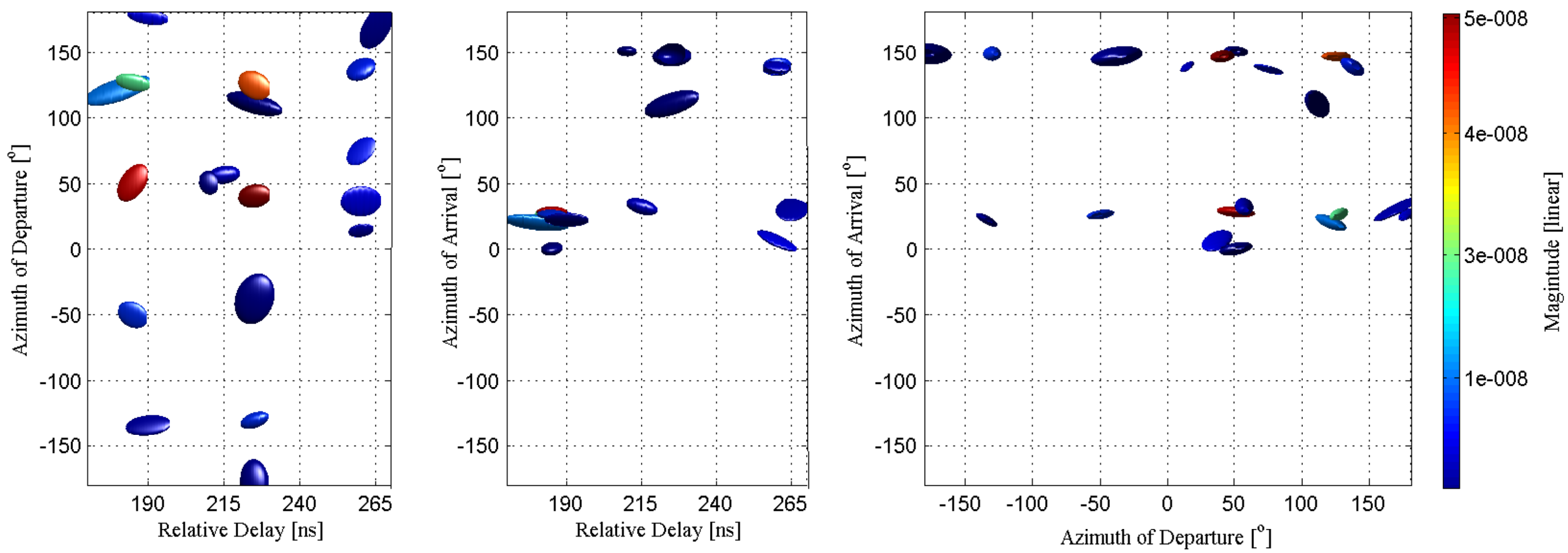

Estimated Biazimuth-Delay Power Spectrum (Movie-view)

Delay 175 ns

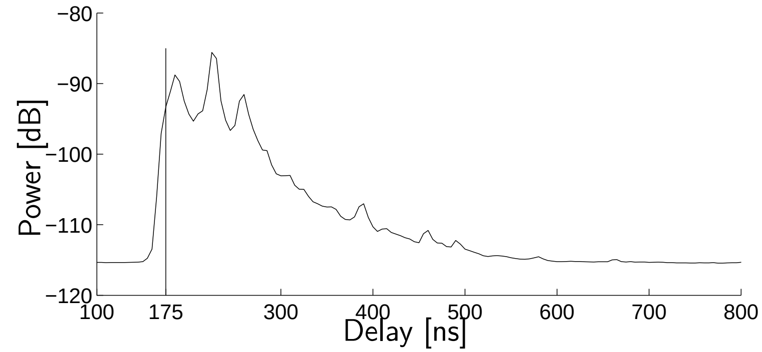

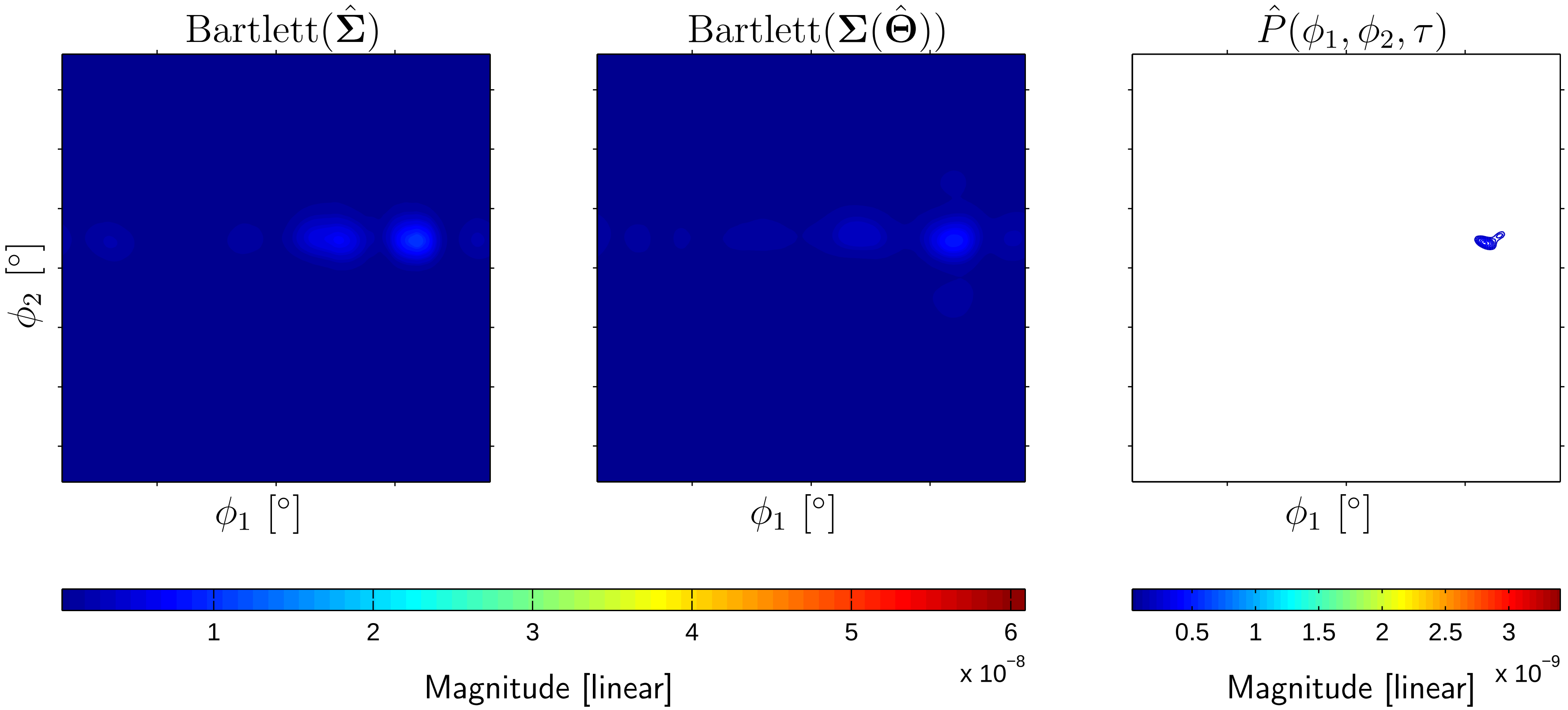

Estimated Biazimuth-Delay Power Spectrum (Movie-view)

Delay 180 ns

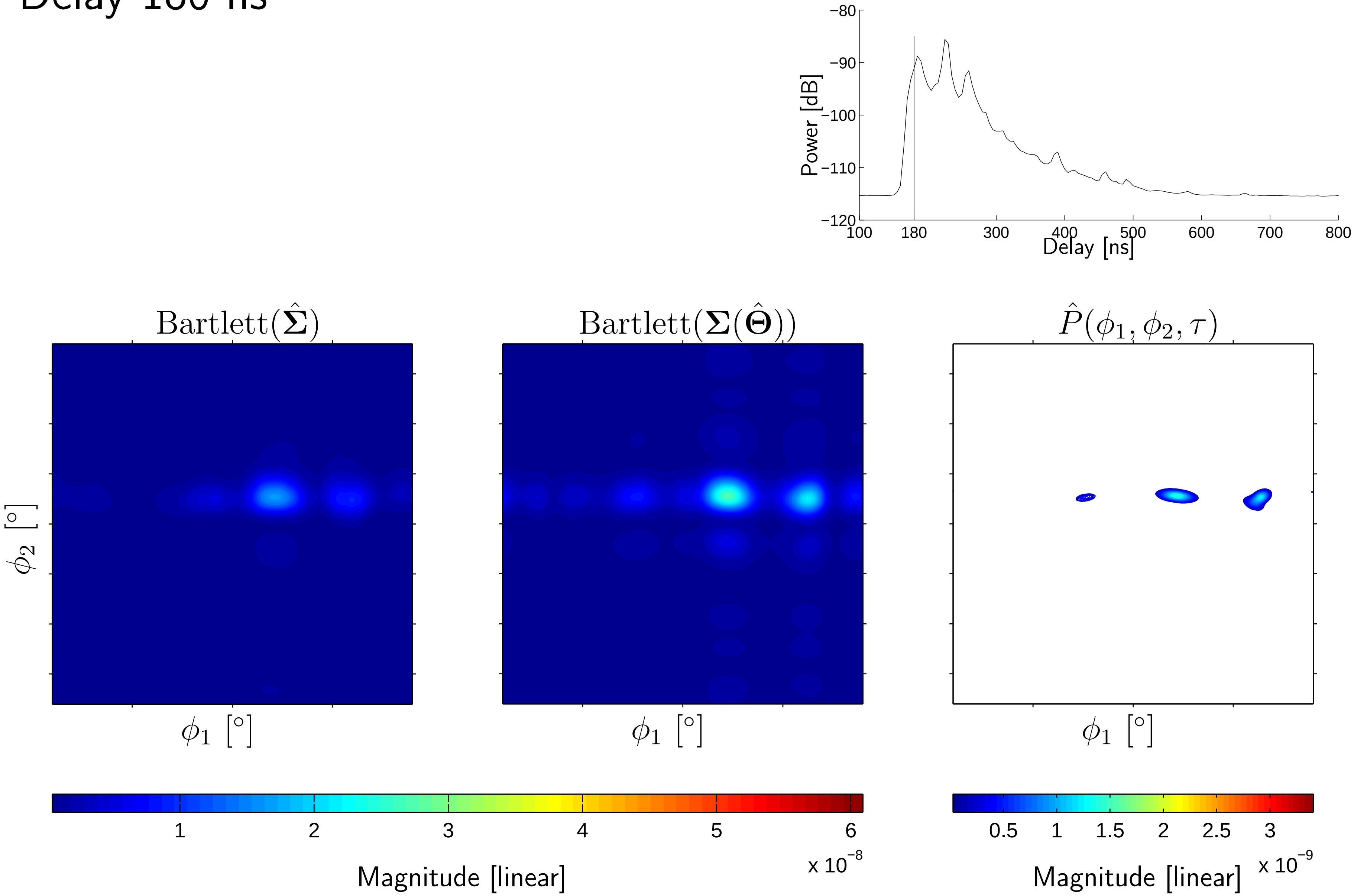

Estimated Biazimuth-Delay Power Spectrum (Movie-view)

Delay 185 ns

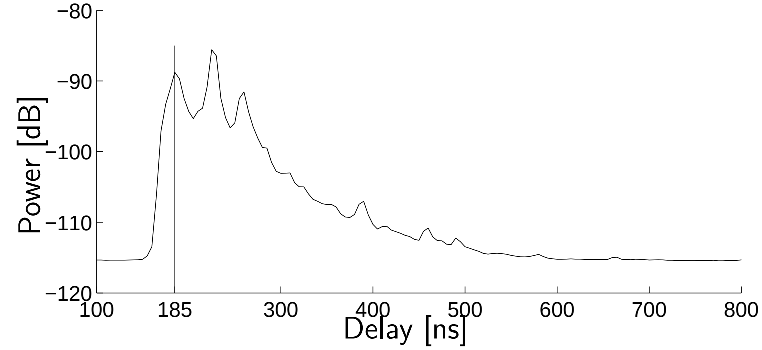

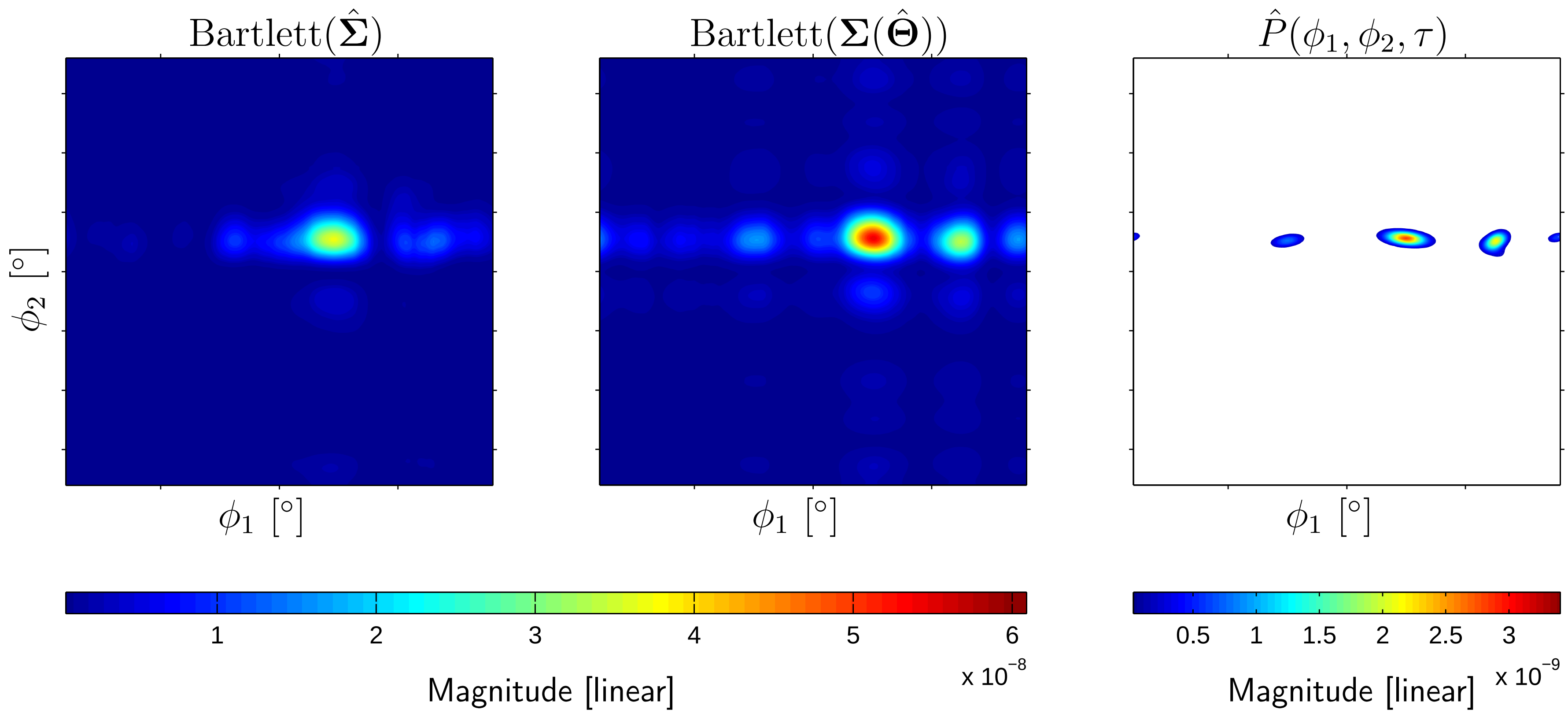

Estimated Biazimuth-Delay Power Spectrum (Movie-view)

Delay 190 ns

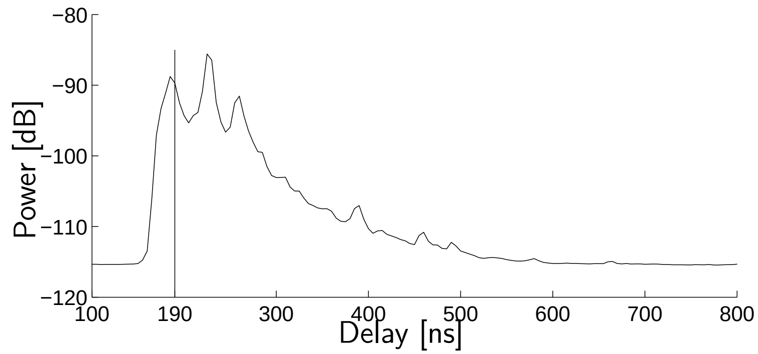

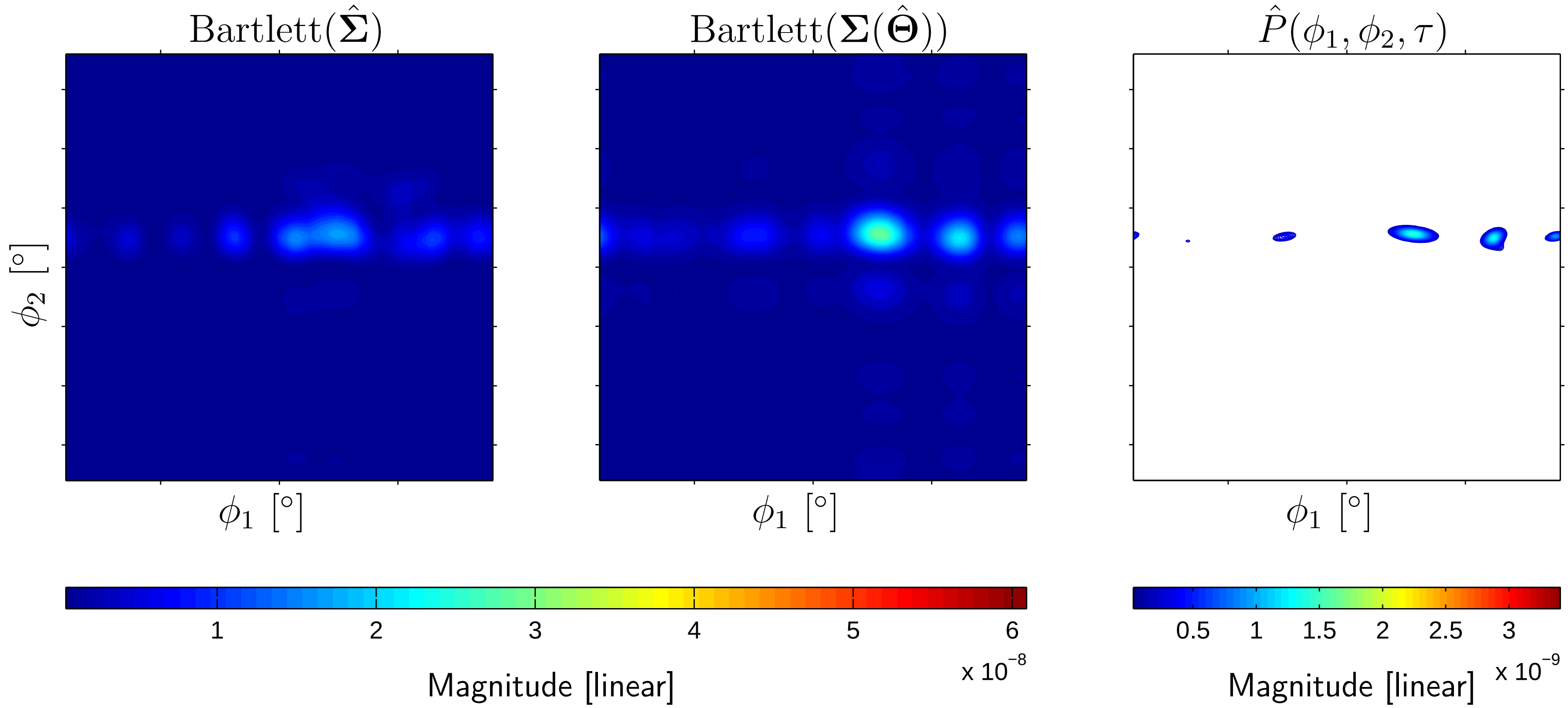

Estimated Biazimuth-Delay Power Spectrum (Movie-view)

Delay 195 ns

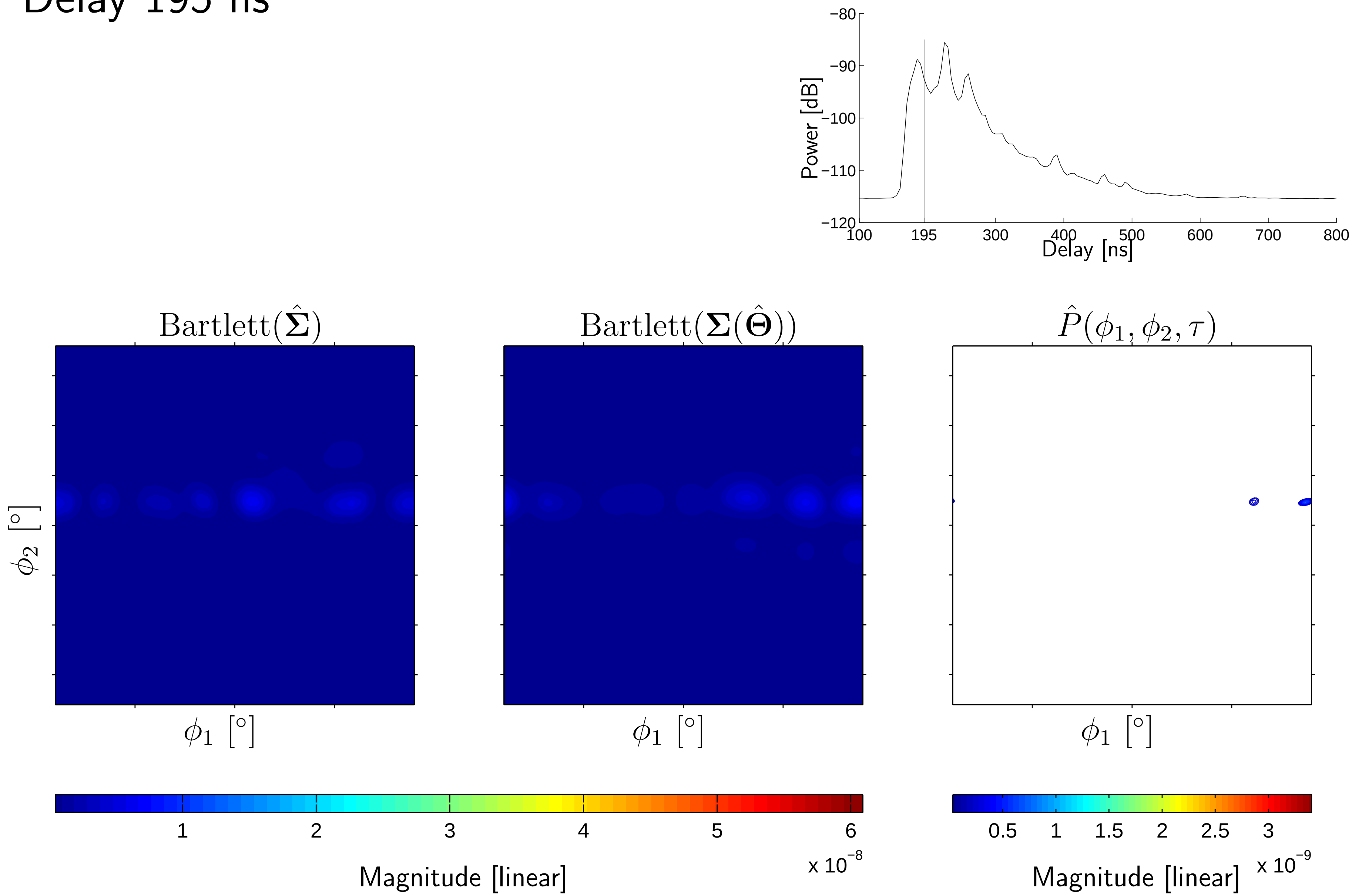

Estimated Biazimuth-Delay Power Spectrum (Movie-view)

Delay 200 ns

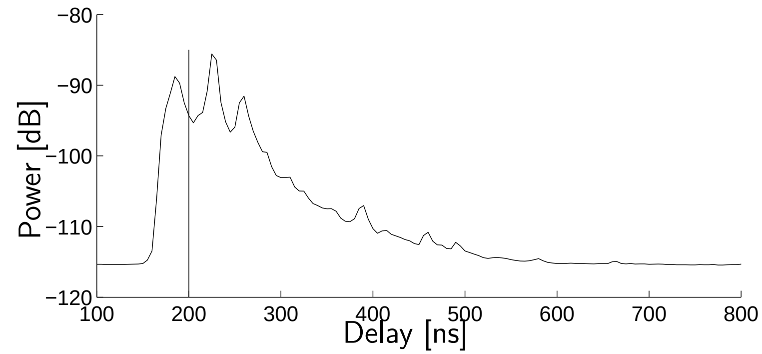

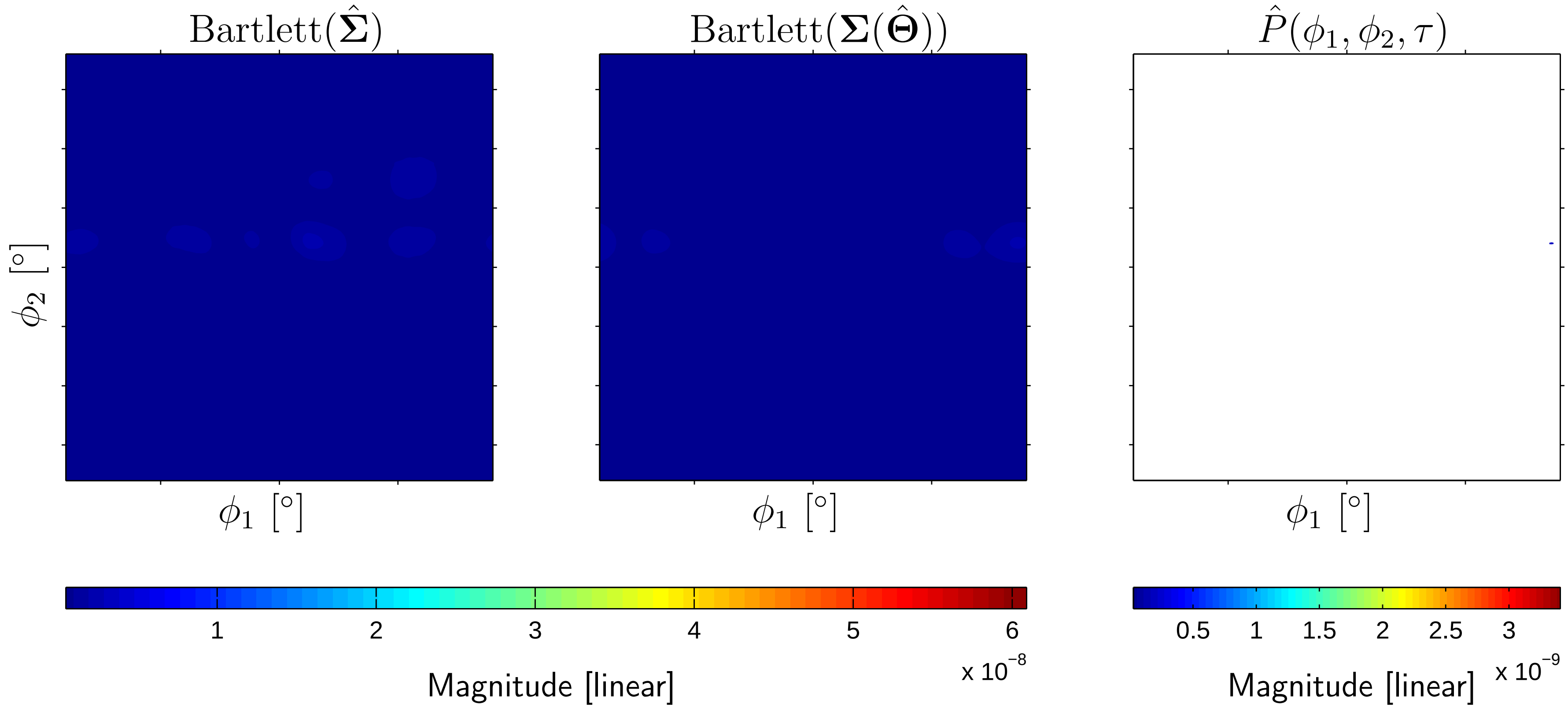

Estimated Biazimuth-Delay Power Spectrum (Movie-view)

Delay 205 ns

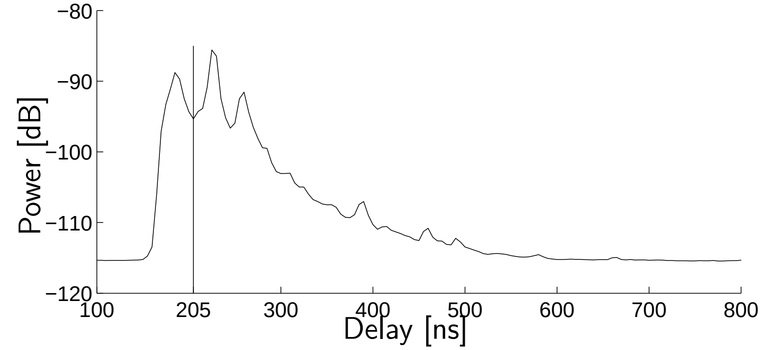

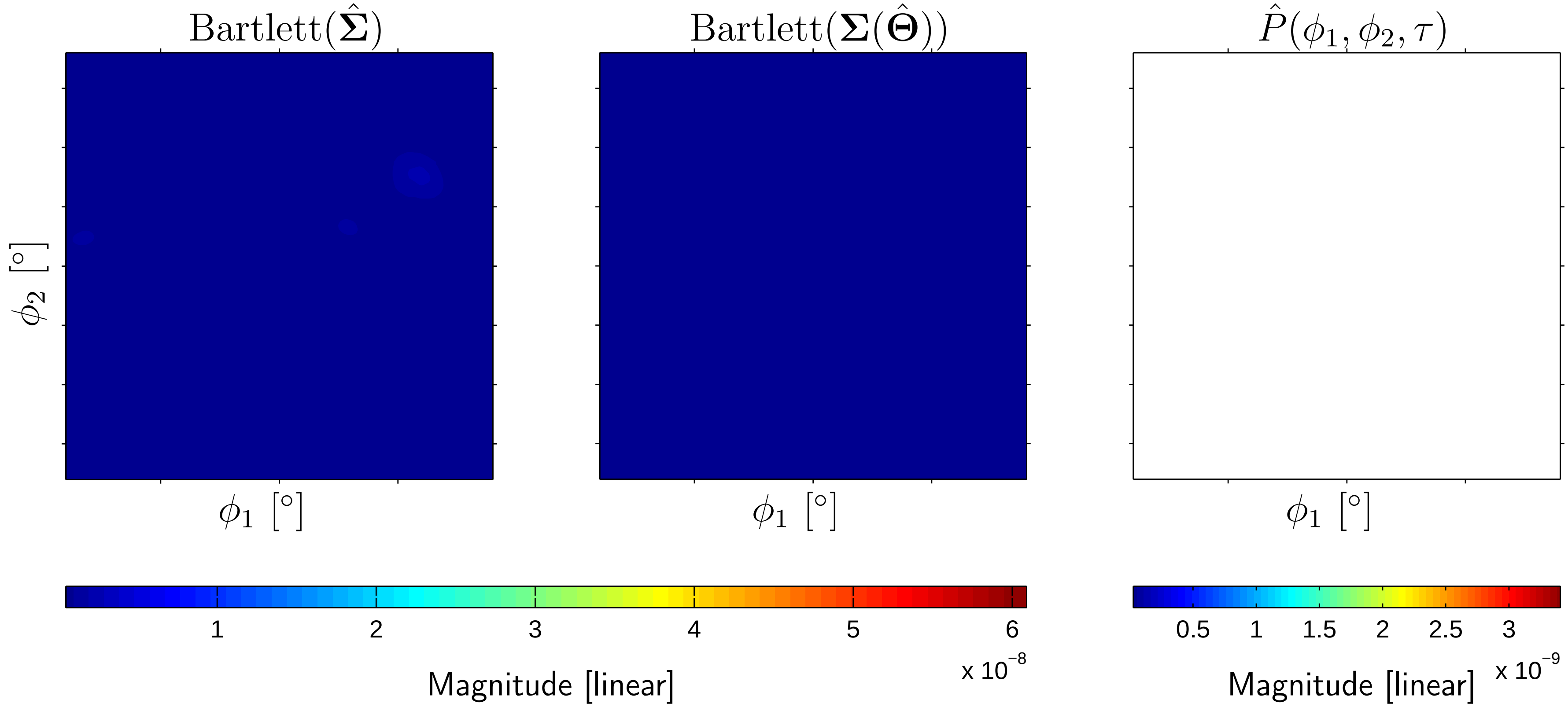

Estimated Biazimuth-Delay Power Spectrum (Movie-view)

Delay 210 ns

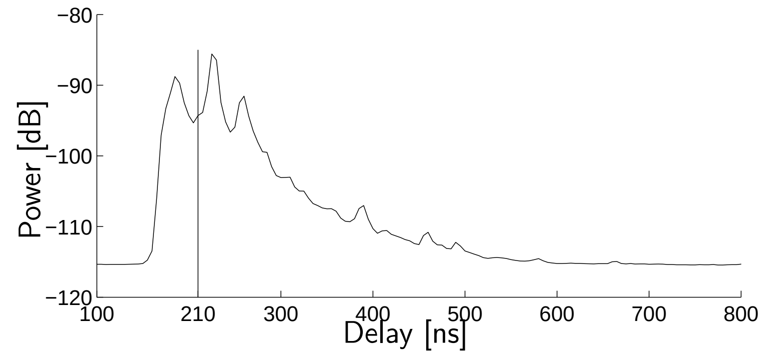

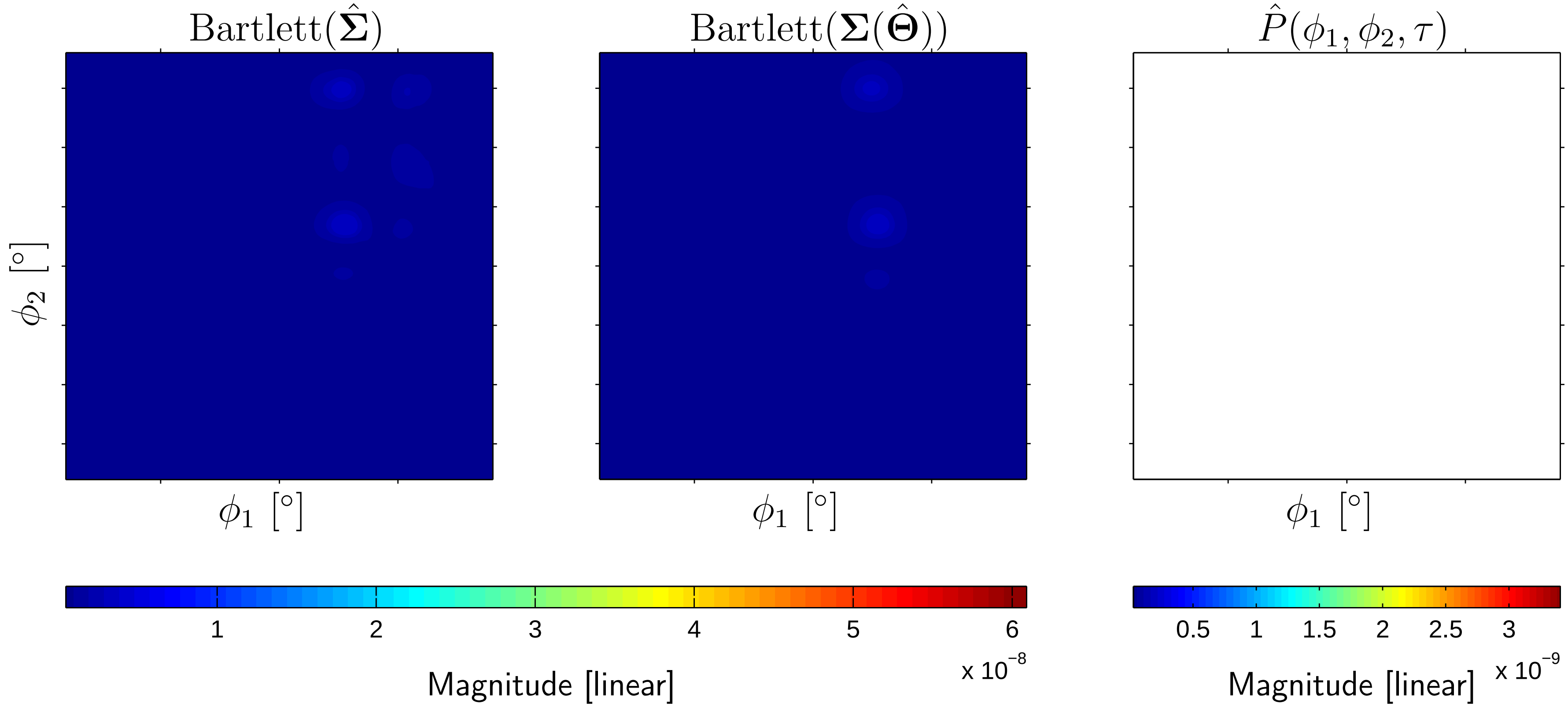

Estimated Biazimuth-Delay Power Spectrum (Movie-view)

Delay 215 ns

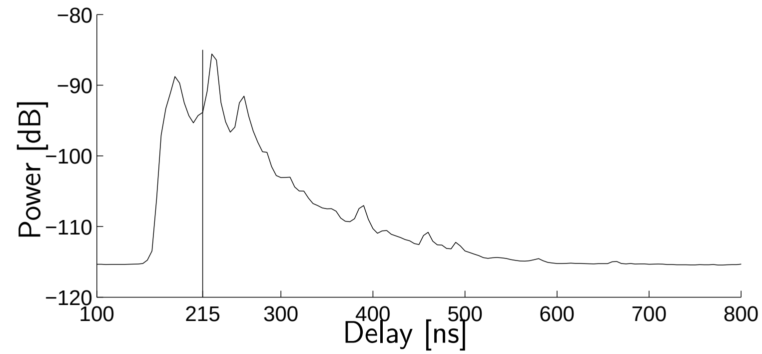

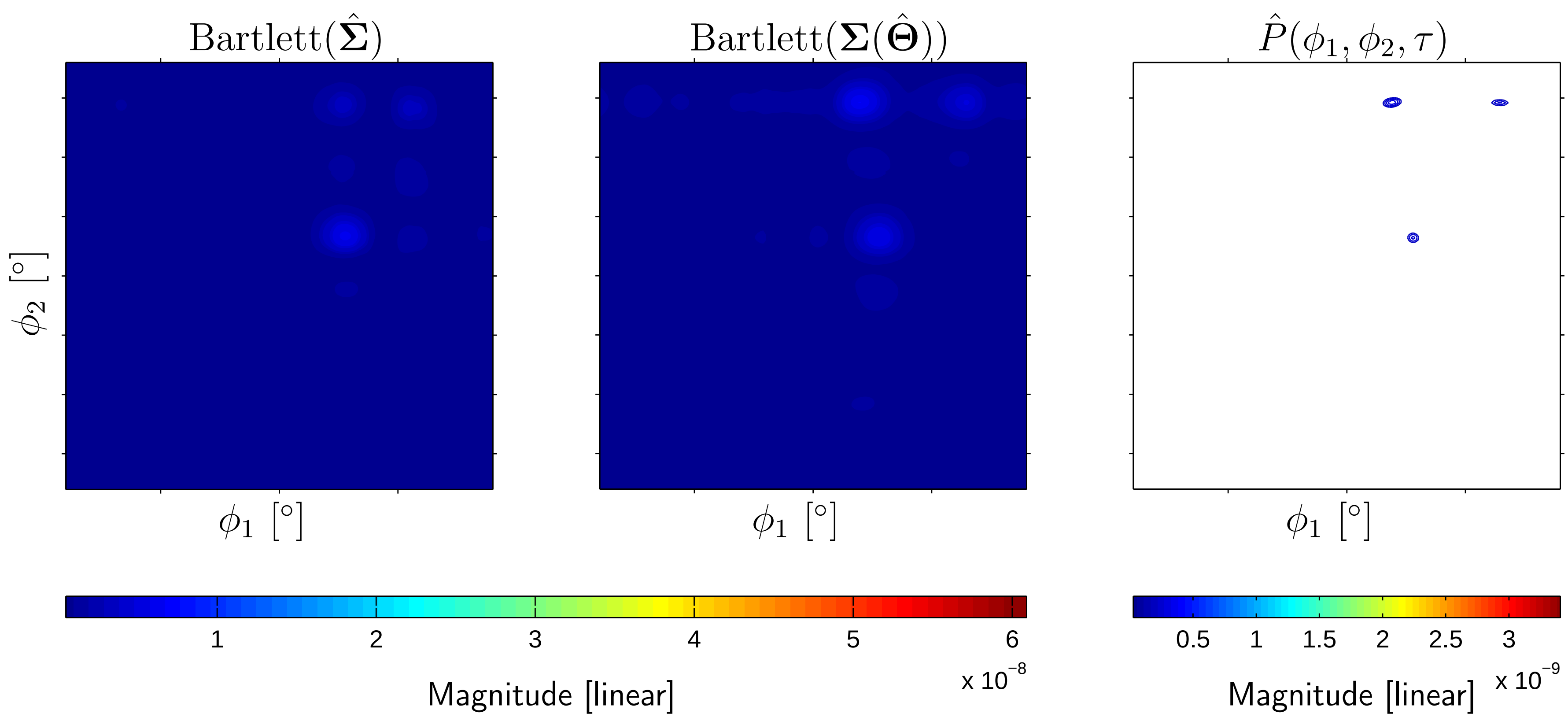

Estimated Biazimuth-Delay Power Spectrum (Movie-view)

Delay 220 ns

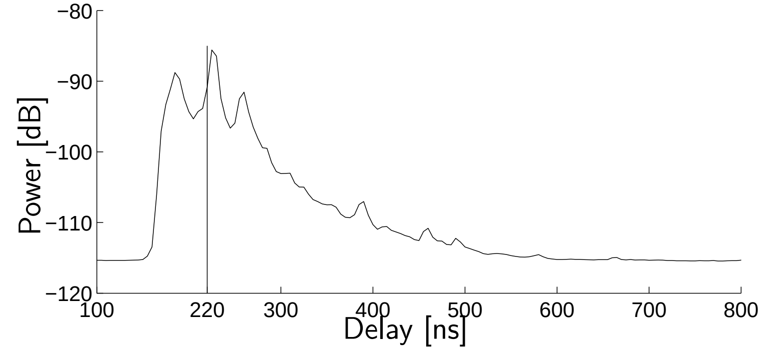

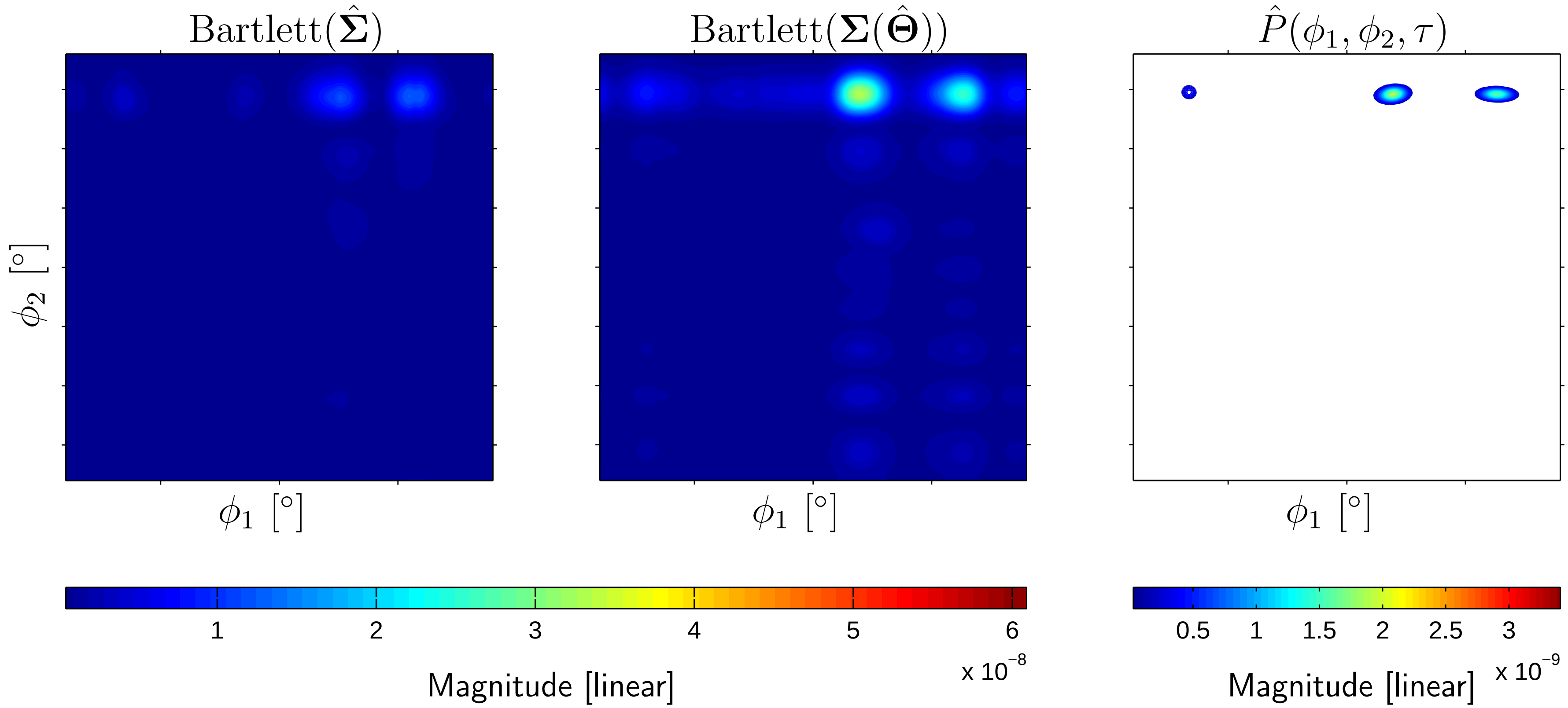

Estimated Biazimuth-Delay Power Spectrum (Movie-view)

Delay 225 ns

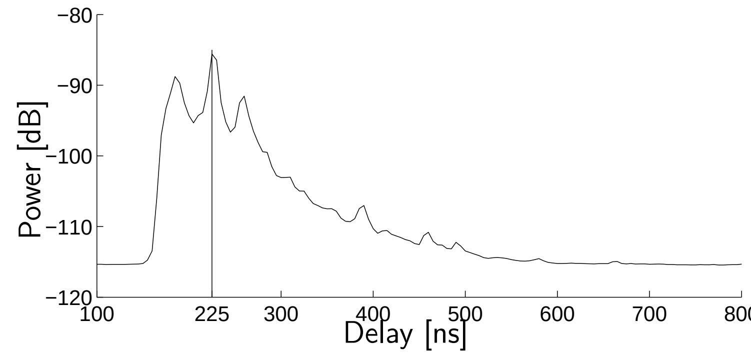

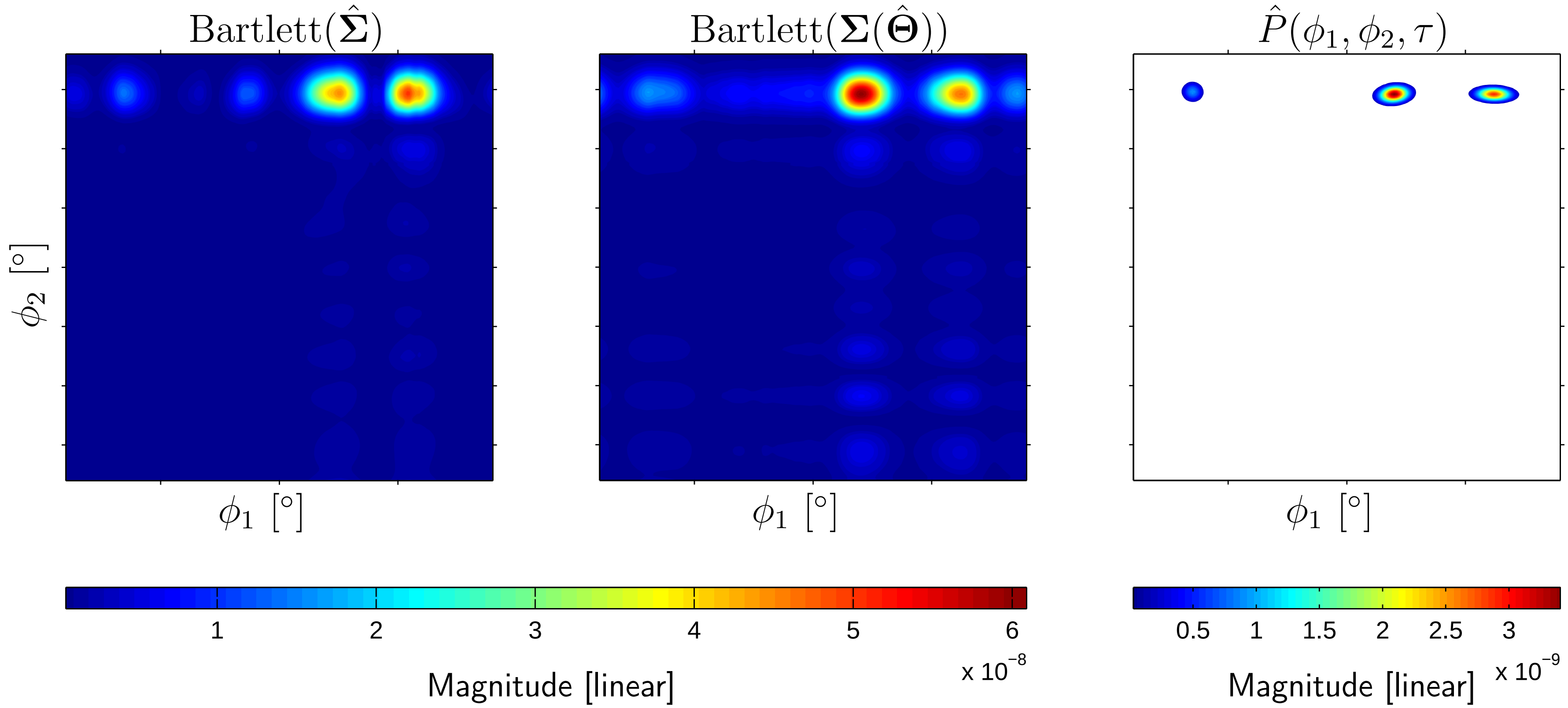

Estimated Biazimuth-Delay Power Spectrum (Movie-view)

Delay 230 ns

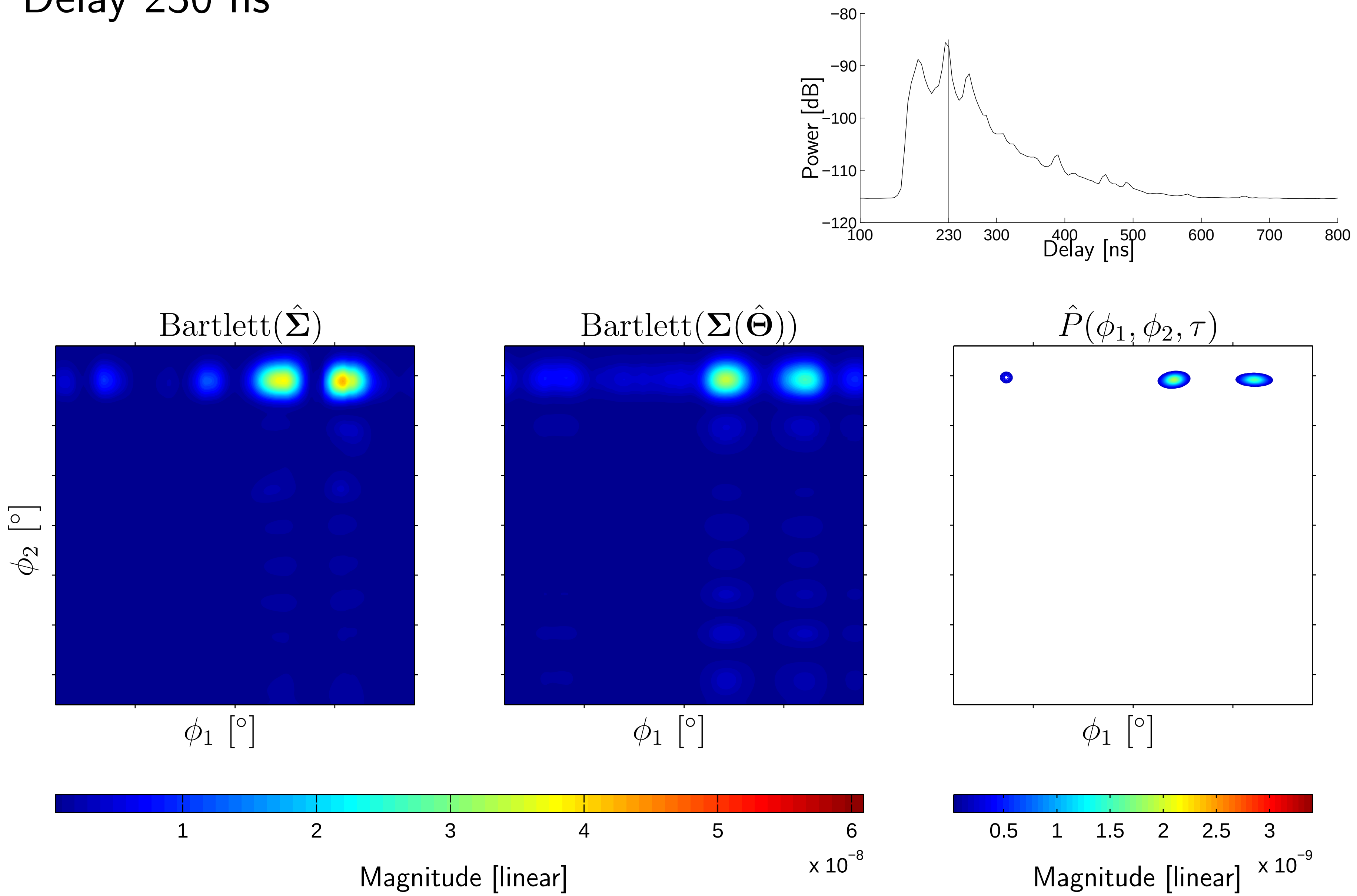

Estimated Biazimuth-Delay Power Spectrum (Movie-view)

Delay 235 ns

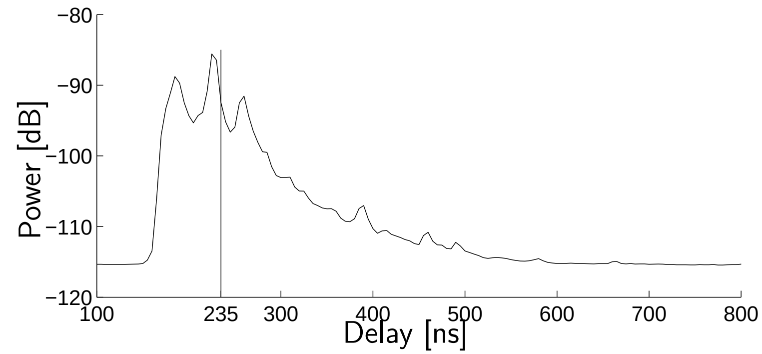

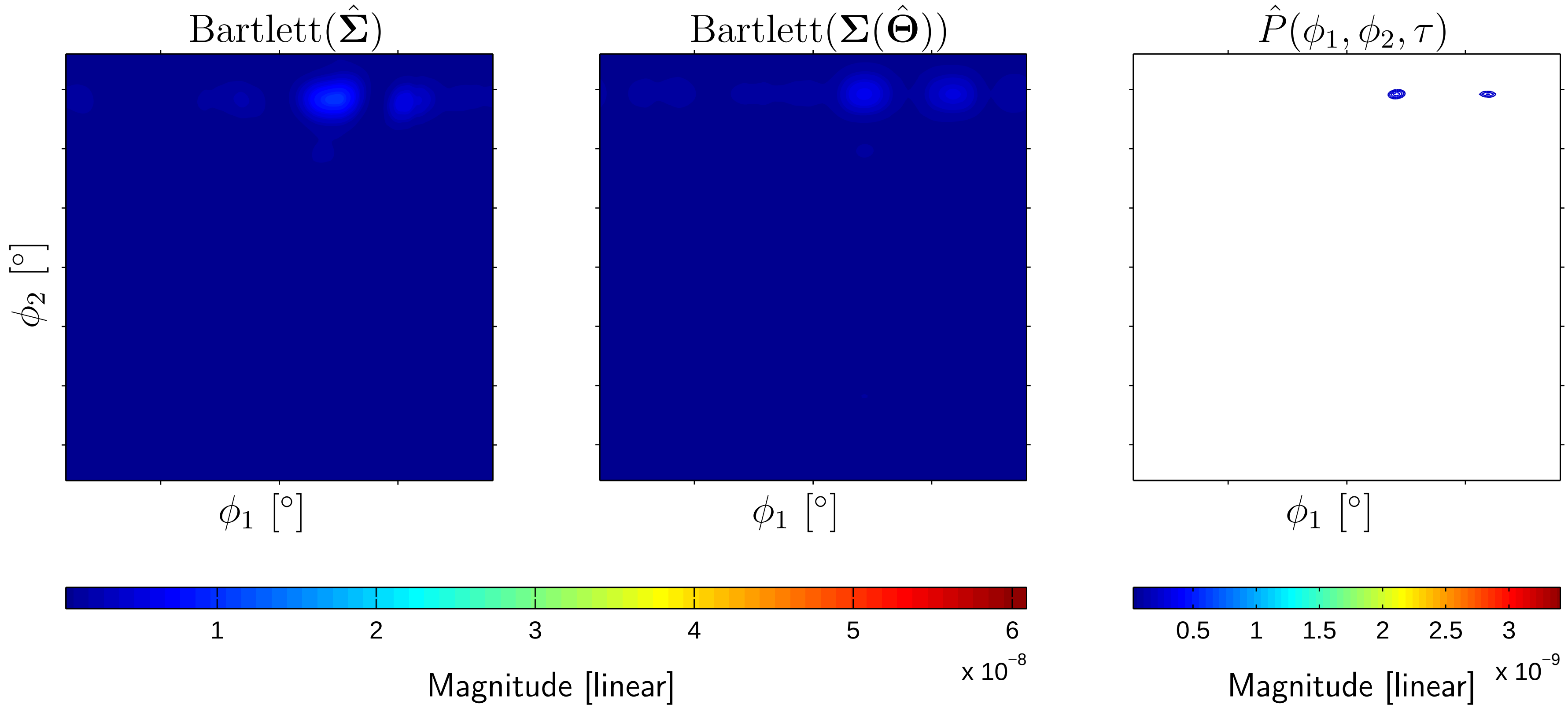

Estimated Biazimuth-Delay Power Spectrum (Movie-view)

Delay 240 ns

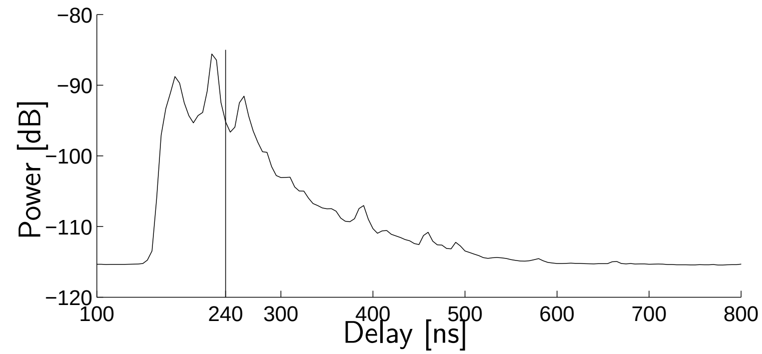

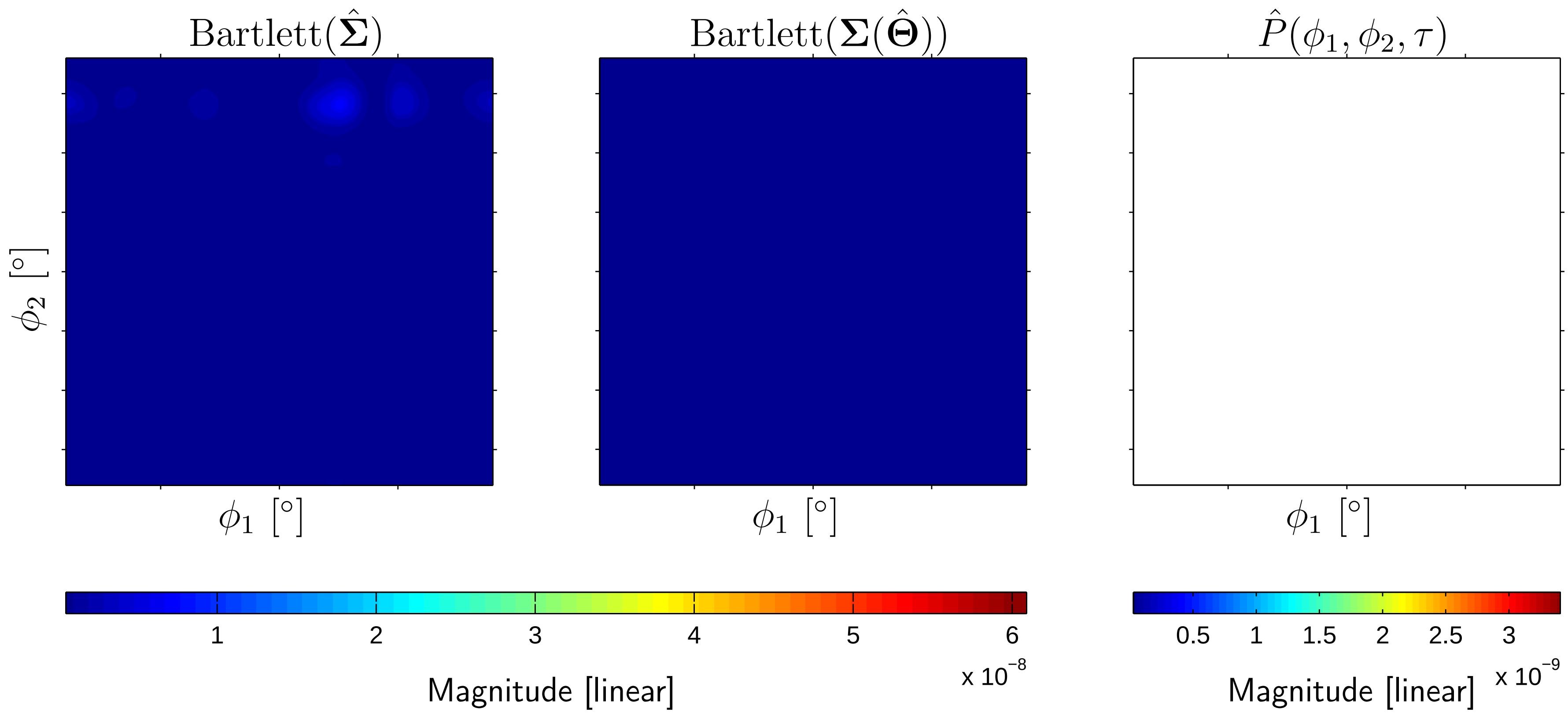

Estimated Biazimuth-Delay Power Spectrum (Movie-view)

Delay 245 ns

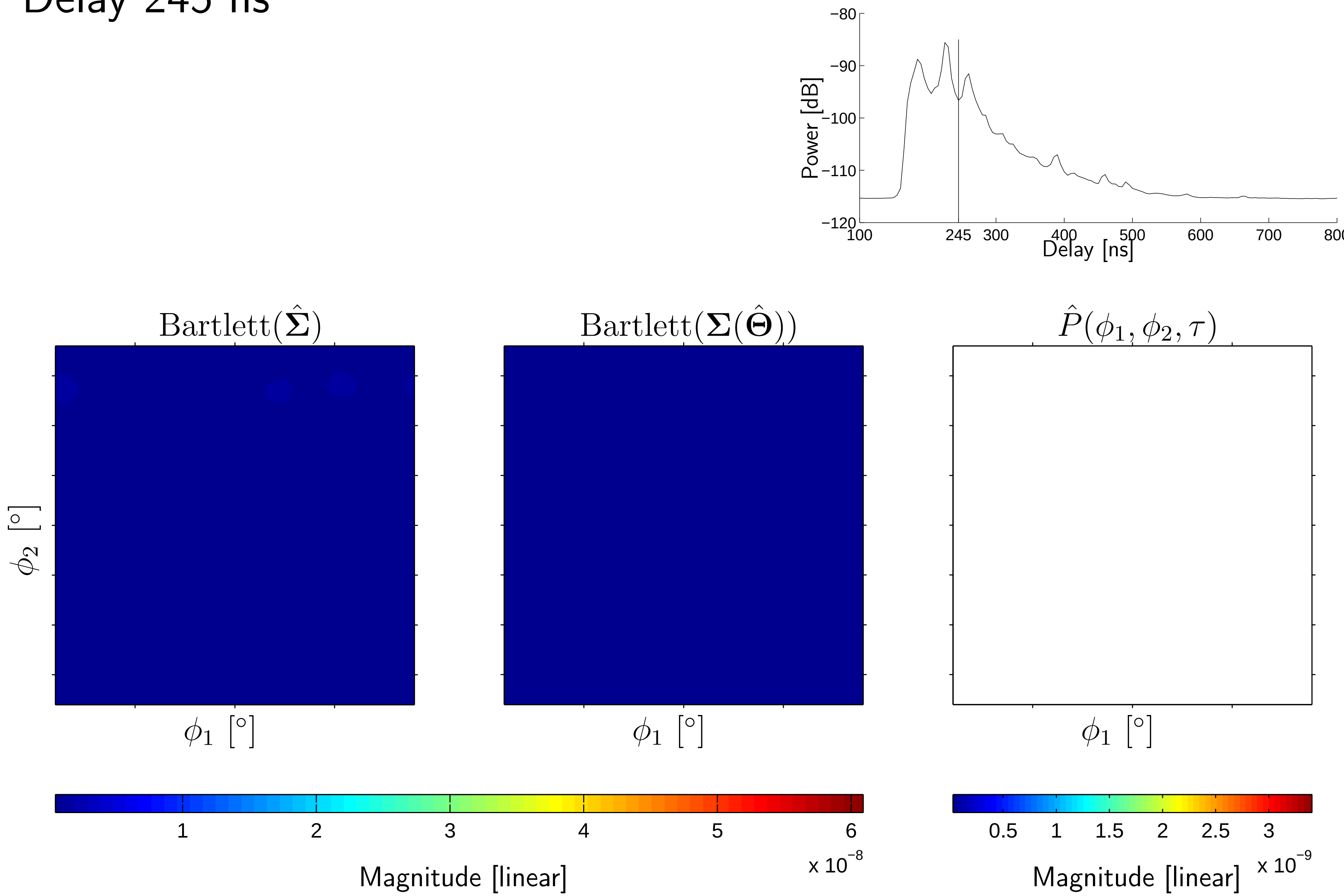

Estimated Biazimuth-Delay Power Spectrum (Movie-view)

Delay 250 ns

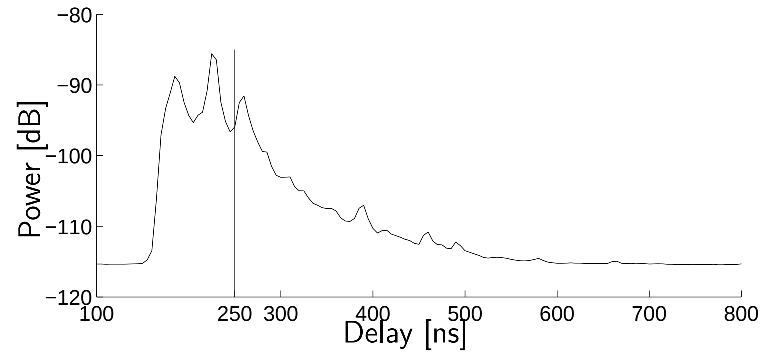

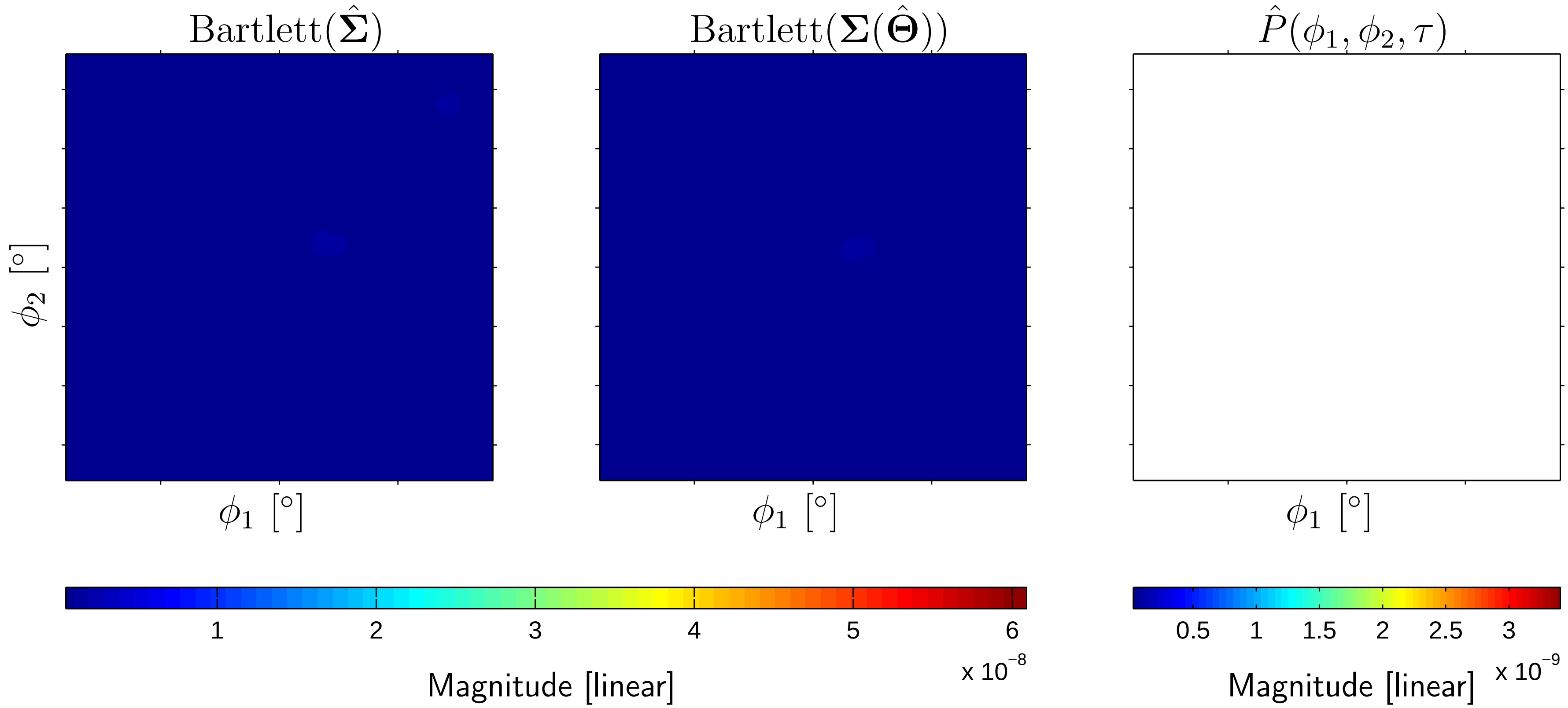

Estimated Biazimuth-Delay Power Spectrum (Movie-view)

Delay 255 ns

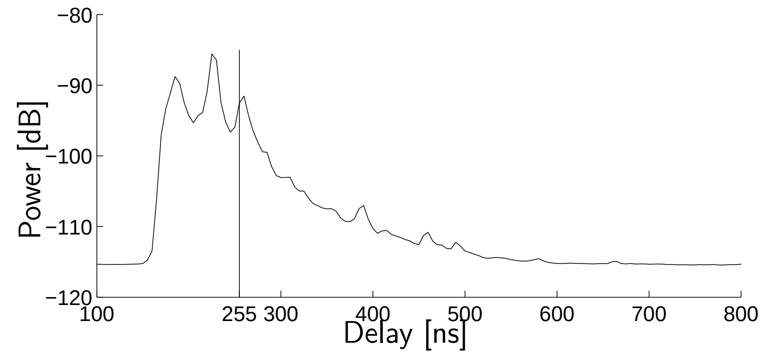

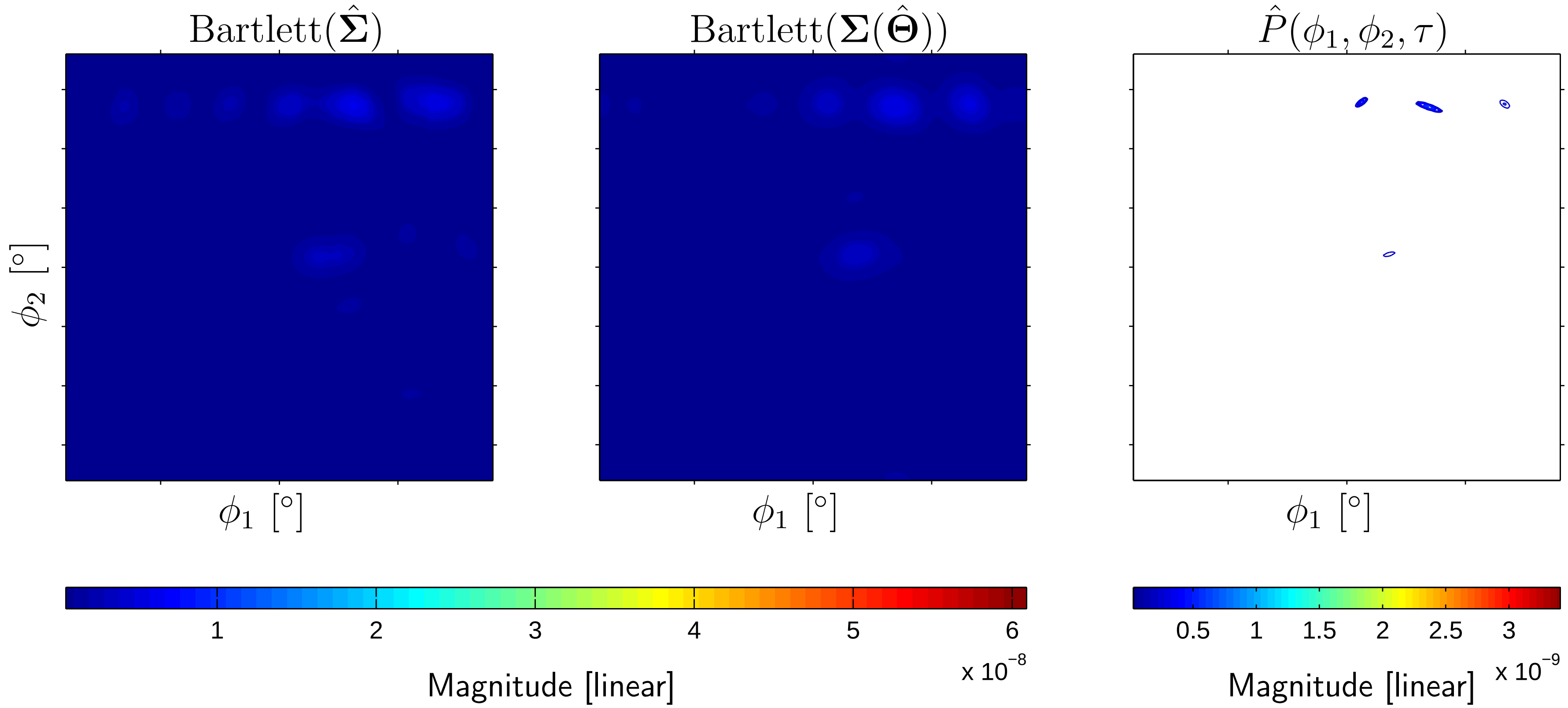

Estimated Biazimuth-Delay Power Spectrum (Movie-view)

Delay 260 ns

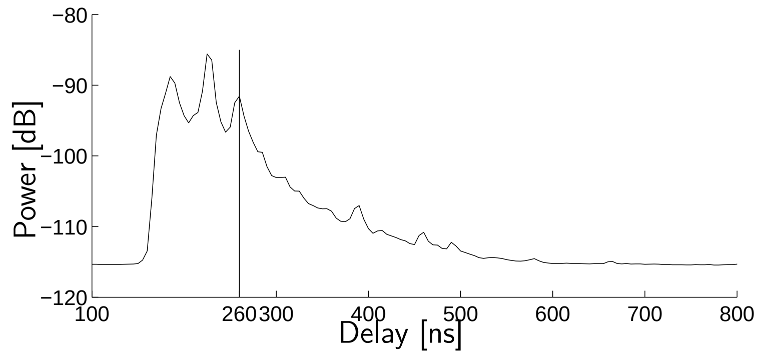

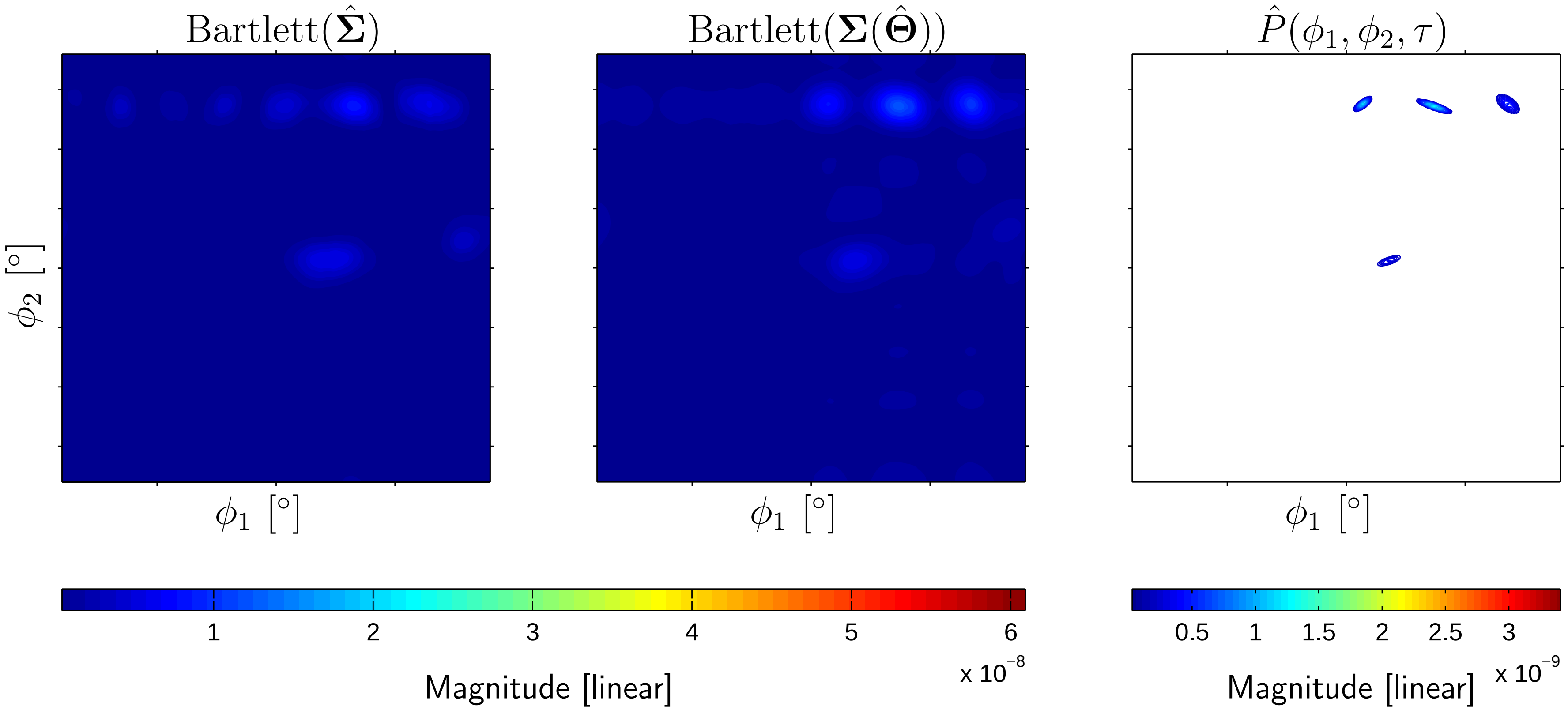

Estimated Biazimuth-Delay Power Spectrum (Movie-view)

Delay 265 ns

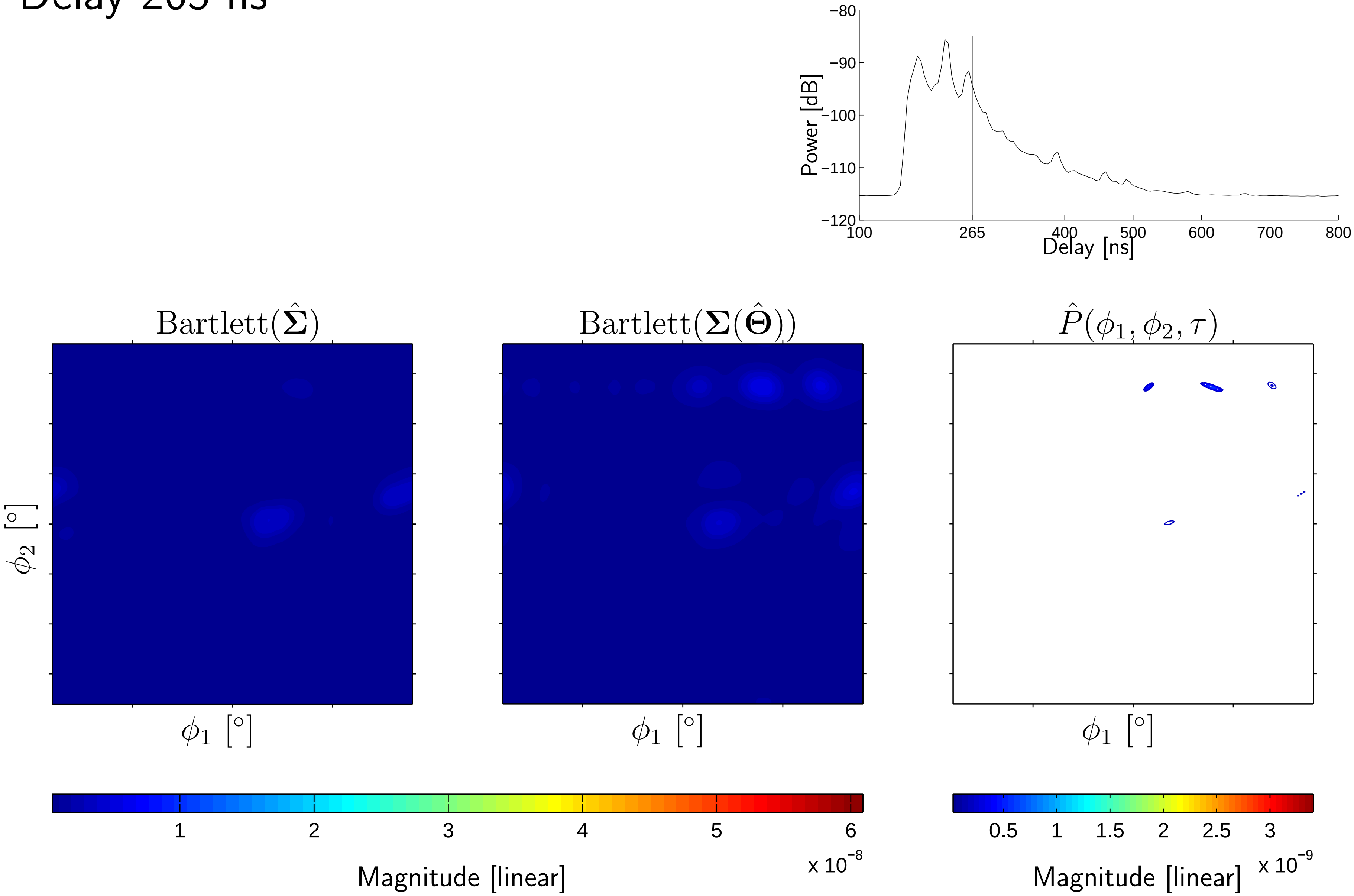

Estimated Biazimuth-Delay Power Spectrum (Movie-view)

Delay 270 ns

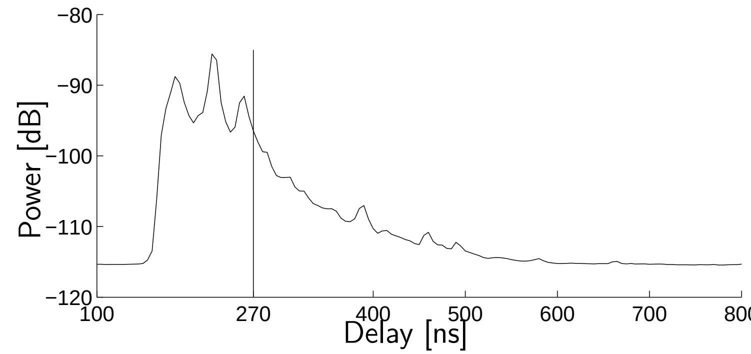

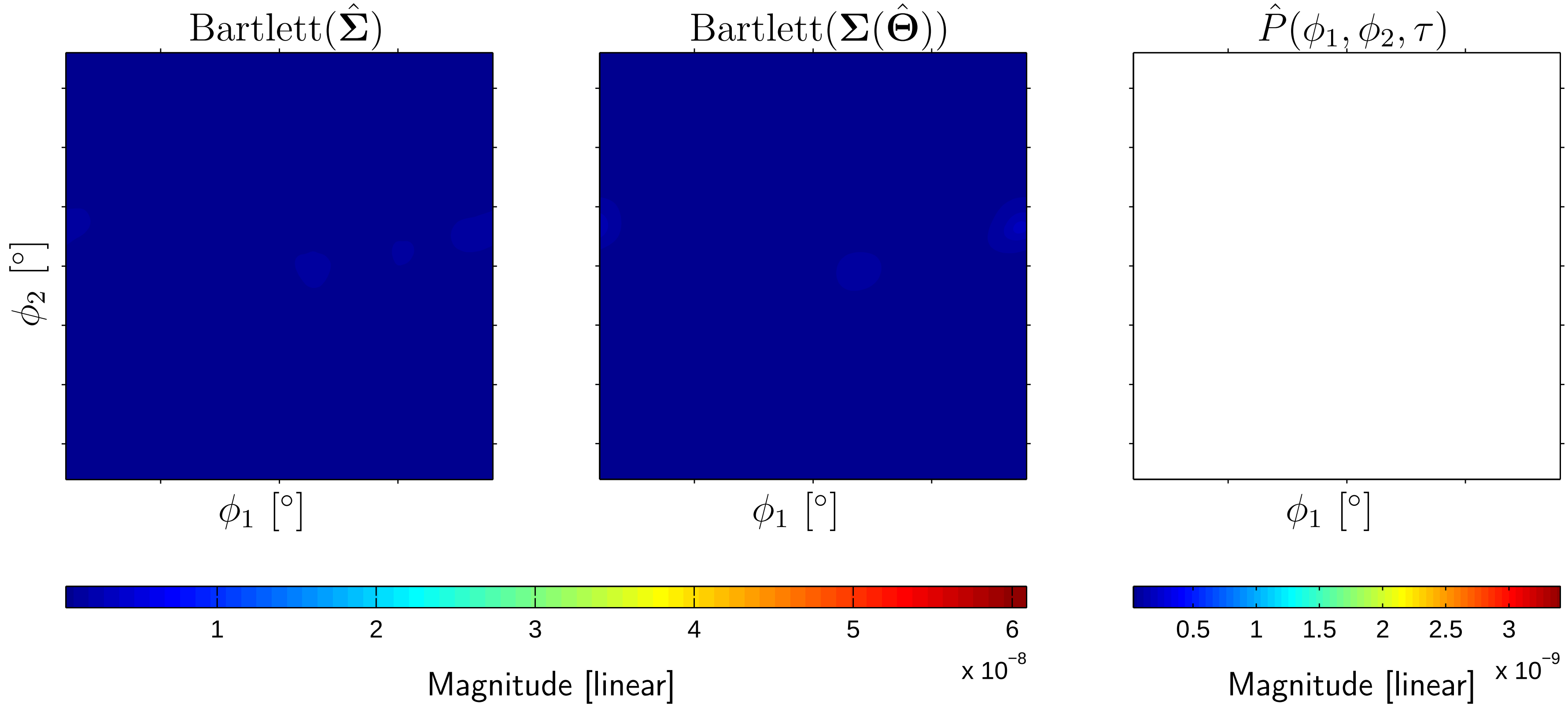

Contents

Summaries and Conclusions

- We applied the principle of constrained entropy maximization to derive probability density functions and use them to characterize the shape of the dispersion power spectrum of individual path components.
- Estimators of the parameters characterizing the dispersion power spectrum were derived.
- Experimental investigations showed that the proposed characterization methods are applicable in real situations.
- Experimental results demonstrated that the path components are noticeably more concentrated compared to their corresponding footprints in the Bartlett spectrum.
- Dependence across multiple dispersion dimensions is observed for individual path components.

References

Besson & Stoica (1999) O. Besson and P. Stoica, "Decoupled estimation of DoA and angular spread for spatially distributed sources", IEEE Transactions on Signal Processing, 1999, 49, 673-680

Trump & Ottersten (1996) T. Trump and B. Ottersten, "Estimation of nominal direction of arrival and angular spread using an array of sensors", Signal Processing, 1996, 50, 57-69

Ribeiro, *et al.* (2005a) C.B. Ribeiro, E. Ollila and V. Koivunen, "Stochastic maximum likelihood method for propagation parameter estimation", Proc. of the 15th IEEE International Symposium on Personal, Indoor and Mobile Radio Communications (PIMRC), 2004

Ribeiro, *et al.* (2005b) C.B. Ribeiro, A. Richter and V. Koivunen, "Stochastic Maximum Likelihood Estimation of Angle- and Delay-Domain Propagation", Proc. of the 16th IEEE PIMRC International Symposium, 2005

Yin, *et al.* (2006a) X. Yin, T. Pedersen, N. Czink and B.H. Fleury, "Parametric Characterization and Estimation of Bi-Azimuth Dispersion of Path Components", Proc. of the 7th IEEE International Workshop on Signal Processing Advances for Wireless Communications (SPAWC), 2006

Yin, *et al.* (2006b) X. Yin, T. Pedersen, N. Czink and B.H. Fleury, "Parametric Characterization and Estimation of Bi-Azimuth and Delay Dispersion of Path Components", Proc. of the First European Conference on Antennas and Propagation (EuCAP), 2006

Yin, *et al.* (2007a) X. Yin, L. Liu, D. Nielsen, N. Czink and B.H. Fleury, "Characterization of the Azimuth-Elevation Power Spectrum of Individual Path Components", Proc. of the International ITG/IEEE Workshop on Smart Antennas (WSA), 2007

Yin, *et al.* (2007b) X. Yin, L. Liu, D. Nielsen, T. Pedersen and B.H. Fleury, "A SAGE Algorithm for the Estimation of Direction Power Spectrum of Individual Path Components", Submitted to the IEEE Global Telecommunications Conference (GLOBECOM), 2007.

Radio Channel Modelling Using Stochastic Propagation Graphs

Contents

Motivation: Specular-to-diffuse Transition

The specular-to-diffuse transition was noticed by Suzuki (1977) and by Pamp&Kunisch (2002).

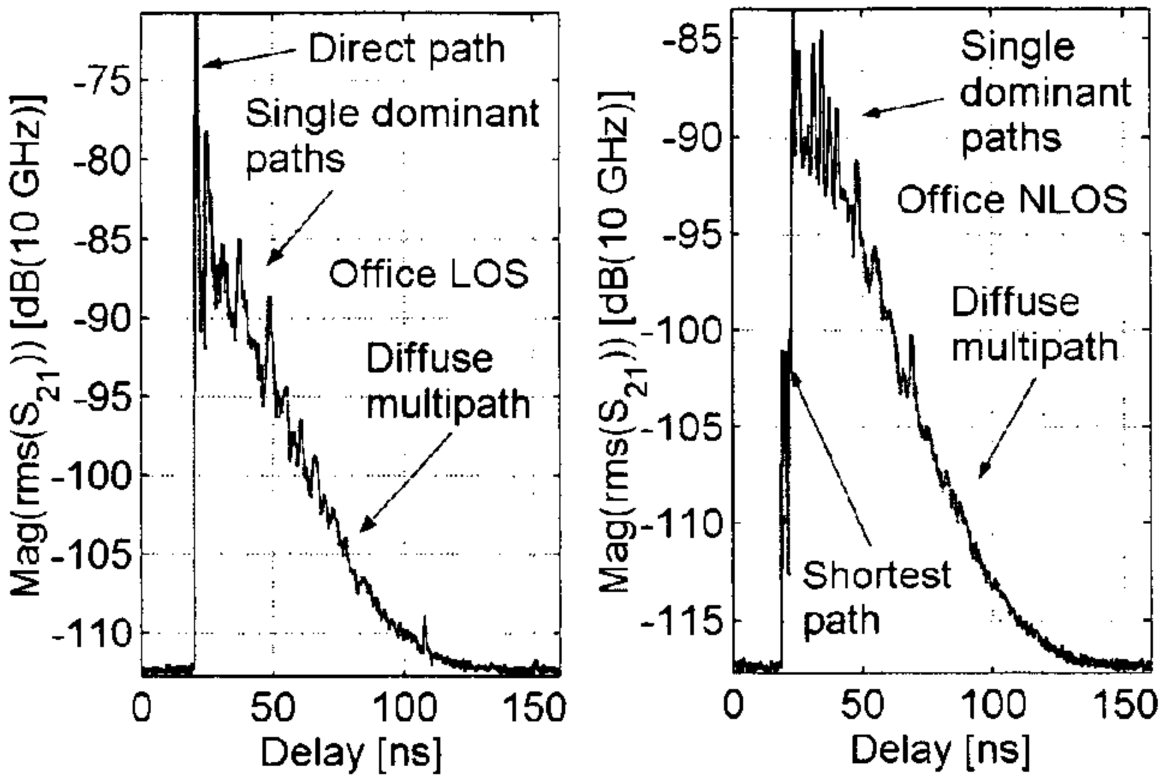

Spatially averaged power delay profiles obtained from a line-of-sight scenario (left) and a non-line-of-sight scenario (right) [Pamp&Kunish2002].

- Not much attention has been paid to this transition effect.
- "Specular" and "diffuse" components are modelled as separate effects.

Motivation: Exponential Power Decay

- Conventional models implement an exponentially decaying power-delay-profile motivated by measurement results.
- This is usually done by including various ad-hoc constraints on the random parameters of the model.
- These approaches do not reflect the underlying physical mechanisms that lead to this exponential decay.
- J. B. Andersen (2006) proposed a model inspired from room acoustical models. It predicts an exponential power decay.

Philosophy, Goals, and Method

Philosophy:

- Model the *environment* instead of the *response* of the environment

Goals:

- The obtained response should exhibit an exponential power decay.
- A joint description of specular and diffuse signal components.

Method:

- Model the propagation environment
- Model the propagation mechanisms
- Compute the response

Model of the Propagation Environment (1)

An atypical propagation environment:

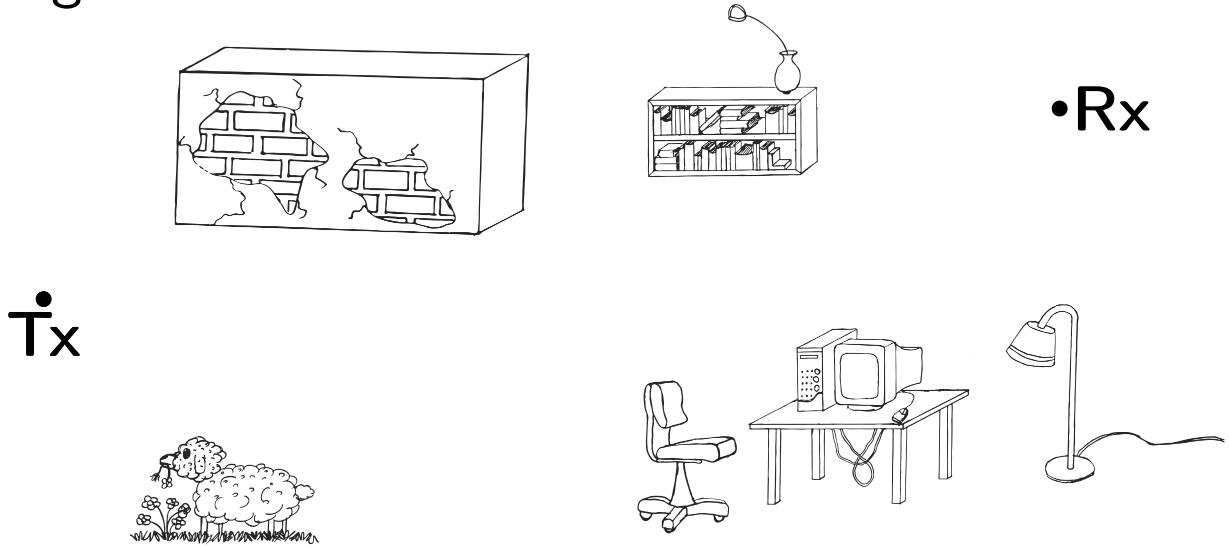

(The propagation environment is static.)

Model of the Propagation Environment (1)

An atypical propagation environment:

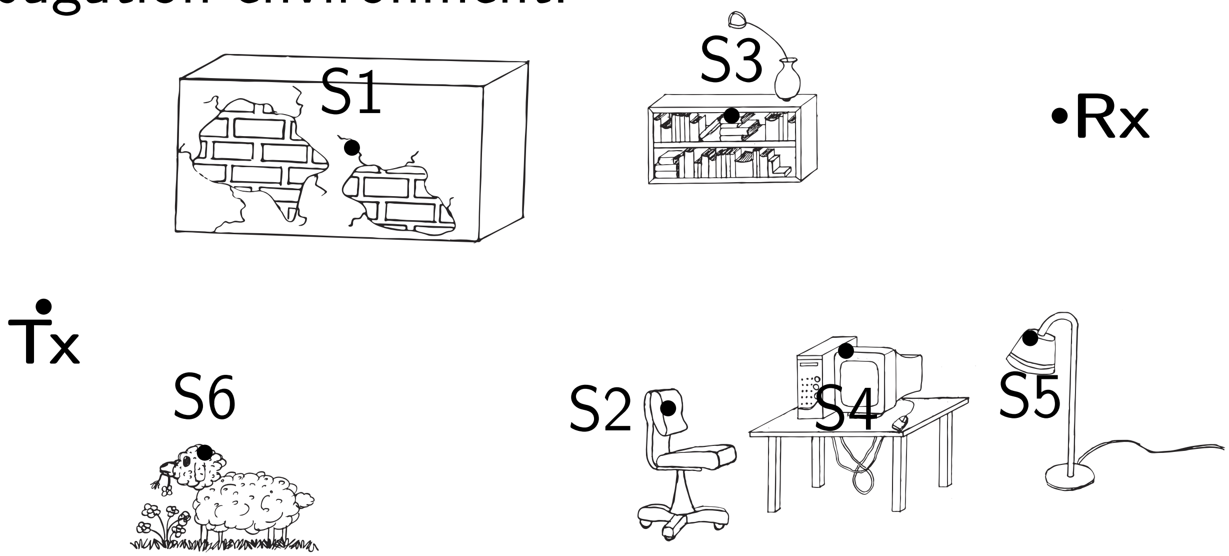

(The propagation environment is static.)

- We model scatterers as the vertices of a signal flow-graph.

Model of the Propagation Environment (1)

An atypical propagation environment:

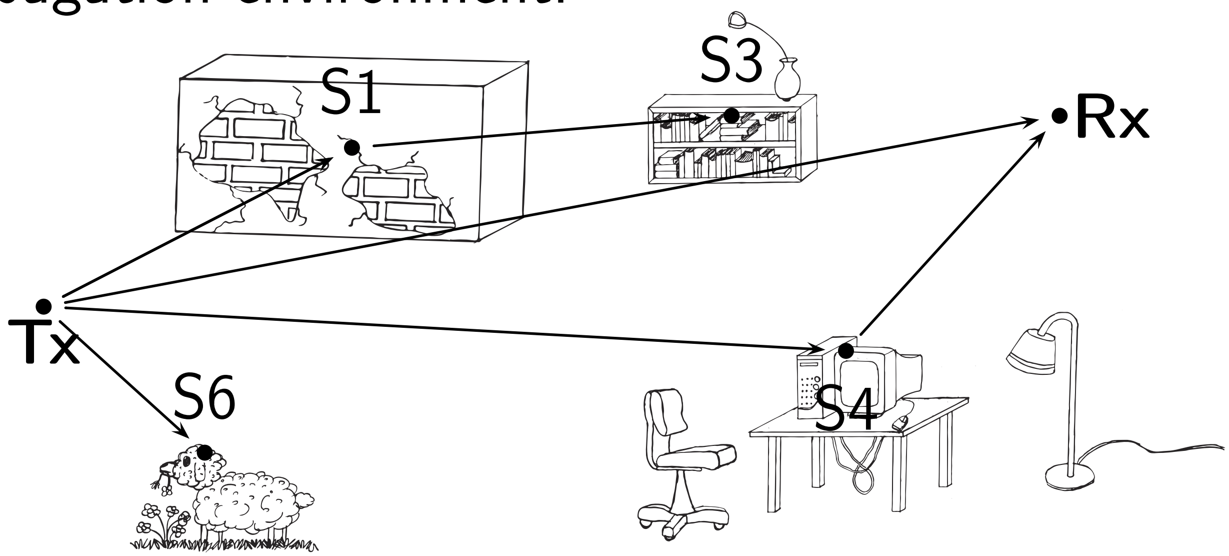

(The propagation environment is static.)

- We model scatterers as the vertices of a signal flow-graph.
- The wave propagation between scatterers is modelled by the edges of the graph.

Model of the Propagation Environment (2)

A propagation graph is a "simple" directed graph $\mathcal{G} = (\mathcal{V}, \mathcal{E})$:

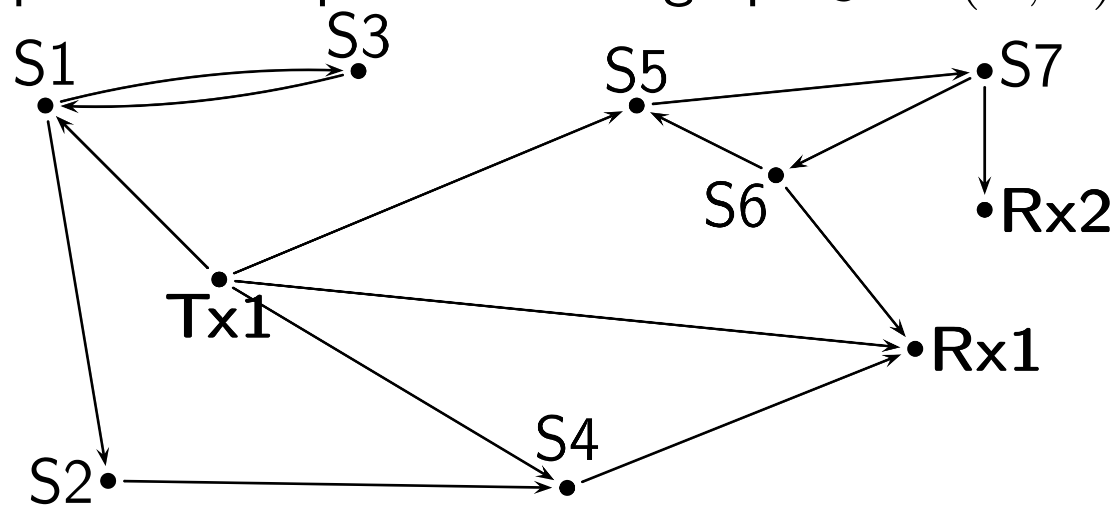

The transmitters (Tx), receivers (Rx), and scatterers (S) are represented by vertices in the vertex set $\mathcal{V} = \{\mathsf{Tx1}, \mathsf{Rx1}, \mathsf{Rx2}, \mathsf{S1}, \mathsf{S2}, \dots\}$.

Wave propagation between the vertices is modelled by edges in the edge set $\mathcal{E}$.
Wave propagation from $v \in \mathcal{V}$ to $v' \in \mathcal{V}$ is possible iff $(v, v') \in \mathcal{E}$.

The position of vertex v is given by $\mathbf{r}_v \in \mathbb{R}^3$.

Model of the Propagation Mechanisms

- The sum of signals impinging via the incoming edges of a scatterer are re-emitted via the outgoing edges

- A signal emitted from the initial vertex of an edge is received in a delayed and attenuated version at the terminal vertex of the edge. Transfer function of edge $e = (v, v')$:

$$A_e(f) = g_e \cdot \exp(j2\pi\tau_e f),$$

$$\tau_e = \frac{|\mathbf{r}_v - \mathbf{r}_{v'}|}{c}, \qquad |g_e|^2 = \left(\frac{g}{1 - |\mathbf{r}_v - \mathbf{r}_{v'}|}\right)^2 \cdot \tfrac{1}{\mathrm{outdegree}(v)},$$

where

- $|g| < 1$ is a constant gain,
- $\mathrm{outdegree}(v)$ is the out-degree of vertex v, and
- c is the speed of light in vacuum.

Response of a Propagation Graph (1)

Relation between the input signal vector $\mathbf{X}(f)$ and the output signal vector $\mathbf{Y}(f)$ in the Fourier domain:

$$\mathbf{Y}(f) = \mathbf{H}(f)\mathbf{X}(f)$$

In the following we derive an expression for the transfer matrix $\mathbf{H}(f)$.

(Four slides of math will follow. Sorry!)

Response of a Propagation Graph (2)

Define the state vector:

$$\mathbf{C}(f) = \begin{bmatrix} \mathbf{X}(f) \\ \mathbf{Y}(f) \\ \mathbf{Z}(f) \end{bmatrix}$$

where $\mathbf{Z}(f)$ is the vector of signals observed at the scatterers.

Decompose $\mathbf{C}(f)$ according to the number of edges k the signals have traversed:

$$\mathbf{C}(f) = \sum_{k=0}^{\infty} \mathbf{C}_k(f) = \begin{bmatrix} \mathbf{X}_k(f) \\ \mathbf{Y}_k(f) \\ \mathbf{Z}_k(f) \end{bmatrix}$$

Response of a Propagation Graph (3)

We have the following recursive equation

$$\mathbf{C}_0(f) = [\mathbf{X}(f)^{\mathsf{t}}, \mathbf{0}^{\mathsf{t}}, \mathbf{0}^{\mathsf{t}}]^{\mathsf{t}}$$
$$\mathbf{C}_{k+1}(f) = \mathbf{A}(f)\mathbf{C}_k(f), \quad k \geq 0$$

where $\mathbf{A}(f)$ is the weighted adjacency matrix of the graph:

$$[\mathbf{A}(f)]_{nn'} = \begin{cases} A_{(v_n, v_{n'})}(f), & (v_n, v_{n'}) \in \mathcal{E} \\ 0, & \text{otherwise} \end{cases}$$

By appropriate vertex indexing:

$$\mathbf{A}(f) = \begin{bmatrix} \mathbf{0} & \mathbf{0} & \mathbf{0} \\ \mathbf{D}(f) & \mathbf{0} & \mathbf{R}(f) \\ \mathbf{T}(f) & \mathbf{0} & \mathbf{B}(f) \end{bmatrix}$$

$$\begin{array}{lllll} \mathbf{D}(f): & \text{transmitters} & \rightarrow & \text{receivers} \\ \mathbf{R}(f): & \text{scatterers} & \rightarrow & \text{receivers} \\ \mathbf{T}(f): & \text{transmitters} & \rightarrow & \text{scatterers} \\ \mathbf{B}(f): & \text{scatterers} & \rightarrow & \text{scatterers.} \end{array}$$

Response of a Propagation Graph (4)

Obviously

$$\mathbf{Y}_1(f) = \mathbf{D}(f)\mathbf{X}(f).$$

By inspection of the series $\mathbf{A}^2(f), \mathbf{A}^3(f), \ldots$ we see

$$\mathbf{A}^k(f) = \begin{bmatrix} \mathbf{0} & \mathbf{0} & \mathbf{0} \\ \mathbf{R}(f)\mathbf{B}^{k-2}(f)\mathbf{T}(f) & \mathbf{0} & \mathbf{R}(f)\mathbf{B}^{k-1}(f) \\ \mathbf{B}^{k-1}(f)\mathbf{T}(f) & \mathbf{0} & \mathbf{B}^k(f) \end{bmatrix}, \; k \geq 2.$$

Thus

$$\mathbf{Y}_k(f) = \mathbf{R}(f)\mathbf{B}^{k-2}(f)\mathbf{T}(f)\mathbf{X}(f), \quad k \geq 2.$$

Response of a Propagation Graph (5)

Summing up signal contributions we obtain:

$$
\begin{aligned}
\mathbf{Y}(f) &= \mathbf{D}(f)\mathbf{X}(f) + \sum_{k=2}^{\infty} \mathbf{R}(f)\mathbf{B}^{k-2}(f)\mathbf{T}(f)\mathbf{X}(f) \\
&= \left[\mathbf{D}(f) + \sum_{k'=0}^{\infty} \mathbf{R}(f)\mathbf{B}^{k'}(f)\mathbf{T}(f)\right]\mathbf{X}(f) \\
&= \underbrace{\left[\mathbf{D}(f) + \mathbf{R}(f)(\mathbf{I} - \mathbf{B}(f))^{-1}\mathbf{T}(f)\right]}_{\mathbf{H}(f)}\mathbf{X}(f).
\end{aligned}
$$

A detailed derivation is given in [Pedersen & Fleury 2007].

How to Generate a Propagation Graph

A propagation graph can be obtained in different ways:

- From a deterministic environment (e.g. by ray-tracing).
- Generate a random environment (scatter locations and weights) and calculate visibilities.
- By randomly generating the vertices and the edges of the graph.

We focus on the third option.

Simulation Study (1)

Simulation scenario:

1. A constant number N of scatterers is assumed.
2. The positions of the N scatterers S$1, \ldots,$ SN are drawn according to a uniform distribution defined on a region $\mathcal{R} \subset \mathbb{R}^3$.
3. The region $\mathcal{R}$ is assumed to be a rectangular solid box.
4. The transmitters and receivers have fixed coordinates.
5. Edge probability: $\Pr((v, v') \in \mathcal{E}) = \begin{cases} P_{\mathrm{dir}} & \text{if } (v, v') = (\mathsf{Tx}, \mathsf{Rx}) \\ 0 & \text{if } v = v' \\ 0 & \text{if } v = \mathsf{Rx} \\ 0 & \text{if } v' = \mathsf{Tx} \\ P_{\mathsf{vis}} & \text{otherwise} \end{cases}$

Simulation Study (2)

Simulation settings:

- $\mathcal{R} = [0, 5] \times [0, 10] \times [0, 3.5]\,\mathrm{m}^3$
- $M_1 = M_2 = 1$
- Transmit antenna position: $[1.8, 2.0, 0.5]^{\mathrm{T}}\,\mathrm{m}$
- Receiver antenna position, $[1.0, 4.0, 1.0]^{\mathrm{T}}\,\mathrm{m}$
- $N = 10$ scatterers placed according to a Bernoulli point process on $\mathcal{R}$
- $g = 0.8$
- $P_{\mathsf{vis}} = 0.8$

Simulation Study (3)

Scenario: $P_{\mathrm{dir}} = 1$ (line-of-sight). Signal bandwidth: 2 GHz to 10 GHz

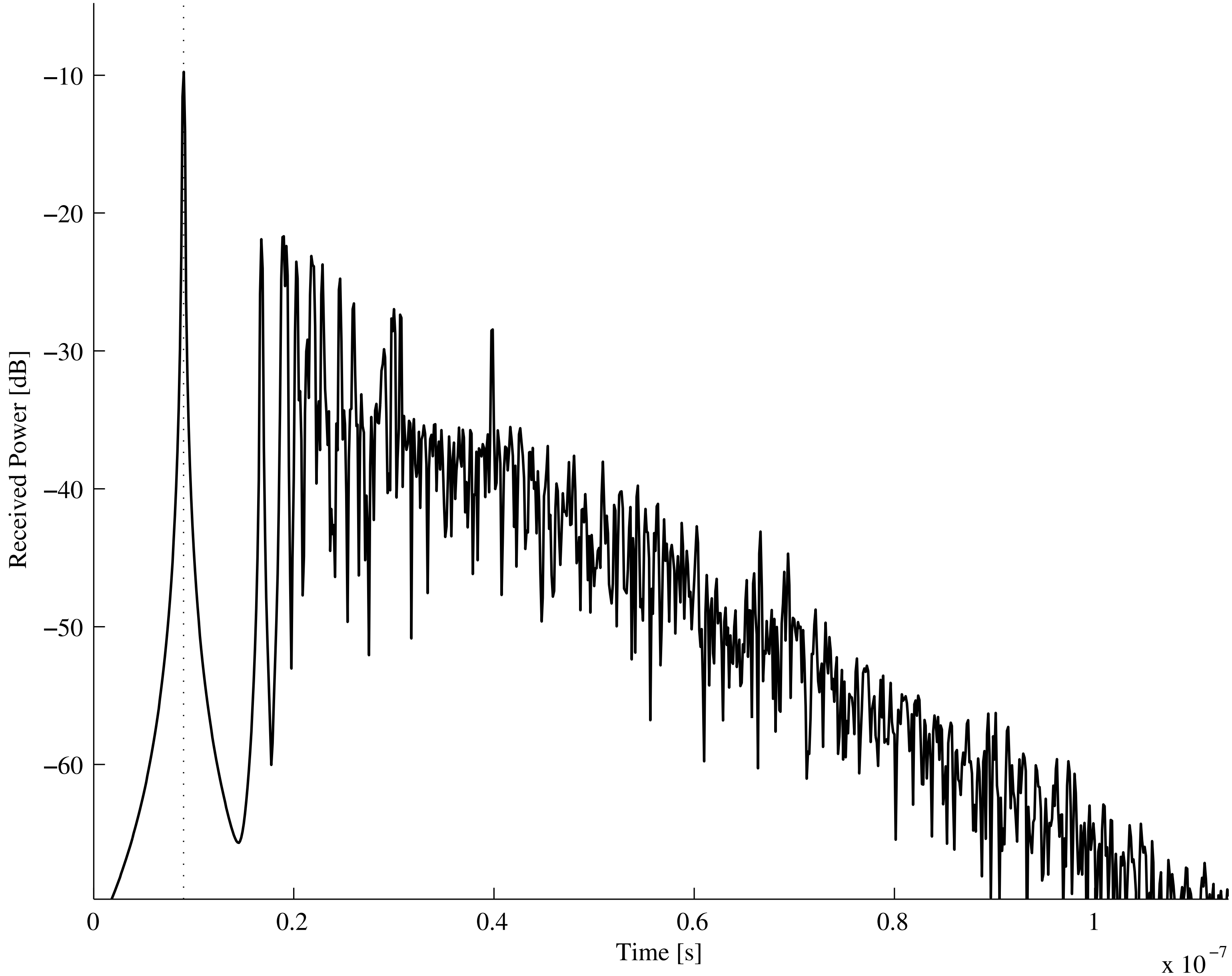

Simulation Study (4)

$P_{\mathrm{dir}} = 1$ (solid) $P_{\mathrm{dir}} = 0$ (dashed), signal bandwidth: 2 GHz to 3 GHz

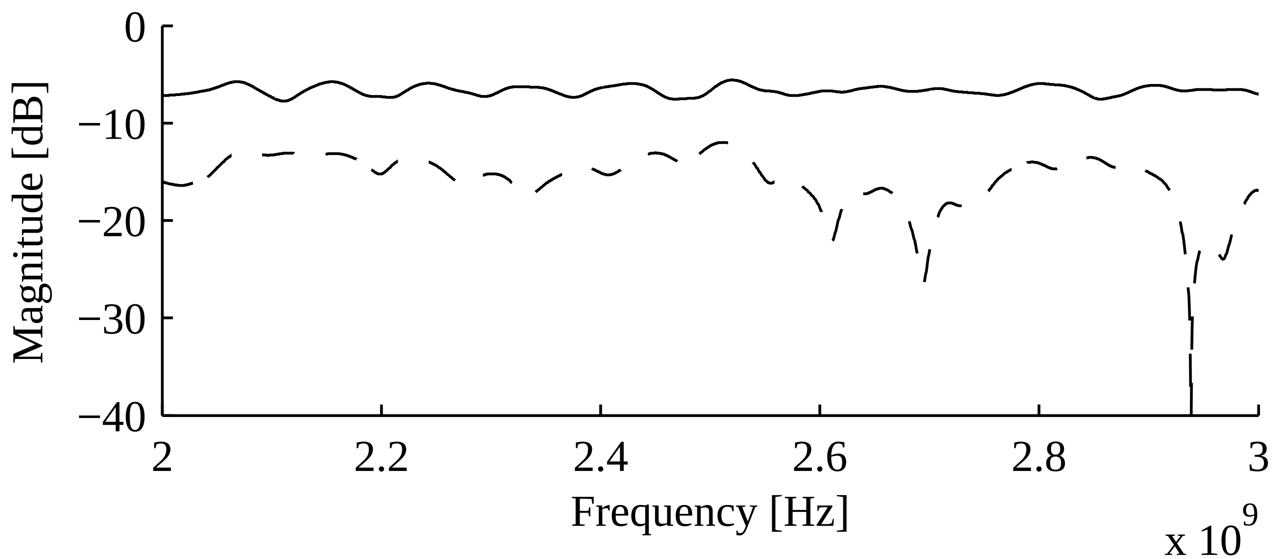

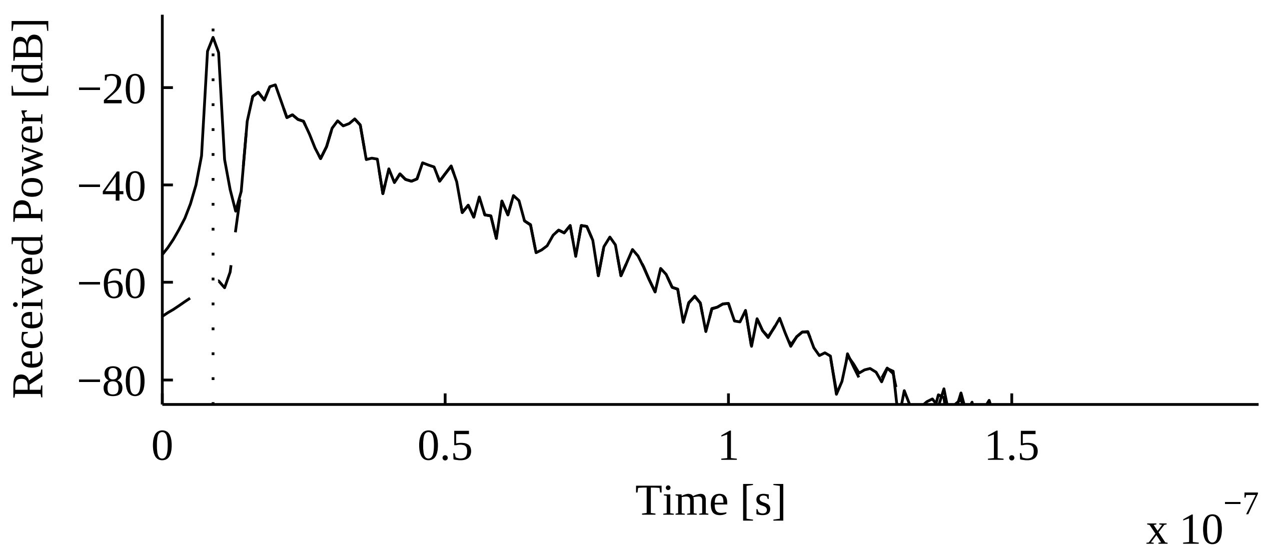

Simulation Study (5)

$P_{\mathrm{dir}} = 1$ (solid) $P_{\mathrm{dir}} = 0$ (dashed), signal bandwidth: 2 GHz to 3 GHz

Estimated delay power spectrum (obtained from 100 realisations):

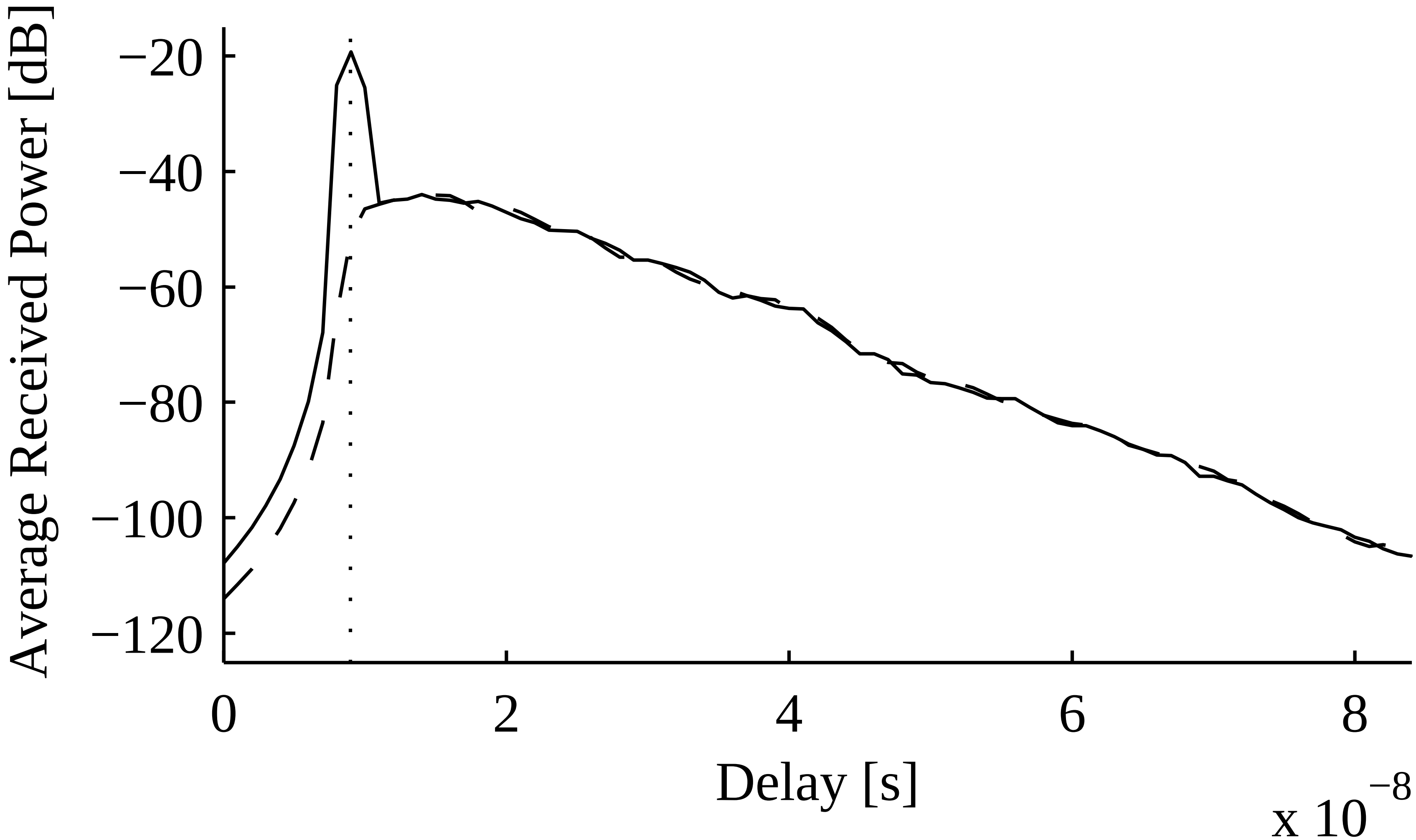

Concluding Remarks

- The structure of the propagation graph yields an exponentially decaying power-delay profile.
- The channel realisations of the channel impulse response obtained with the model exhibit a transition from specular contributions for low delays to a diffuse part at long delays as observed in measurements.
- The propagation graph model can be easily extended to include dispersion in directions of departure and arrival.
- The model has been described in [Pedersen & Fleury 2006] and [Pedersen & Fleury 2007]

Acknowledgements: The work is supported by Elektrobit Oy, Finland, and has been performed within NEWCOM, the Network of Excellence in Wireless Communications

References

Suzuki (1977) H. Suzuki, "A statistical model for urban radio propagation channel", IEEE Transactions on Communication Systems, 1977 , 25 , 673-680

Kunish & Pamp (2002) J. Kunisch and J. Pamp "Measurement results and modeling aspects for the UWB radio channel", Ultra Wideband Systems and Technologies, 2002. Digest of Papers. 2002 IEEE Conference on, 2002 , 19-24

Kunish & Pamp (2003) J. Kunisch and J. Pamp, "An ultra-wideband space-variant multipath indoor radio channel model", Ultra Wideband Systems and Technologies, 2003 IEEE Conference on, 2003 , 290-294

Andersen et. al. (2006) J. B. Andersen, J. Ø. Nielsen, G. Bauch, and M. Herdin, "The Large Office Environment-Measurement and Modeling of the Wideband Radio Channel", The 17th Annual IEEE INternational Symposium on Personal Indoor and Mobile Radio Communications, 2006

Pedersen & Fleury (2006) T. Pedersen and B. H. Fleury "A Realistic Radio Channel Model Based on Stochastic Propagation Graphs", Proceedings 5th MATHMOD Vienna – 5th Vienna Symposium on Mathematical Modelling, 2006, 1,2, 324

Pedersen & Fleury (2007) T. Pedersen and B. H. Fleury "Radio Channel Modelling Using Stochastic Propagation Graphs", accepted for publication at ICC 2007.